ZBTB2-mediated mechanisms behind the expression of a specific subset of HIF-1 target genes under hypoxia

Christalle Cheuk Tung Chow

Table of Contents

Abstract

Hypoxic, or low-oxygen, conditions arise in a variety of physiological and pathophysiological situations in multicellular organisms. The cellular response to hypoxia is largely controlled by the action of the transcription factor hypoxia-inducible factor 1 (HIF-1), but it alone is insufficient to trigger the full expression of genes under hypoxic conditions. While interactions between HIF-1 and other coactivating proteins are suggested to be required for activation of certain genes, much remains to be elucidated regarding the underlying mechanisms. The aim of this project is to explore how coactivators can influence the expression of HIF-1 target genes under hypoxic conditions, and to ultimately shed more light on the mechanisms behind the cellular response to hypoxia. My colleagues and I have previously reported that zinc finger and BTB-domain containing 2 (ZBTB2) increases HIF-1 activity and promotes the expression of some HIF-1 target genes. Therefore, I focused on ZBTB2 as a representative coactivator of HIF-1 in order to investigate the project aim. The current study demonstrates through ChIP-Seq analysis that ZBTB2 is recruited to a subset of HIF-1 target genes. Inspection of one of these genes, EGFR antisense RNA 1 (EGFR-AS1), revealed that it is upregulated under hypoxic conditions in a ZBTB2- and HIF-1-dependent manner, and that overexpression of ZBTB2 results in a further increase in gene expression. HIF-1 is shown to bind to a hypoxia-response element (HRE) situated in the intron of EGFR-AS1, and HIF-1 recruitment to the HRE is found to be required for the effects of ZBTB2 on gene expression to be observed. In addition, expression of EGFR-AS1 under hypoxia was shown to require p300-mediated histone 3 lysine 27 acetylation (H3K27ac), and ZBTB2 overexpression increased H3K27ac at the EGFR-AS1 gene locus. Furthermore, ATPase Na+/K+ Transporting Subunit Alpha 2 (ATP1A2), another gene where HIF-1 and ZBTB2 are co-recruited to the gene locus, was found to be subjected to the same mode of regulation as EGFR-AS1. On the other hand, carbonic anhydrase 9 (CA9), a known HIF-1 target gene that does not have ZBTB2 recruitment, was not

upregulated by ZBTB2. Finally, there was an attempt to identify ZBTB2's consensus binding motif using various wet-lab experimental and *in silico* methods, but a clear motif could not be identified. Together, the results in this thesis demonstrate that, under hypoxic conditions, ZBTB2 is a coactivator of HIF-1 that is recruited to the vicinity of the HREs in a subset of HIF-1 target genes to enable their full expression. These findings shed further light onto the molecular mechanisms behind HIF-1's role as a master regulator of the cellular response to hypoxia.

List of Abbreviations

ANOVA	Analysis of variance
AP-1	Activator protein 1
ARNT	Aryl hydrocarbon receptor nuclear translocator
ATF	Activating transcription factor
ATP1A2	ATPase Na+/K+ Transporting Subunit Alpha 2
bHLH	Basic helix-loop-helix
BNIP3	BCL2/adenovirus E1B 19 kDa protein-interacting protein 3
BTB	Broad-Complex, Tramtrack, and Bric-a-brac
BWA	Burrows-Wheeler Aligner
bZIP	Basic leucine zipper
C2H2	Cys2His2
CA9	Carbonic anhydrase 9
CBP	CREB-binding protein
cDNA	Copy DNA
CDS	Coding sequence
ChIP	Chromatin immunoprecipitation
ChIP-Seq	ChIP Sequencing
CIAP	Calf intestine alkaline phosphatase
CMV	Human cytomegalovirus
CMVmp	Human cytomegalovirus minimal promoter
CREB	ATF/cAMP responsive element binding protein
CRISPR	Clustered regularly interspaced short palindromic repeats
DAVID	Database for Annotation, Visualization and Integrated Discovery
dCas9	Catalytically inactive Cas9
DMEM	Dulbecco's Modified Eagle Medium
DNA	Deoxyribonucleic acid
DNase	Deoxyribonuclease
EDTA	Ethylenediaminetetraacetic acid
EGFP	Enhanced green fluorescent protein
EGFR-AS1	EGFR Antisense RNA 1
EPAS1	Endothelial PAS Domain Protein 1
EPO	Erythropoietin
FBS	Fetal bovine serum
FIH-1	Factor-inhibiting HIF-1
GEO	Gene Expression Omnibus
GO	Gene ontology
H3K27ac	Histone 3 lysine residue 27 acetylation
HCl	Hydrochloric acid
hEF-1α	Human elongation factor 1α-subunit
HEPES	4-(2-hydroxyethyl)-1-piperazineethanesulfonic acid
HIF	Hypoxia inducible factor
HNF-4	Hepatocyte nuclear factor 4
HRE	Hypoxia response element
KEGG	Kyoto Encyclopedia of Genes and Genomes
MMP	Matrix metalloproteinase
NaCl	Sodium chloride
NGS	Next-generation sequencing

ODD   Oxygen-dependent degradation
p53   Tumor protein p53
PAS   Per-Arnt-Sim
PBS   Phosphate buffered saline
PCR   Polymerase chain reaction
PHD   Prolyl-4-hydroxylases
PMSF   Phenylmethylsulfonyl fluoride
POZ   Poxvirus and zinc finger
PS   Penicillin-streptomycin mixed solution
PVDF   Polyvinylidene fluoride
qRT-PCR   Quantitative Real-Time PCR
RIPA buffer Radioimmunoprecipitation assay buffer
RNA   Ribonucleic acid
RNAPII   RNA polymerase II
RNase   Ribonucleic acid
RPM   Rotations per minute
SDS   Sodium dodecyl sulfate
SELEX   Systematic evolution of ligands by exponential enrichment
sgRNA   Single guide RNA
siRNA   Small interfering RNA
STAT3   Signal transducer and activator of transcription-3
SV40   Simian vacuolating virus 40
T3   Bacteriophage T3
T7   Bacteriophage T7
TAD   Transactivation domain
TBS-T   Tris-buffered saline with Tween
TE   Tris-EDTA
TF   Transcription factor
Tris   Tris(hydroxymethyl)aminomethane
UCSC   University of California, Santa Cruz
VHL   von Hippel-Lindau
ZBTB2   Zinc finger and BTB-domain containing 2
ZF   Zinc finger

Chapter 1

Introduction

1.1   Hypoxia and HIFs

Hypoxic, or low-oxygen, conditions arise in both physiologic and pathophysiologic contexts and can play roles in a variety of processes including embryonic development, heart disease, and cancer progression (1). In cancers, abnormal metabolism and uncontrolled cell proliferation cause tumors to outgrow the surrounding oxygen supply and results in an oxygen gradient within the tumor microenvironment. While cells in the proximity of blood vessels are able to obtain sufficient oxygen and nutrients and remain under normoxic (normal oxygen) conditions, cells further away experience hypoxic conditions and undergo changes that cause an increase in malignant characteristics including invasiveness and radioresistance (Figure 1.1) (2, 3).

The cellular response to hypoxic conditions is controlled largely by the transcription factors in the hypoxia inducible factor (HIF) family. Members of this family include HIF-1α, HIF-2α, HIF-3α, and HIF-1β (Figure 1.2) (4). Among these, HIF-1α is the most well-studied, and is considered to be the master regulator of the hypoxia response. There are several crucial domains in HIF-1α: the basic helix-loop-helix (bHLH) motif domain and Per-Arnt-Sim (PAS) domains participate in DNA binding and protein dimerization, the oxygen-dependent degradation (ODD) domain causes HIF-1α to be degraded in response to increases in oxygen concentration, and finally the two transactivation domains (TAD) serve as scaffolds for transcription co-regulators such as prolyl-4-hyrdoxylases (PHDs) and factor inhibiting HIF-1 (FIH-1) (5, 6). HIF-2α, also known as Endothelial PAS Domain Protein 1 (EPAS1), contains the same key domains as HIF-1α and shares high structural similarity (7). HIF-3α undergoes extensive alternative splicing, and most of its isoforms lack the C-terminal TAD (C-TAD) found in HIF-1α and HIF-2α (8). The final member of the HIF family is HIF-1β, or aryl hydrocarbon receptor nuclear translocator (ARNT), and it is unique among the HIFs in that it does not contain the ODD domain common to the alpha subunits (5). Each of the HIF-α

subunits binds with HIF-1β to form heterodimers which can activate transcription of downstream genes. Studies have suggested that HIF-1 (the heterodimer consisting of HIF-1α and HIF-1β) drives the initial response to acute hypoxia, while HIF-2 (consisting of HIF-2α and HIF-1β) regulates the chronic response (9). Research on HIF-3 (HIF-3α and HIF-1β) is scarce in comparison to the other HIFs, but there is evidence showing HIF-3α can negatively affect HIF-1 and HIF-2-dependent gene expression by binding competitively with HIF-1β (10, 11).

The ability of HIF heterodimers to promote transcription of genes in response to low oxygen concentrations is regulated through post-translational modifications on the HIF-α subunits modulated by prolyl-4-hydroxylases (PHDs) and factor-inhibiting HIF-1 (FIH-1) (6). These enzymes function by hydroxylating key residues by using oxygen as a substrate, and they also require Fe^{2+}, α-ketoglutarate, and ascorbate as co-factors. PHDs regulate HIF-α subunit stability: for instance, they hydroxylate HIF-1α at two proline residues, P402 and P564, located in the ODD domain, which causes HIF-1α to be recognized and ubiquitylated by von Hippel-Lindau tumor suppressor (VHL)-containing E3 ligase and ultimately proteolyzed by the 26S proteasome (Figure 1.3) (6, 12). On the other hand, FIH-1 affects HIF transactivation activity: FIH-1 hydroxylates N803 located in the C-terminal TAD of HIF-1α, thereby preventing association with the p300/CREB-binding protein (CBP) coactivator protein complex (13–17). In this fashion, HIF-α subunits are inactivate and degraded in the presence of oxygen. However, once under hypoxia, PHDs and FIH-1 can no longer function. This means that HIF-α subunits are no longer degraded and are able to associate with p300/CBP, and this allows them to form a heterodimer with HIF-1β, which is constitutively expressed and stable due to the lack of ODD domain (17). The completed HIF heterodimer can then enter the nucleus and bind to DNA containing hypoxia-response element (HRE) sequences (5'-RCGTG-3') to promote transcription of genes required for the hypoxic response (6, 17, 18).
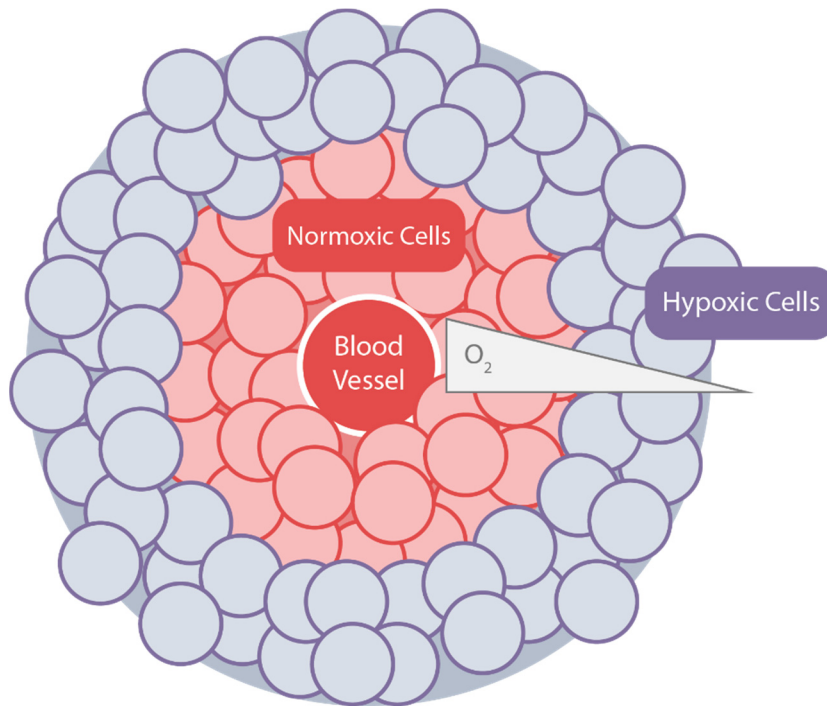
Figure 1.1 A schematic diagram showing tumor cells around a blood vessel. The region proximal to the blood vessel is well-oxygenated, and cells are under normoxic conditions. Oxygen levels decrease as distance from the blood vessel increases, causing the cells on the periphery to experience hypoxic conditions.
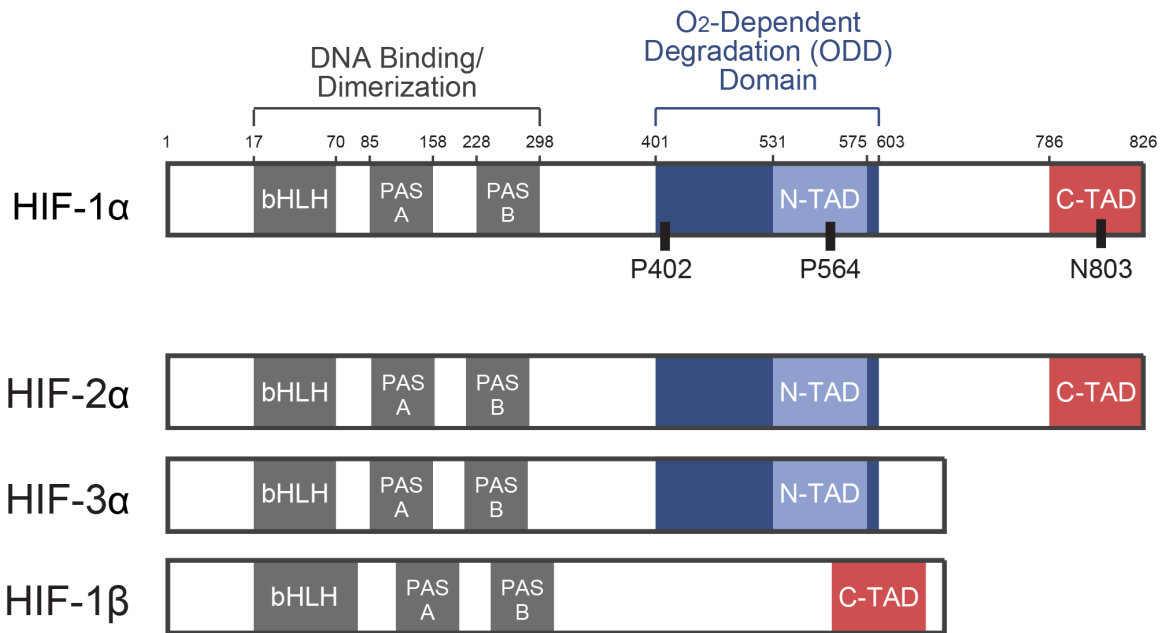
Figure 1.2 A schematic diagram showing the domains in the members of the hypoxia inducible factor (HIF) family. Key residues in HIF-1α, the master regulator of the cellular response to hypoxia, are shown.
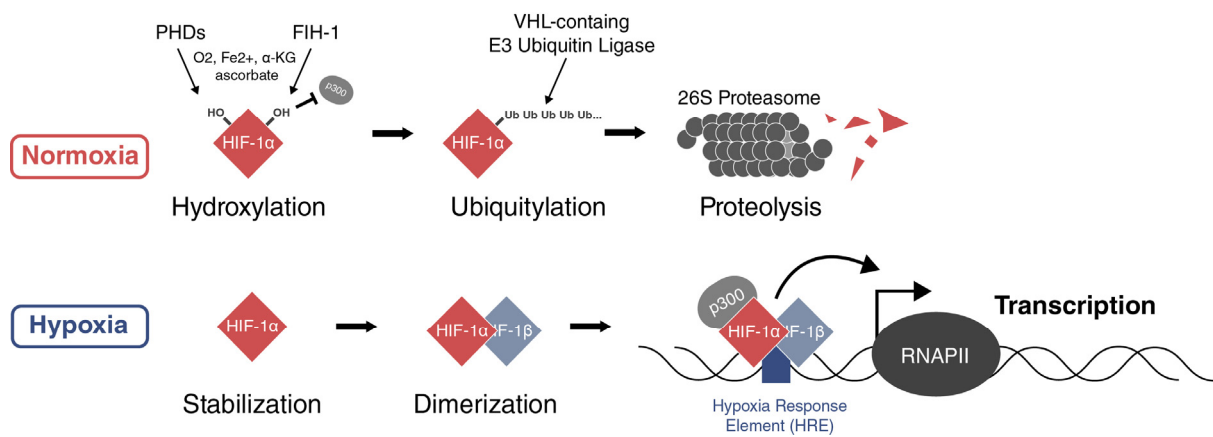
Figure 1.3 HIF-1 protein stability and transcriptional activity are regulated by oxygen concentration. Under normoxic conditions, HIF-1α is hydroxylated by oxygen-dependent PHDs and FIH-1. These modification either tag HIF-1α for proteasomal degradation or inhibit its interaction with transcriptional activator p300. Under hypoxia, PHDs and FIH-1 cannot function, and HIF-1α can form a heterodimer with HIF-1β and activate the expression of downstream genes.

1.2   HIFs require additional factors to promote transcription

The basic pathway of HIF-1-dependent gene regulation described above is well-studied; however, the mechanisms behind it are highly complex and much remains to be characterized. One major remaining question is what determines which genes are modulated by HIF-1 in response to hypoxia. For instance, while the HRE sequence is abundant across the human genome, HIF-1 is actually only recruited to a small percentage of them (19). In addition, many HIF-1 targets are expressed in a cell type-dependent manner (20, 21): Benita *et al* performed a study to identify HIF-1 target genes that form the core response to hypoxia by comparing gene expression in 6 different cell types, and found that only 81 out of 200 of the top predicted HIF-1 targets responded to hypoxia in three or more cell types (21). Therefore, it is reasonable to expect that additional elements participate in determining which HIF-1 target genes are fully expressed under hypoxic conditions.

Various transcription factors and proteins have been reported to influence HIF-1-dependent gene regulation. For example, HIF-1-dependent upregulation of erythropoietin (EPO), a protein hormone expressed in the kidney and liver and a key player in erythropoiesis, requires interaction of HNF-4 (hepatocyte nuclear factor 4) with the HIF-1α PAS domain (22). Additionally, signal transducer and activator of transcription-3 (STAT3), a transcription factor that mediates the inflammatory response, has been shown in certain cell types to interact with HIF-1 and bind to HIF-1 target gene promoters to enhance recruitment of p300/CBP and RNA polymerase II (RNAPII) (23). Given the evidence that coactivating proteins can heavily influence HIF-1-dependent gene regulation, it is of high interest to identify new coactivators and characterize their mechanisms in order to better understand the cellular response to hypoxia.

1.3 Zinc finger transcription factors and ZBTB2

One factor that has drawn attention as a modulator of HIF-1α-dependent gene regulation is the protein zinc finger and BTB-domain containing 2 (ZBTB2) (Figure 1.4). As its name suggests, ZBTB2 contains a BTB (Broad-Complex, Tramtrack, and Bric-a-brac)/POZ (poxvirus and zinc finger) domain and four zinc finger motifs (ZF1-4), and it has been reported to play roles in both transcriptional activation and repression through a diverse range of mechanisms (24–27). Our lab has previously established that ZBTB2 can act as a coactivator for HIF-1α: in HCT116 cells lacking tumor suppressor protein p53 (p53), ZBTB2 increases HIF-1's transactivation activity, leading to the expression of downstream genes that increase invasive properties such as matrix metalloproteinase 2 (MMP2) and MMP9 (24). However, this effect is abrogated by the presence of p53. Our previous study has also shown that deletion of either the N-terminus region (residues 1-23), the BTB/POZ domain, ZF2, or ZF3 abrogates ZBTB2's ability to increase HIF-1 transactivation activity, signifying that these are domains important for ZBTB2's function as a coactivator.

BTB/POZ domains are often found at the N-termini of zinc finger proteins that are known to function as scaffolds for protein-protein interactions (28). In the case of many zinc finger proteins including ZBTB2, this domain is crucial for homodimerization and proper functioning of the protein. We have found in our previous study that substitution of four key residues in the amino acids in positions 1-23 or deletion of the BTB/POZ domain results in loss of ZBTB2 homodimerization (24).

The zinc fingers found in ZBTB2 are of the Cys2His2 (C2H2) subtype. As the name implies, C2H2 zinc fingers are DNA-binding motifs that typically consist of cysteine and histidine amino acids, with other amino acid residues interspersed in between. Canonically, each zinc finger has a β-sheet-β-sheet-α-helix structure, with the α-helix making contact with DNA bases

at 4 positions. Interactions at these 4 positions largely determine binding specificity (29, 30) (Figure 1.5). Zinc finger transcription factors often contain several zinc finger motifs in tandem, allowing them to recognize and interact with longer DNA sequences. As the results from our previous publication showed that some of the zinc finger domains in ZBTB2 are required for its ability to induce HIF-1 transactivation activity (24), it is likely that DNA binding is important in the process, and therefore it is of interest to see if ZBTB2 has a consensus binding motif. However, ZBTB2's binding sequence has not yet been successfully identified.
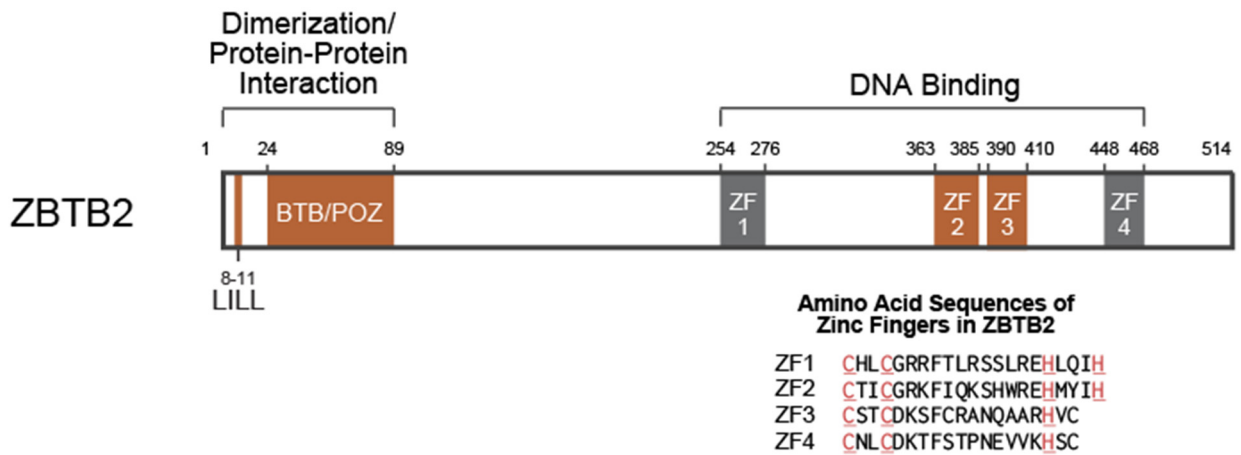
Figure 1.4 A schematic diagram showing the key domains of ZBTB2. Domains that were previously found to be required for ZBTB2 to function as a HIF-1 coactivator are highlighted in orange.
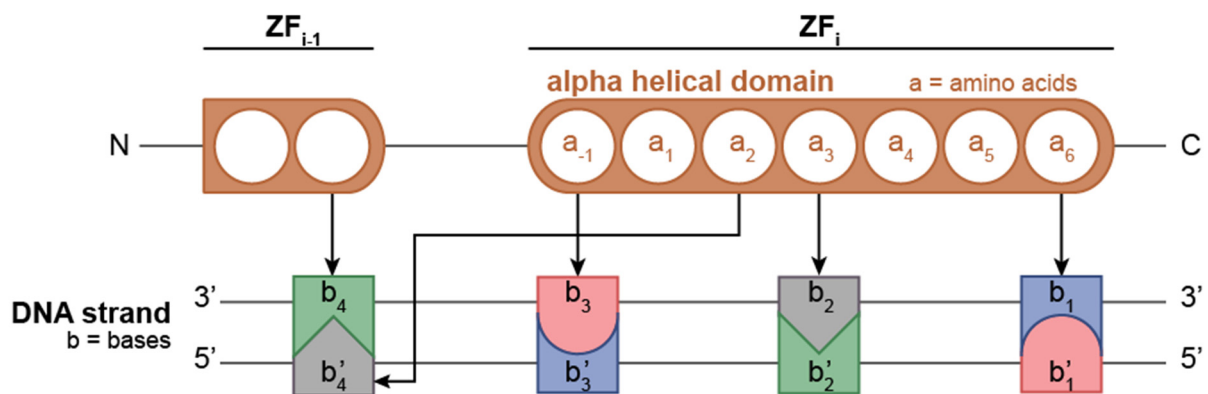
Figure 1.5 A schematic diagram showing how C2H2 zinc finger proteins interact with DNA. Two successive zinc fingers (ZF$_{i-1}$ and ZF$_i$) are shown. Amino acids inside the α-helical domain are represented by a$_n$, with a$_{-1}$ representing the amino acid right before the helix. Bases on the primary DNA strand are labeled b$_1$-b$_4$, and the bases on the complementary strand are labeled b$_1$'-b$_4$'. Arrows represent the canonical contacts between the ZFs and DNA. Figure adapted from publications by Persikov *et al* (29, 30).

1.4   Project Aims and Summary

The aim of this project is to further characterize how ZBTB2 can influence the regulation of HIF-1 target genes, and to ultimately shed more light on the mechanisms behind the cellular response to hypoxia. Based on our previous findings and the existing reports on how transcription factors can modulate expression of HIF-1 target genes, I hypothesize that ZBTB2 can act as a coactivator for a subset of HIF-1 genes to enable their full expression under hypoxia.

Chapter 3 describes the work I performed to examine the interplay between ZBTB2 and HIF-1 and to investigate mechanistically how the two factors can co-regulate gene expression under hypoxia. ZBTB2 is demonstrated to be a novel factor that is required for the expression of a subset of HIF-1 target genes. ZBTB2 and HIF-1 are shown to be co-recruited to certain genes, and a detailed examination of the regulatory mechanism of one of these genes, the long non-coding RNA EGFR Antisense RNA 1 (EGFR-AS1), shows that it is upregulated under hypoxic conditions in a HIF-1, ZBTB2-, and p300-dependent manner. Additionally, ZBTB2 is shown to be recruited to the vicinity of the HRE located in the intron of EGFR-AS1 only if HIF-1 is present, and mutation of the HRE is shown to abolish the effects of ZBTB2 on the expression of the gene. It is also demonstrated that p300 activity is required for hypoxia-dependent induction of EGFR-AS1 expression, and that ZBTB2 overexpression is able to increase histone 3 lysine residue 27 acetylation (H3K27ac) at the intron HRE region. Finally, it is shown that the expression of another HIF-1-ZBTB2 candidate target gene, ATPase Na^+/K^+ transporting subunit alpha 2 (ATP1A2), is regulated through similar mechanisms. On the other hand, ZBTB2 did not upregulate the expression of carbonic anhydrase 9 (CA9) or BCL2/adenovirus (BNIP3), two HIF-1 target genes that do not have ZBTB2 recruitment. Together, the results in this chapter demonstrate that ZBTB2 is recruited a subset of HIF-1 target genes in a HIF-1-dependent manner, which leads to increased histone acetylation and increased gene expression.

In **Chapter 4**, I attempt to identify ZBTB2's consensus binding motif through both experimental and *in silico* methods. As it has been previously established that some of the zinc finger domains in ZBTB2 are important for its ability to co-regulate HIF-1 target genes, identifying ZBTB2's binding motif may allow for further identification of potential targets. Further analysis of the ZBTB2-myc ChIP-Seq data obtained through the present study shows that certain binding motifs are enriched in the vicinity of ZBTB2 peaks. Systematic Evolution of Ligands by EXponential enrichment (SELEX) was used as another approach to identify potential ZBTB2 binding motifs *in vitro*. Furthermore, online tools were employed to predict ZBTB2 binding motifs, and a literature search was performed to find previously reported ZBTB2 binding motifs. Finally, I attempt to locate the putative motifs in the ZBTB2 target genes we identified to assess their utility in predicting ZBTB2 targets.

Chapter 2

Materials and Methods

2.1 Plasmids

2.1.1 pEF6B/ZBTB2-myc His, pEF6B/ZBTB2 4A-myc His, pEF6B/ZBTB2 ΔZF3-myc His
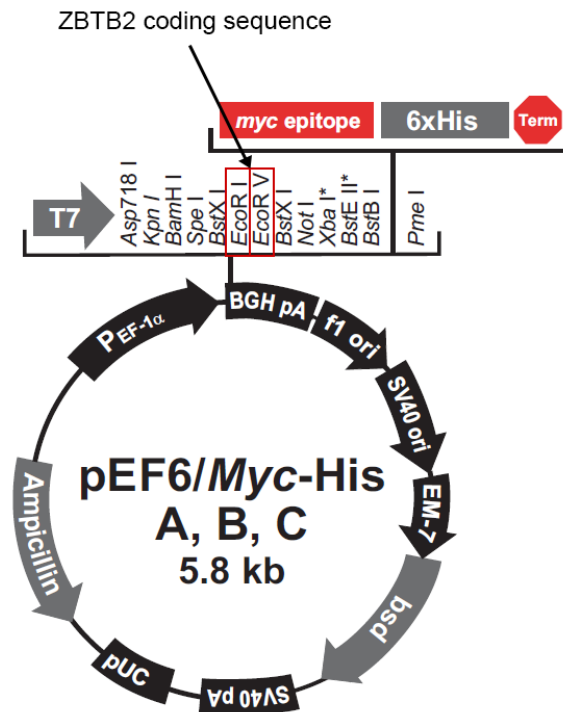
Figure 2.1 The plasmid map of the pEF6/myc-His vector. Plasmid map from Thermo Fisher Scientific.

The DNA fragment encoding ZBTB2 coding sequence (CDS) was amplified from the cDNA of HeLa, a cervical cancer cell line, by PCR using 5'-AAGAATTCACCATGGATTTGGCCAACCATGG-3' as the forward primer and 5'-AAGATATCGTCTAGTAAGACGGTTTCTTG-3' as the reverse primer. The fragment was inserted into the pEF6/myc-His B plasmid (Thermo Fisher Scientific) using the EcoRI and EcoRV sites in order to create a vector that overexpresses myc- and His-tagged ZBTB2 from a constitutively active human elongation factor 1α-subunit (hEF-1α) promoter.

Overexpression vectors for mutants ZBTB2 4A and ZBTB2 ΔZF3 were generated by site-directed mutagenesis or deletion respectively. The forward primer used for making ZBTB2 4A

19

was 5'- TGGAGCCGCAGCTGCCCAACAGTTAAACGC-3' and the reverse primer was 5'-TGGGCAGCTGCGGCTCCATGGTTGGCC-3'. The forward primer used for making ZBTB2 ΔZF3 was 5'-CCGGGAAGCCTCTCAACCAGAGCATCGAC-3' and the reverse primer was 5'-CTCTGGTTGAGAGGCTTCCCGGTGTGTAT-3'. The resulting fragments were cloned into the EcoRI and EcoRV sites of pEF6/myc-His.

2.1.2 pcDNA4A/EGFP-myc His
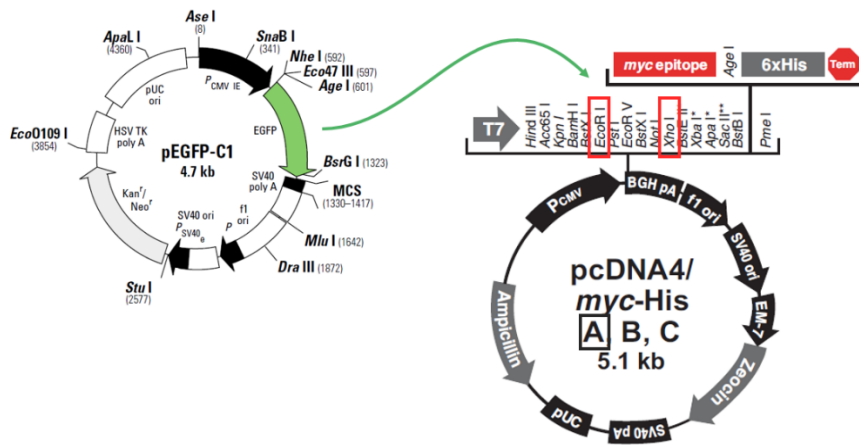
Figure 2.2 The EGFP coding sequence from the pEGFP-C1 vector was inserted into the pcDNA4/myc-His A vector. pEGFP-C1 plasmid map from Takara. pcDNA4/myc-His plasmid map from Thermo Fischer Scientific.

The DNA fragment encoding the EGFP CDS was amplified from the pEGFP-C1 vector (Takara Bio/Clontech) by PCR using 5'-ATGAATTCGCTAGCGCTACCGGTCGCCACC-3' as the forward primer and 5'-ATACTCGAGCTTGTACAGCTCGTCCATCCC-3' as the reverse primer. The DNA fragment was inserted into the pcDNA4/myc-His A (Thermo Fisher Scientific) vector using the EcoRI and XhoI restriction enzyme cut sites. This vector overexpresses myc- and His-tagged EGFP from a constitutively active human cytomegalovirus (CMV) promoter. This vector was used to visually check transfection efficiency and was used as a negative control for immunoprecipitation experiments using myc tag antibodies.

Figure 2.3 The plasmid map of the pcDNA6/V5-His vector. Plasmid map from Thermo Fisher Scientific.

The DNA fragment encoding ZBTB2 CDS was taken from the pEF6B/ZBTB2-myc His plasmid (24) and was inserted between the EcoRI and EcoRV cut sites in the pcDNA6/V5-His B plasmid. This construct is used to express V5- and His-tagged ZBTB2 from a CMV promoter.

2.1.4 lentiCRISPRv2/EGFR-AS1 Intron HRE
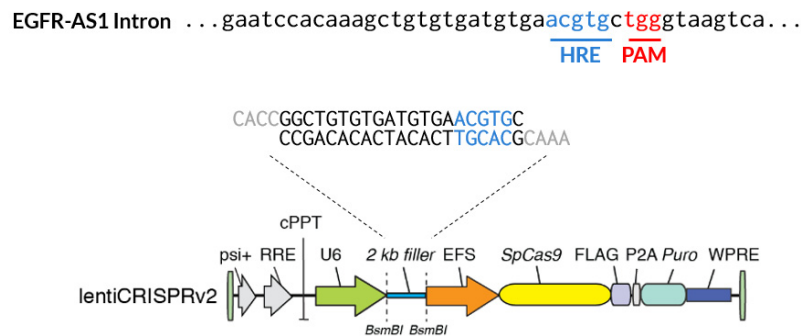
Figure 2.4 sgRNA targeting the HRE in the EGFR-AS1 intron was inserted into the lentiCRISPRv2 vector. Plasmid map from GeCKO.

The lentiCRISPRv2 vector (GeCKO) is a one-vector lentiviral system for genome editing. It contains expression cassettes for hSpCas9 and a guide RNA. The vector was cut with BsmBI, and a single guide RNA (sgRNA) scaffold containing the indicated guide sequence targeting the EGFR-AS1 intron HRE was inserted. The guide RNA sequence was designed using CRISPRdirect (https://crispr.dbcls.jp/) (31). Additionally, the vector contains a puromycin resistance gene to allow for the selection of cells infected with the lentivirus. This vector was used to generate cells containing mutations and/or deletions of the HRE in the EGFR-AS1 intron.

2.1.5   pX330-U6-Chimeric_BB-CBh-hSpCas9 vector
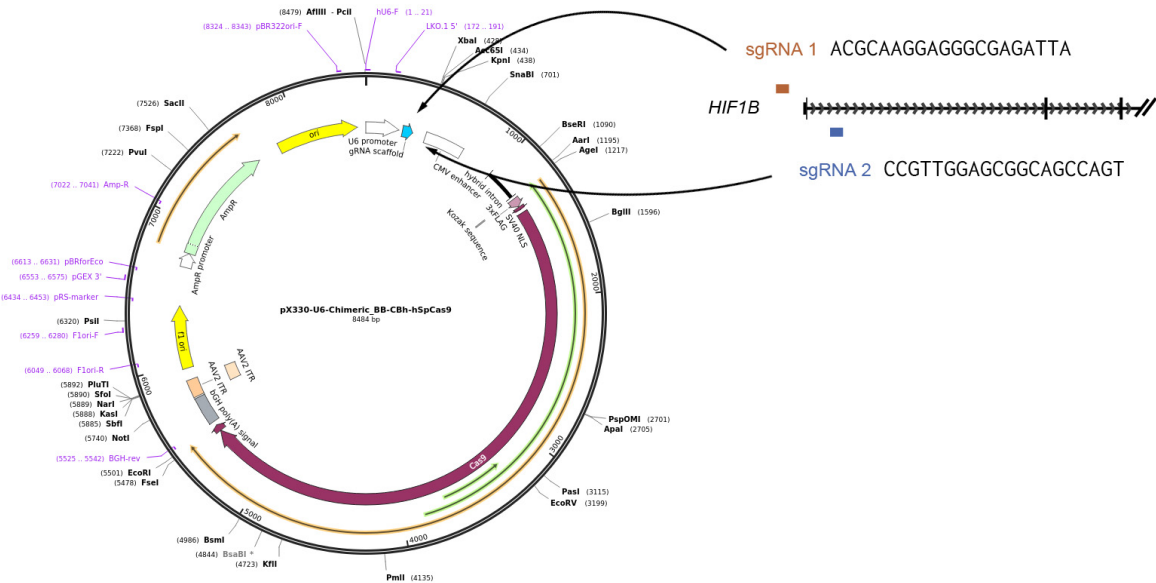
Figure 2.5 sgRNAs targeting HIF1B were inserted into the pX330 vector. Plasmid map from Addgene.

This vector allows for co-expression of hSpCas9 and a guide RNA, and was used for the generation of HIF-1β knockout HeLa cells. Guide RNA sequences targeting intron 1 or upstream of exon 1 were designed by CRIPSRdirect, and cloned into the BbsI site of pX330-U6-Chimeric_BB-CBh-hSpCas9 (pX330) (Addgene). Expression of these 2 guide RNAs will facilitate the deletion of exon 1 of HIF-1β.
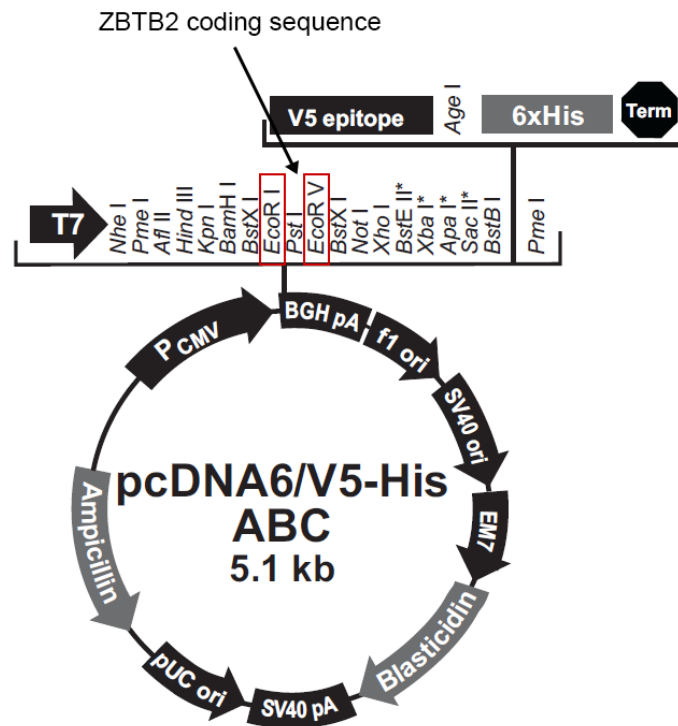
2.1.6   pcDNA4A/HIF-1β myc His
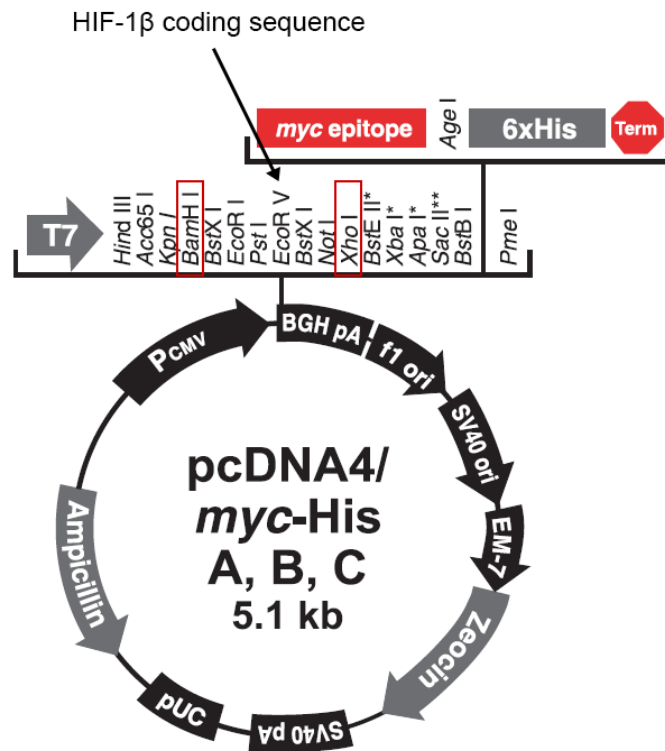
Figure 2.6 The plasmid map of the pcDNA4/myc-His vector. Plasmid map from Thermo Fisher Scientific.

The DNA fragment encoding the CDS of HIF-1β was amplified from HeLa cDNA using the forward primer 5'- ATAGGATCCGCCGCCATGGCGGCGACTAC'-3' and the reverse primer 5'- ATACTCGAGTTCTGAAAAGGGGGGAAAC-3'. It was inserted into the multiple cloning site of pcDNA4/myc-His A (Thermo Fisher Scientific) using the BamHI and XhoI sites. This vector expresses myc- and His-tagged HIF-1β from a CMV promoter, and was used to overexpress HIF-1β in rescue experiments using HIF-1β knockout cells.

2.1.7   pGL3-CMVmp
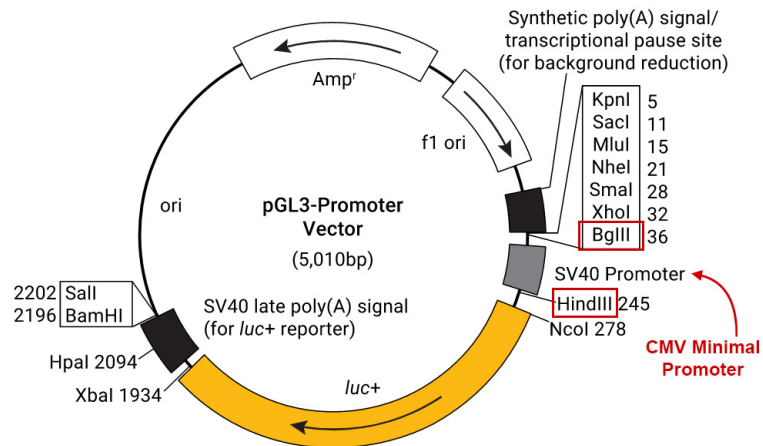
Figure 2.7 The plasmid map of the pGL3 Vector. The SV40 promoter was replaced with the CMV minimal promoter to yield pGL3-CMVmp. The EGFR-AS1 intron was inserted in the middle of the *Firefly* luciferase coding sequence to yield pGL3-CMVmp/EGFR-AS1 Intron. Plasmid map from Promega.

This vector codes for the *Firefly* luciferase used in luciferase reporter assays. The pGL3-CMVmp vector was created by inserting the human cytomegalovirus minimal promoter (CMVmp) between the BglII and HindIII sites in the pGL3 promoter vector (Promega).

2.1.8 pGL3-CMVmp/EGFR-AS1 Intron
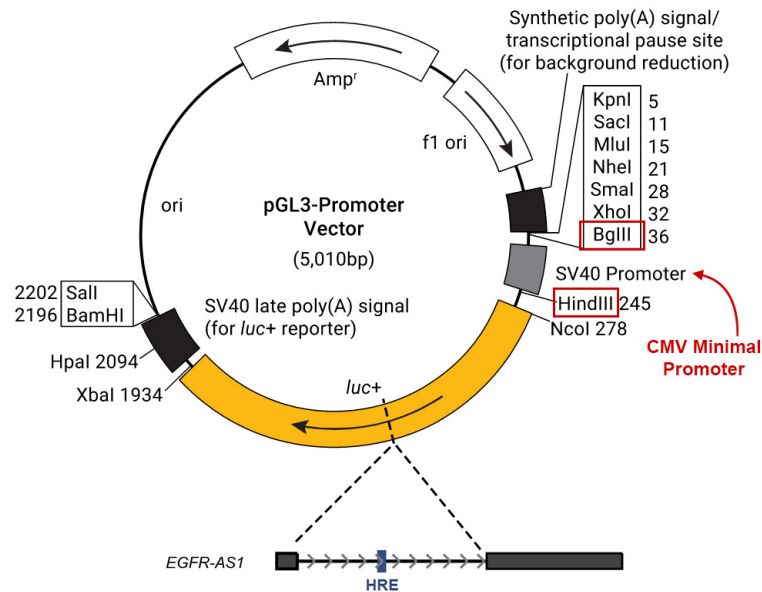
Figure 2.8 The EGFR-AS1 intron was inserted into the middle of the *Firefly* luciferase coding sequence in the pGL3-CMVmp vector. Plasmid map from Promega.

pGL3-CMVmp/EGFR-AS1 Intron, a version of the pGL3-CMVmp vector with the EGFR-AS1 intron inserted inside the *Firefly* luciferase coding sequence after nucleotide 828, was generated by PCR. First, full-length EGFR-AS1 containing the intron was amplified from HeLa cDNA using the forward primer 5'-ATAAAGCTTGTCTGTTTCCTCAGAACACC'-3' and the reverse primer 5'- ATACTCGAGTTGCATCGGTACTGAACATATAC-3'. To insert the intron into the luciferase coding sequence, several PCR reactions were performed. The following primers were used.
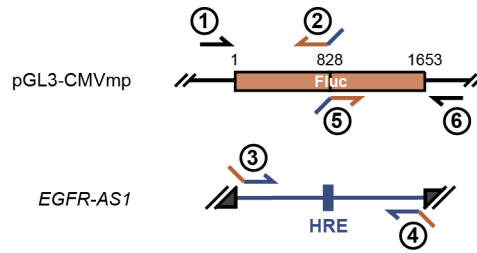
Figure 2.9 A schematic diagram showing the positions of the primers used to generate pGL3-CMVmp/EGFR-AS1 Intron.

#	Primer	Sequence (5' -> 3')
1	pGL3/CMVmp Luciferase XhoI Forward	gggctcgagatctGGTAGGC
2	Luciferase (N) – EGFR-AS1 Reverse	ccctccaactgattacCTCAGAAACAGCTCTT
3	Luciferase (N) – EGFR-AS1 Forward	AAGAGCTGTTTCTGAGgtaatcagttggaggg
4	EGFR-AS1 – Luciferase (C) Reverse	GTAATCCTGAAGGCTCctacaagaagacaaac
5	EGFR-AS1 – Luciferase (C) Reverse	gtttgtcttcttgtagGAGCCTTCAGGATTAC
6	pGL3/CMVmp Luciferase XbaI Reverse	cgacTCTAGATTACACGGCG

The PCR reactions to obtain the desired construct were set up as detailed below:

PCR	Primers	Template	Product
A	1, 2	pGL3/CMVmp	N-terminal luciferase fragment
B	3, 4	EGFR-AS1 fragment	EGFR-AS1 intron
C	5, 6	pGL3/CMVmp	C-terminal luciferase fragment
D	1, 4	Annealed products of PCR A and B	N-terminal luciferase fragment + EGFR-AS1 intron
E	1, 6	Annealed products of PCR C and D	N-terminal luciferase fragment + EGFR-AS1 intron + C-terminal luciferase fragment

PCR reactions A-C will yield fragments for the N-terminal luciferase fragment, the intron, and the C-terminal luciferase fragment respectively. These fragments will have overhangs from the primers that allow them to anneal with other fragments. The final fragment was inserted between the XhoI and XbaI sites in pGL3-CMVmp.*2.1.9   pGL3-CMVmp/EGFR-AS1 Intron HRE mut and pGL3-CMVmp/EGFR-AS1 Intron ChIP motif mut*
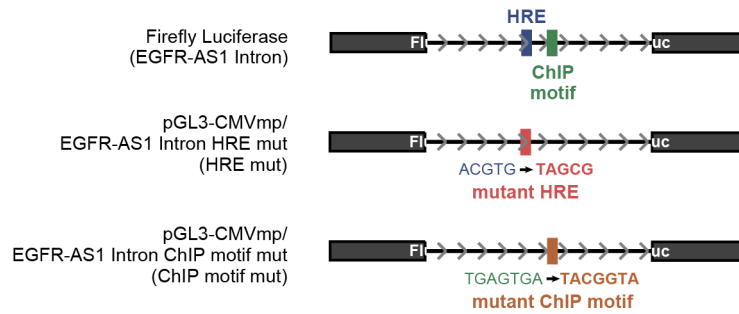
Figure 2.10 A schematic diagram showing the mutation introduced into pGL3-CMVmp/EGFR-AS1 Intron in order to create pGL3-CMVmp/EGFR-AS1 Intron HRE mut and pGL3-CMVmp/EGFR-AS1 Intron ChIP motif mut.

pGL3-CMVmp/EGFR-AS1 Intron HRE mut and pGL3-CMVmp/EGFR-AS1 Intron ChIP motif mut were generated by introducing mutations into pGL3-CMVmp/EGFR-AS1 Intron by PCR. First, a fragment containing the mutation was amplified from pGL3-CMVmp/EGFR-AS1 Intron using 5'-CTCACTATAGCTGCGCCTCC-3' as the forward primer and either 5'-CTTACCCAG**CGCTA**TCACATCACAC-3' (for HRE mut) or 5'-CCCAGGGTGG**TACCGTA**GCCCTGCAC-3' (for ChIP motif mut) as the reverse primer. The reverse primers contain a scrambled HRE or ChIP motif sequence (indicated in bold). A second PCR was performed using the PCR product from the first PCR as the forward primer and 5'-CGGGCATTGATATCTCAGCT-3' as the reverse primer to yield the insert fragment. The insert fragment and pGL3-CMVmp/EGFR-AS1 Intron vector were cut with SpeI and EcoRV. To prevent re-ligation, the vector was dephosphorylated with calf intestine alkaline phosphatase (CIAP) (Takara Bio, 2250). The insert fragment was phosphorylated with T4 polynucleotide kinase (Takara Bio, 2021). The insert fragment and vector were ligated together to yield pGL3-CMVmp/EGFR-AS1 Intron HRE mut or ChIP motif mut.

2.1.10 pRL/CMV (Promega)
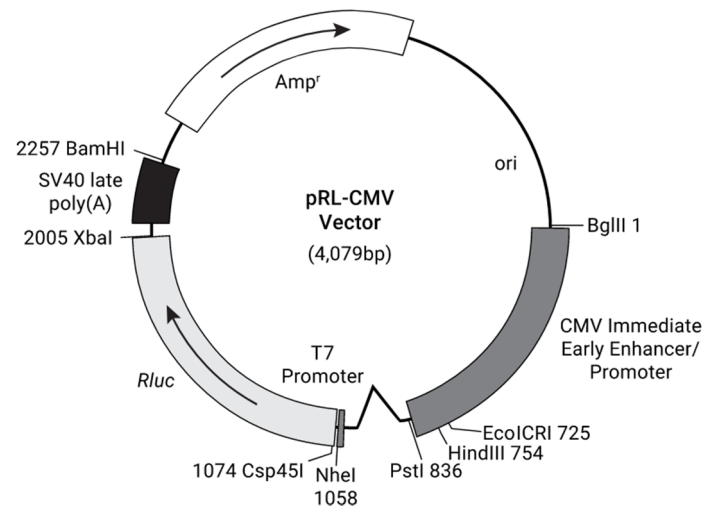
Figure 2.11 The plasmid map of the pRL-CMV vector. Plasmid map from Promega.

This is a vector used to express *Renilla* luciferase (Promega, E2261) and is used an internal control in luciferase report assays.

2.1.11 pcDNA-dCas9-p300 Core
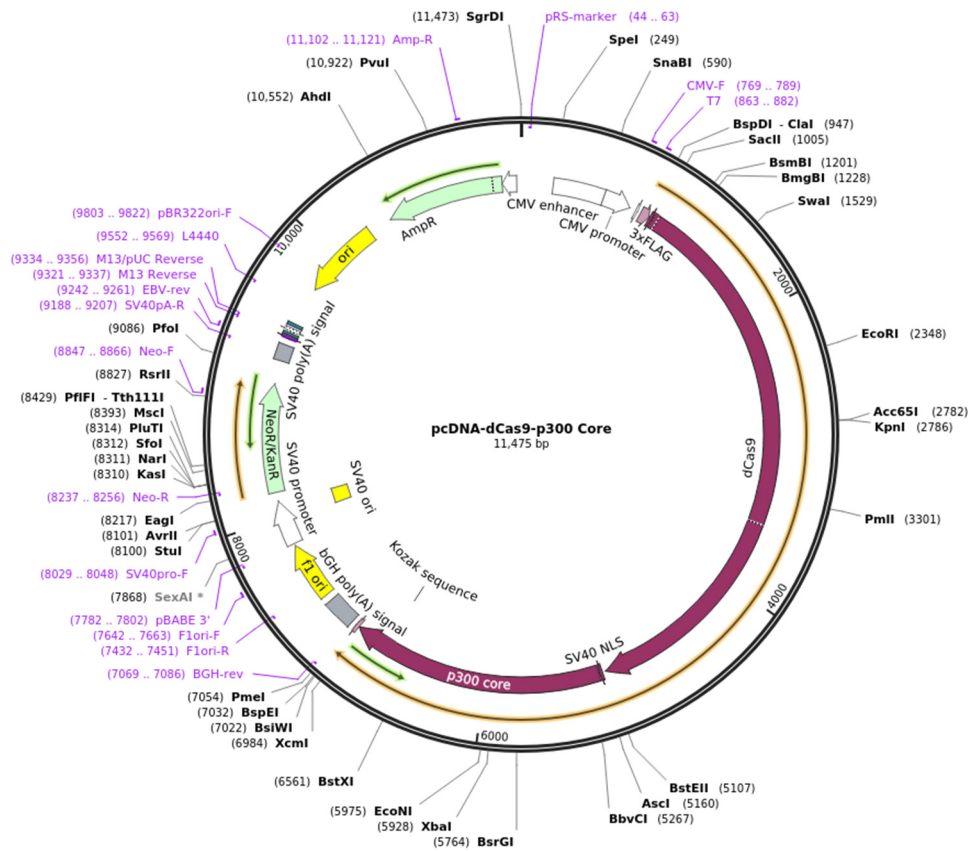
Figure 2.12 The plasmid map of the pcDNA-dCas9-p300 Core vector. Plasmid map from Addgene.

The vector was obtained from Addgene (Addgene #61357). This vector was used to express a fusion protein consisting of catalytically inactive Cas9 (dCas9) and the p300 Core histone acetyltransferase domain. Co-expression with a sgRNA targeting a specific sequence will cause dCas9-p300^{Core} to induce H3K27ac at a specific gene locus.

2.1.12 pX330-Cas9(-) and pX330-Cas9(-)/EGFR-AS1-Intron-HRE
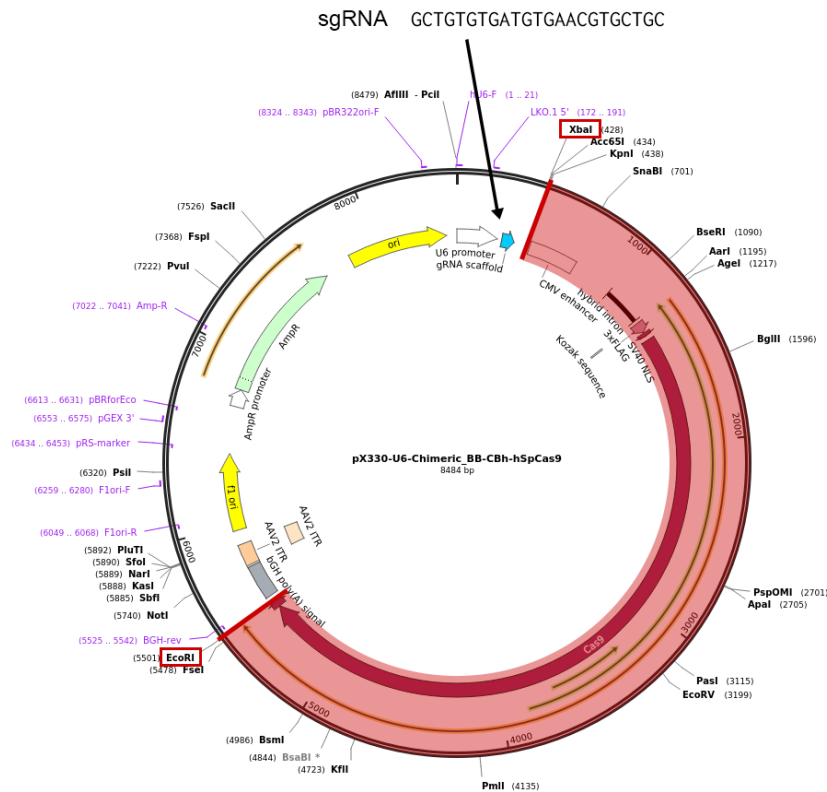
Figure 2.13 pX330-Cas9(-) was generated by removing the Cas9 coding sequence from pX330. pX300-Cas9(-)/EGFR-AS1 Intron HRE was created by inserting the sequence for a sgRNA to target the EGFR-AS1 intron HRE into the sgRNA scaffold. Plasmid map from Addgene.

In order to express sgRNA for use with the pCDNA-dCas9-p300 Core vector, a version of the pX330 vector lacking Cas9 was generated. The pX330 vector was cut with XbaI and EcoRI, and T4 Polymerase was used to create blunt ends. The plasmid was then recircularized by ligation. Afterwards, the same EGFR-AS1 intron HRE sgRNA used to generate lentiCRISPRv2/EGFR-AS1 Intron HRE was inserted into the gRNA scaffold in the vector using the BbsI cut site.
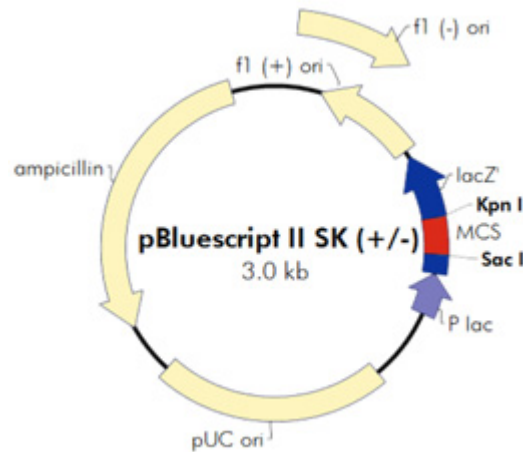
Figure 2.14 The plasmid map of the pBluescript II SK (+/-) vector. Plasmid map from Agilent.

The pBlueScript II SK (+) vector was used to facilitate sequencing of DNA fragments obtained from Systematic Evolution of Ligands by Exponential Enrichment (SELEX) and for genotyping clones obtained from CRISPR experiments. The vector features common sequencing primer sites, such as the T7 and T3 promoters, as well as a *lacZ* gene fragment that contains a multiple cloning site. Bacteria that take up pBlueScript II SK (+) with an intact *lacZ* gene will produce blue colonies when grown on a substrate containing Blue-Gal or another chromogenic β-galactosidase substrate in the presence of isopropyl β-D-1-thiogalactopyranoside. On the other hand, if a DNA fragment is cloned into the multiple cloning site, the *lacZ* gene is disrupted, and the colonies will remain white. Plasmids can be isolated from white colonies, and the insert can be sequenced.

2.2   Cell culture and reagents

A human cervical cancer cell line, HeLa, and a human embryonic kidney cell line that stably expresses the SV40 large T antigen and neomycin gene products, HEK293TN, were obtained from the American Type Culture Collection (Manassas, VA, USA). Cells were cultured in Dulbecco's Modified Eagle Medium (4.5 g/L-Glucose) with L-Gln and Sodium Pyruvate (DMEM) (Nacalai Tesque, 08458-16). Media was supplemented with 10% heat-inactivated fetal bovine serum (FBS) (EQUITECH-BIO, 268-1) and 1% penicillin-streptomycin mixed solution (PS) (Nacalai Tesque, 26253-84). Cells were maintained at 37°C in a 5% CO_2 incubator. For hypoxic treatment, cells were incubated in a RUSKINN INVIVO2 500 Hypoxic Work Station set at < 0.1% O_2, 5% CO_2, and 4% H_2, and 91% N_2 gas. p300 bromodomain inhibitor SGC-CBP30 was purchased from Sigma-Aldrich (SML1133).

2.3   Plasmid Transfection

Plasmids were transfected into cells using either PEI MAX (Polysciences, 24765) or PolyFect Transfection Reagent (Qiagen, 201105). For experiments performed in 6-well dishes, HeLa cells were seeded at a density of 1.5×10^5 cells per well, and allowed to adhere for a minimum of 4 hours. For experiments using PEI MAX, 1.5 µg of Plasmid DNA and 4.5 µL of PEI MAX were mixed in 100 µL serum- and antibiotic-free DMEM and incubated at room temperature for 10 minutes. After incubation, the entire volume was added to the well. For transfections using PolyFect, 1.5 µg of plasmid DNA and 12 µL of PolyFect Transfection Reagent were mixed in 98.5 µL serum- and antibiotic-free DMEM and incubated at room temperature for 10 minutes. 600 µL of DMEM containing 10% FBS and 1% PS was added, and the entire volume was added to the well. After transfection, cells were incubated in normoxic conditions

overnight before being transferred into the hypoxic chamber for 24 hours. Volumes were scaled accordingly for experiments performed using other cell culture vessels.

2.4   Small-interfering RNA (siRNA) Transfection

siRNA was transfected using Lipfectamine[TM] RNAiMAX Transfection Reagent (Thermo Fisher Scientific, 13778-030). For experiments performed in 6-well dishes, HeLa cells were seeded at a density of 1.5×10^5 cells per well, and allowed to adhere for a minimum of 4 hours. The media was then replaced with 1 mL antibiotic-free DMEM. The transfection mixture was prepared as follows: 2 µL of 50 nM siRNA was mixed with serum- and antibiotic-free DMEM. Separately, 2 µL of Lipofectamine[TM] RNAiMAX was mixed with 100 µL serum- and antibiotic-free DMEM. The two mixtures were combined and incubated at room temperature for 10 minutes. 200 µL of the combined mixture was added to one well. Volumes were scaled appropriately according to the type of culture dish. Commercial siRNA purchased from Invitrogen were used for the following targets: HIF-1α (HSS104775, HSS179231), HIF-1β (HSS100699, HSS100700), HIF-2α (HSS103261, HSS176568), ZBTB2 (HSS126563, HSS183975), and EP300 (HSS103258, HSS103259). Stealth™ RNAi Negative Control Medium GC Duplexes (Invitrogen, 452001) were used as negative controls.

2.5   Western Blotting

Cells were seeded into 6-well plates and subjected to the indicated treatments, and incubated under normoxia or hypoxia for 24 hours. Cells were washed with 1× PBS, and then 80 µL of RIPA buffer (50 mM Tris-HCl pH 8.0, 150 mM NaCl, 1% IGEPAL, 0.5% sodium deoxycholate, 0.1% SDS) supplemented with ProteoGuard EDTA-Free Protease Inhibitor Cocktail (Takara Bio, 35672) was added to each well. Cells were harvested by scraping.

Sonication of the cell lysates was performed with a Bioruptor UCW-210 (Cosmo Bio) (5 cycles, output power 5, 30 seconds on/off). Afterwards, lysates were centrifuged at 12,000 RPM for 10 min at 4ºC, and the supernatant was transferred to a clean tube. Protein concentration was quantified by DC Protein Assay (Bio-Rad, 5000116). 30-50 μg of protein were loaded into each lane of a 7.5% polyacrylamide gel, and electrophoresis was performed using a constant current of 40 mA for roughly 2 hours. Protein bands were transferred to a 0.45 μm PVDF membrane (Amersham Hybond) *via* semidry transfer and then blocked with 5% skim milk for 1 hour. The membrane was divided as needed and was then incubated with the desired primary antibody at a suitable concentration in 5% milk overnight at 4ºC. The following day, membranes were washed in 1× TBS-T (20 mM Tris-HCl pH 7.5, 500 mM NaCl, 0.1% Tween-20) (10 minutes × 3 times), and incubated with the appropriate secondary antibody in 1% skim milk at room temperature for at least 1 hour. Detection of bands was performed by using ECL Prime Western Blotting Detection Reagents (Cytiva, RPN2232) and Amersham Imager 680 (Amersham).

Antibodies:

Anti-human β-actin mouse monoclonal antibody (Santa Cruz, sc-69879)
Anti-human HIF-1α mouse monoclonal antibody (BD Biosciences, 610958)
Anti-human HIF-2α mouse monoclonal antibody (Santa Cruz, sc-13596)
Anti-human HIF-1β mouse monoclonal antibody (Novus, NB100-124)
Anti-human ZBTB2 rabbit polyclonal antibody (Abcam, ab117756)
Anti-myc tag mouse monoclonal antibody (Cell Signaling Technology, 2276)
Anti-mouse IgG HRP-linked whole antibody antibody (Cytiva, NA931)

2.6   CRISPR/Cas9-mediated knockout of HIF-1β

HeLa cells were seeded at a density of 5×10^4 cells per well in 6-well plates and allowed to adhere for at least 4 hours. The cells were then transfected with pX330 vectors coding for the sgRNAs targeting HIF-1β. The cells were allowed to proliferate for 48 hours, and afterwards they were reseeded at low density (30-200 cell/10 cm dish). Cells were allowed to grow until

colonies could be isolated with glass O-rings, and were subsequently moved to larger culture vessels for further propagation. HIF-1β knockout clones were screened by performing PCR using the forward primer 5'-CGGCAACCACTCAGACGAAT-3' and the reverse primer 5'-GGTTATGGTTCCGGACAGGT-3'.

2.7   Lentiviral Transfection

HEK293TN cells were seeded at a density of 3×10^6 cells per 10 cm dish in antibiotic-free DMEM with 10% FBS and allowed to adhere overnight. The following day, transfection mixtures were assembled with the following components:

Component	Amount per 10 cm dish
pPACK HI-GAG	1 μg
pPACK HI-REV	1 μg
pVSV-G	1 μg
lentiCRISPRv2 plasmid	3 μg
Polyfect	50 μL
Serum- and Antibiotic-Free DMEM	Up to 350 μL

The mixture was incubated at room temperature for 10 minutes, and afterwards 1 mL of antibiotic-free DMEM with 10% FBS was added. The entire volume was added to the 10 cm dish to transfect the cells. After 18 hours, the media was replaced with fresh DMEM containing 10% FBS and 1% penicillin-streptomycin solution. Following an additional 48 hours of incubation, the media was collected and passed through a 20 μm filter. The collected medium was diluted 1:2 with fresh DMEM containing 10% FBS and 1% penicillin-streptomycin solution. The cells to be transduced (HeLa cells seeded at 1.8×10^6 cells per 10 cm dish) were pretreated with media containing 8 μg/mL polybrene for 30 minutes. Afterwards, the lentiviral mixture was added to the cells and they were incubated for 48 hours. The cells were passaged, and then incubated in media containing 2.0 μg/mL puromycin for 7 days.

For experiments where stable clones were desired, cells were seeded at low density (30-200 cells per 10 cm dish) and maintained in media containing 0.2 μg/mL puromycin. Cells were allowed to proliferate until colonies could be isolated. Colonies were isolated using glass O-rings and moved to larger culture vessels for further propagation.

2.8 RNA Purification and Quantitative Real-Time PCR

Cells for RNA purification were harvested using Sepasol-RNA I Super G (Nacalai Tesque, 09379-84) and purified according to the manufacturer's instructions. The purified RNA was quantified using a NanoDrop 2000 (Thermo Fisher Scientific). RNA samples were treated with DNase I (Thermo Fisher Scientific, 1806815) according to the manufacturer's instructions. Quantitative Real-Time PCR (qRT-PCR) was performed using TB Green Premix Ex Taq II (Takara Bio, RR820) and a Thermal Cycler Dice Real Time System Single (Takara Bio, TP-850) according to the manufacturer's instructions. Primers used for each target are listed in the following table.

Target	Forward Primer (5'→3')	Reverse Primer (5'→3')
β-actin	TGGCACCCAGCACAATGAA	CTAAGTCATAGTCCGCCTAGAAG
RPS18	GCAGAATCCACGCCAGTACAAG	GCTTGTTGTCCAGACCATTGGC
HIF-1α	TCATCCAAGAAGCCCTAACGTG	TTTCGCTTTCTCTGAGCATTCTG
HIF-2a (EPAS1)	CACTGCAGACTTGTCCAGTGCTC	CACTGCTCGGATTGTCACACCTA
HIF-1β (ARNT)	CTACCCGCTCAGGCTTTC	CACCAAACTGGGAAGTACGAG
ZBTB2	AGCAGCTGCCAGTGATAATTTG	TTGCCAGTAAACTATCAGCATTGAC
EP300	CCTTTGTGTGTGTGTTCAAGTG	GAGGTGCAAGGCAGGAGCATA
EGFR-AS1	CATATTCTGGAATTCAGGTCAC	GTCCTCCTCATTGCTTGCAT
ATP1A2	CTCATGGCTGTAAGGTGGAT	CTTCAACACAGTTGGTGGAG
CA9	ACCAGACAGTGATGCTGAGTGCTAA	TCAGCTGTAGCCGAGAGTCACC
BNIP3	GGCCATCGGATTGGGGATCT	AACGAACCAAGTCAGACTCCAG

2.9 Chromatin Immunoprecipitation Sequencing (ChIP-Seq)

HeLa cells were seeded at a density of 2×10^6 cells per 10 cm dish, and transfected with either pEF6B/ZBTB2-myc His or pcDNA4A/EGFP-myc His (negative control). 3 biological

replicates were prepared, and two 10 cm dishes were used per replicate. The following day, cells were moved into the hypoxic chamber (< 0.1% O_2) for 24 hours. Cell samples for ChIP-Seq were prepared according to Active Motif's Epigenetic Services ChIP Cell Fixation protocol. Briefly, 1 mL Formaldehyde Solution (11% formaldehyde, 0.1 M NaCl, 1 mM EDTA pH 8.0, 50 mM HEPES pH 7.9) was added to 10 cm dish of cells containing 10 mL media, and the cells were incubated at room temperature for 15 minutes. The fixation reaction was quenched with 500 µL 2.5 M glycine solution in water and incubated at room temperature for 5 minutes. Cells were scraped into a 15 mL conical tube and kept on ice. Cells were then pelleted by centrifuging at 800 × g at 4°C for 10 minutes. The supernatant was removed and the pellet was resuspended in 10 mL PBS-Igepal (1× PBS pH 7.4, 0.5% Igepal). Cells were pelleted once again as before, and resuspended in 10 mL fresh PBS-Igepal. 100 µL PMSF (100 mM in ethanol) was added to each tube. Cells were then pelleted a third time, and the supernatant was completely removed. Cells were snap-frozen in liquid nitrogen and sent to Active Motif for sample processing and analysis. Analysis of next-generation sequencing (NGS) data was performed according to Active Motif's protocol. The BWA algorithm with default settings was used to map sequence reads (75-nt long) to the genome. Reads that did not pass Illumina's purity filter, had more than 2 mismatches, did not map uniquely to the genome, or were duplicated were removed. Coverage plots were generated by extending 5'-ends of the align reads (tags) at their 3'-end to 150-200 bp. The extended tags were divided into 32-nt bins and density was determined by the number of fragments in each bin. The UCSC genome browser (http://genome.ucsc.edu) (32) was used to visualize coverage plots. HOMER (http://homer.ucsd.edu/homer/motif/) (33) was used to identify enriched binding motifs within 100 bp of the top 1000 peaks. ChIP-Atlas (https://chip-atlas.org/) (34) was used to obtain data for HIF-1α and HIF-1β genome occupancy. ChIP-Seq data can be accessed through the NCBI's Gene Expression Omnibus (GEO Series accession number GSE223754) (35).

Antibodies:

Anti-myc tag mouse recombinant antibody (Active Motif, 91203)

2.10 Comparison of genes containing HIF and/or ZBTB2-myc peaks

A list of transcripts and Known Gene IDs (hg38 assembly, GENCODE V41 track, knownGene table), and a list of Known Gene IDs and the corresponding gene symbols (hg38 assembly, GENCODE V41 track, kgXref table) were obtained from the UCSC Table Browser (http://genome.ucsc.edu/cgi-bin/hgText) (36). ChIP-Atlas (https://chip-atlas.org) was used to obtain HIF-1α, HIF-2α, and HIF-1β genomic intervals reported from several cell lines (34, 37). The datasets were uploaded to the Galaxy web platform (http://usegalaxy.org) (38) for analysis. The "Intersect" tool was used to find transcripts that overlapped with HIF-1α genomic intervals, and gene symbols were assigned to each transcript by referencing the Known Gene IDs/gene symbols list. ChIP-Seq was used to identify genes containing ZBTB2 peaks, and a list of genes was generated to include those with peaks in at least two out of three biological replicates and that had peaks with 2 times the intensity of those in the negative control conditions. The two lists were compared using the "Compare two Datasets" tool on Galaxy to generate a list of genes containing both HIF-1 α and ZBTB2-myc peaks.

2.11 ChIP-qPCR

ChIP-qPCR samples were prepared using the EZ-ChIP Kit (Millipore, 17-371). 250 μL of 37% formaldehyde (Sigma, F8775) was added to a confluent 10 cm dish of cells containing 10 mL of DMEM. The dish was incubated at room temperature for 2 minutes. The reaction was then quenched by addition of 1 mL 1.25 M glycine solution in water and incubated at room

temperature for 5 minutes. Cells were then washed twice with ice-cold PBS, and scraped into 500 µL PBS containing 1× Protease Inhibitor Cocktail II (Millipore, 20-283). The cell pellet was isolated by centrifugation, and resuspended in 600 µL SDS Lysis Buffer (1% SDS, 10mM EDTA, 0.5% Triton X-100, 50mM Tris pH 8.1, 1× Protease Inhibitor Cocktail II). Cell lysates were split into 300 µL aliquots and chromatin was sheared by sonication using a Biorupter UCW-310 (Cosmo Bio) (32 cycles, 30 seconds on/off). Lysates were cleared by centrifugation, and 200 µL of the lysate was diluted in 1.8 mL ChIP Dilution Buffer (0.01% SDS, 1.1% Triton X-100, 1.2mM EDTA, 16.7mM Tris-HCl, pH 8.1, 167mM NaCl, 1× Protease Inhibitor Cocktail II) per immunoprecipiation reaction. Immunoprecipitation was performed using Dynabeads G Immunoprecipitation Kit (Thermo Fisher Scientific, 10007D). 50 µL beads per reaction were incubated with the desired antibody on a rotator for 10 minutes at room temperature. Lysates were then incubated with antibody-conjugated beads overnight at 4°C. Beads were isolated with a magnetic stand and washed sequentially with Low Salt Immune Complex Wash Buffer (20mM Tris-HCl, pH 8.1, 150mM NaCl, 1% Triton X-100, 2mM EDTA, 0.1% SDS), High Salt Immune Complex Wash Buffer (20mM Tris-HCl, pH 8.1, 500mM NaCl, 1% Triton X-100, 2mM EDTA, 0.1% SDS), LiCl Immune Complex Wash Buffer (10mM Tris, pH 8.1, 0.25M LiCl, 1% IGEPAL-CA630, 1mM EDTA, 1% deoxycholic acid), and twice with TE Buffer (10mM Tris-HCl, 1mM EDTA, pH 8.0). DNA was eluted by incubating the beads with 200 µL Elution Buffer (1% SDS, 100 mM NaHCO$_3$) for 30 minutes at room temperature. Crosslinks were reversed by addition of 8 µL 5M NaCl and incubation for 5 hours at 65°C. Samples were then treated with RNase A for 30 minutes at 37°C, followed by treatment with Proteinase K for 1 hour at 45°C. DNA was isolated from the sample using the QIAquick PCR Purification Kit (QIAGEN, 28106) and subjected to qRT-PCR experiments using the following primer sets.

Antibodies & Amount per IP

Normal mouse IgG polyclonal antibody (Millipore, 12-371B)	3 µg
Normal rabbit IgG polyclonal antibody (R&D Systems, AB-105-C)	1.5 µg
Anti-human HIF-1α mouse monoclonal antibody (abcam, ab1)	3 µg
Anti-myc tag mouse monoclonal antibody (CST, 2276)	3 µg
Anti-V5 tag mouse monoclonal antibody (MBL International, M215-3)	3 µg
Anti-human H3K27ac rabbit polyclonal antibody (Abcam, ab4729)	1.5 µg

Primers

Target	Forward Primer (5'→3')	Reverse Primer (5'→3')
CA9 Promoter HRE	TCTCGTTTCCAATGCACGTACAGC	AGTGACAGCAGCAGTTGCACAGT
EGFR-AS1 Intron HRE	CCTAGGAATCCACAAAGCTG	CTGACTAACTGTGGCCCCAG
ATP1A2 Intron HRE	AGAGTGGTGTAATCATGCAGGG	CAGGGGGAGACACTAACACTG

2.12   Luciferase Reporter Assay

HeLa cells were seeded at a density of 6.0×10^3 cells per well in 24-well plates, and at least 3 wells were seeded per condition. For experiments involving siRNA-mediated knockdown, cells were transfected after 4 hours of incubation at 37ºC as described above. The following day, cells were co-transfected with the overexpression vectors for *Firefly* and *Renilla* luciferases. Transfection mixtures were assembled as described in the table below.

Component	Amount per 24 well dish	
	No additional plasmid	With additional plasmid
pRL/CMV (*Renilla* luciferase)	0.33 µg	0.17 µg
pGL3/CMVmp (*Firefly* luciferase)	0.07 µg	0.03 µg
Additional plasmid (if required)		0.20 µg
PEI MAX	1.2 µL	
Serum- and Antibiotic-Free DMEM	Up to 25 µL	

The day after transfection, cells either incubated under normoxia or moved into the hypoxic chamber ($< 0.1\%$ O_2) and incubated for 24 hours. Cells were harvested with $1\times$ Passive Lysis Buffer (Promega, E1941) and incubated at -30ºC for at least 1 hour. *Firefly* and *Renilla*

luciferase activity were measured with the Dual-Luciferase Reporter Assay System according to the manufacturer's instructions (Promega, E1910).

2.13   Systematic Evolution of Ligands by Exponential Enrichment (SELEX)

SELEX was performed to determine the ZBTB2 binding motif *in vivo*. First, nuclear lysate was obtained from HeLa cells overexpressing myc-tagged ZBTB2 using the NE-PER Nuclear and Cytoplasmic Extraction Reagent Kit (Thermo Fisher Scientific, 78833). A library consisting of random 50 base-long double-stranded DNA flanked with T7 and T3 primer annealing sites was purchased from Invitrogen. Lysates and the DNA library were pre-cleared by rotating with magnetic beads from the Dynabeads G Immunoprecipitation Kit (Thermo Fisher Scientific, 10007D) for 1 hour at room temperature. After pre-clearing, binding reactions were assembled as follows:

10× Binding Buffer (100 mM Tris-HCl pH 7.5, 500 mM KCl)	6.0 µL
LightShiftTM Poly(dI-dC) (Thermo Fisher Scientific, 20148E) (1 µg/µL)	1.5 µL
Nuclear Extract	50 µg
DNA Library	60 fmol
MilliQ Water	Up to 60 µL

Binding reactions were incubated at 37ºC for 20 minutes. Magnetic beads from the Dynabead G Immunoprecipitation Kit were prepared according to the manufacturer's instructions. For each binding reaction, 50 µL beads were conjugated with 1 µg of anti-myc tag mouse monoclonal antibody (CST, 2276). The binding reactions and beads were incubated on a rotator overnight at 4ºC. The beads were washed three times with wash buffer (1× Binding Buffer with 0.02% Tween), and DNA was eluted by boiling in TE Buffer for 5 minutes at 95ºC. The eluted DNA was purified using the QIAquick PCR Purification Kit (QIAGEN, 28106) and used as the DNA library for the next round of SELEX. After 9 rounds, the resulting DNA was cloned into the pBlueScript SK (+) vector. Plasmids were isolated from white colonies using the

QIAprep Spin Miniprep Kit (QIAGEN, 27106) and sequenced using M13 primer M4 (5'-GTTTTCCCAGTCACGAC-3'). Recurring motifs in the obtained sequences were analyzed by using MEME (http://meme-suite.org/) (39).

2.14   Statistical Analysis

Error bars represent the standard deviation (s.d.). Statistical significance of the difference between two independent samples was calculated using the Student's t-test. ANOVA with Dunnett's or Sidak's tests were employed to calculate the statistical significance of the difference between samples in datasets with multiple comparisons. Differences with a p-value < 0.05 were considered significant. ns: not significant, * $p < 0.05$, ** $p < 0.01$, *** $p < 0.001$, and **** $p < 0.0001$.

Chapter 3

Identification of HIF-1-ZBTB2 targets and characterization of the mechanisms behind their regulation

3.1   ZBTB2 is recruited to a subset of HIF-1 target gene loci

In order to identify potential ZBTB2 and HIF-1 targets on a genome-wide scale, I first examined ZBTB2 genome occupancy by performing ChIP-Seq using HeLa cells that overexpressed either EGFP-myc (negative control) or ZBTB2-myc. The cells were incubated under hypoxia ($< 0.1\%$ O_2) for 24 hours. Three biological replicates were prepared per condition. Chromatin-protein crosslinking was performed through addition of formaldehyde, and DNA was sheared *via* sonication. The isolated DNA was analyzed by next-generation sequencing (NGS), and reads were mapped and binned to genomic intervals to determine density. Regions with high density were considered to be peaks. A total of 41,838 peaks were identified in the ZBTB2-myc condition, and 9,631 peaks were called in the negative control (Figure 3.1A, B). 14,989 of the ZBTB2-myc peaks were common to at least 2 biological replicates, while 7,496 peaks were common to all three.

To find candidate HIF-1-ZBTB2 target genes, a list of 4,425 candidate ZBTB2 target genes were generated from the ChIP-Seq data by taking genes with ZBTB2-myc peaks in at least 2 out of 3 replicates that were at least two times larger than those observed in the negative control EGFP-myc samples. Aggregate data on HIF-1α genomic occupancy in multiple cell lines was obtained from ChIP-Atlas and used to create a list of 39,480 coding and non-coding genes containing HIF-1α peaks in either gene body or promoter region (2 kb upstream of the transcription start site). This list was compared with the list of ZBTB2 genes, and 2,914 overlapping genes were found (Figure 3.1C).
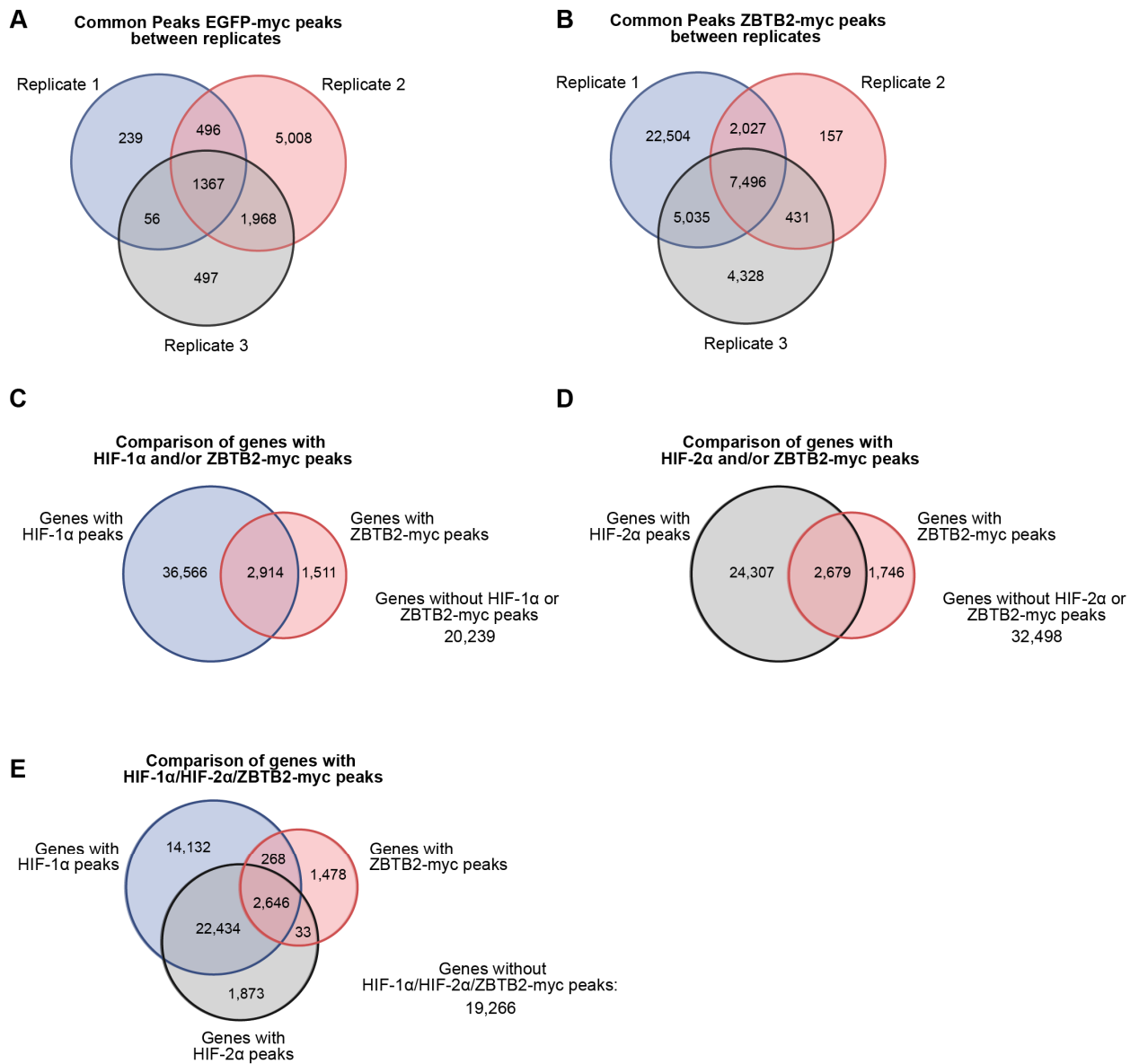
Figure 3.1 ChIP-Seq was performed to identify genes with ZBTB2 recruitment. (A-B) Venn diagrams showing the number of peaks detected in each of the negative control EGFP-myc (A) or ZBTB2-myc (B) ChIP-Seq samples. (C-E) Venn diagram showing the overlap between genes with ZBTB2-myc peaks with genes with HIF-1α peaks (C), with HIF-2α peaks (D), or with both (E). Data for the genes with HIF-1α and HIF-2α peaks were obtained from ChIP-Atlas.

HIF-2 is another gene that controls the hypoxic response and has both distinct and shared target genes with HIF-1 (9, 19, 40). I then postulated that ZBTB2 may have a role in determining which HIF regulates a specific gene. I compared genes with ZBTB2 peaks and genes reported to have HIF-2α peaks in ChIP-Atlas, and observed that 2,689 contained both HIF-2α and ZBTB2-myc peaks (Figure 3.1D). When genes with ZBTB2-myc, HIF-1α, and HIF-2α peaks were compared together, it was found that 2,646 genes contained reported peaks for all 3 genes (Figure 3.1E). Based on the fact that most of genes with ZBTB2-myc peaks and reported peaks for one of the HIFs also had peaks for the other HIF, it is unlikely that ZBTB2 is a factor in determining if a gene is a HIF-1 or a HIF-2 target.

To see if there are any enriched functions or pathways among the genes containing both HIF-1α and ZBTB2 peaks, I utilized the Database for Annotation, Visualization and Integrated Discovery (DAVID) to perform Kyoto Encyclopedia of Genes and Genomes (KEGG) pathway enrichment analysis and Gene Ontology (GO) analysis (41, 42) (Figure 3.2). KEGG pathway enrichment analysis found that genes involved in HIF-1 signaling, various cancers, and cardiomyopathy were enriched among candidate HIF-1α/ZBTB2 downstream genes (Figure 3.2A). GO analysis showed that genes containing HIF-1α and ZBTB2-myc peaks encode proteins involved in a wide variety of biological pathways and molecular functions, such as cell migration, transcriptional factor activity, and signal transduction (Figure 3.2B).
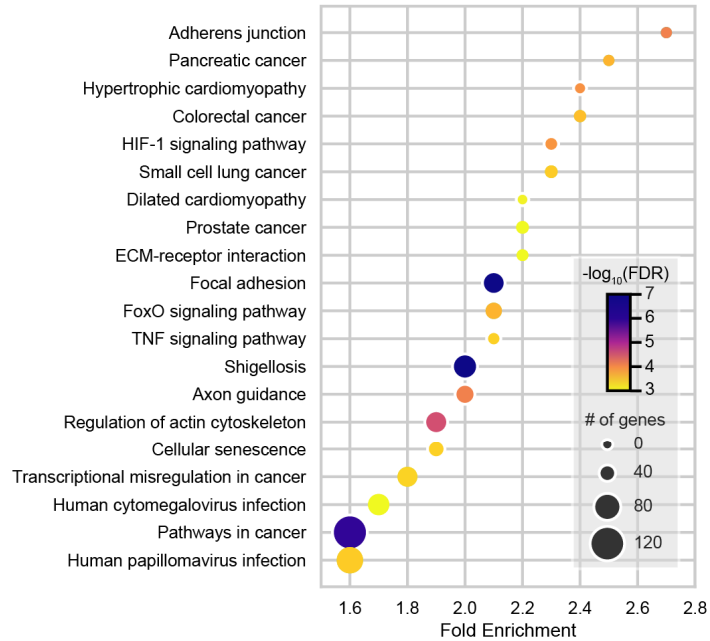
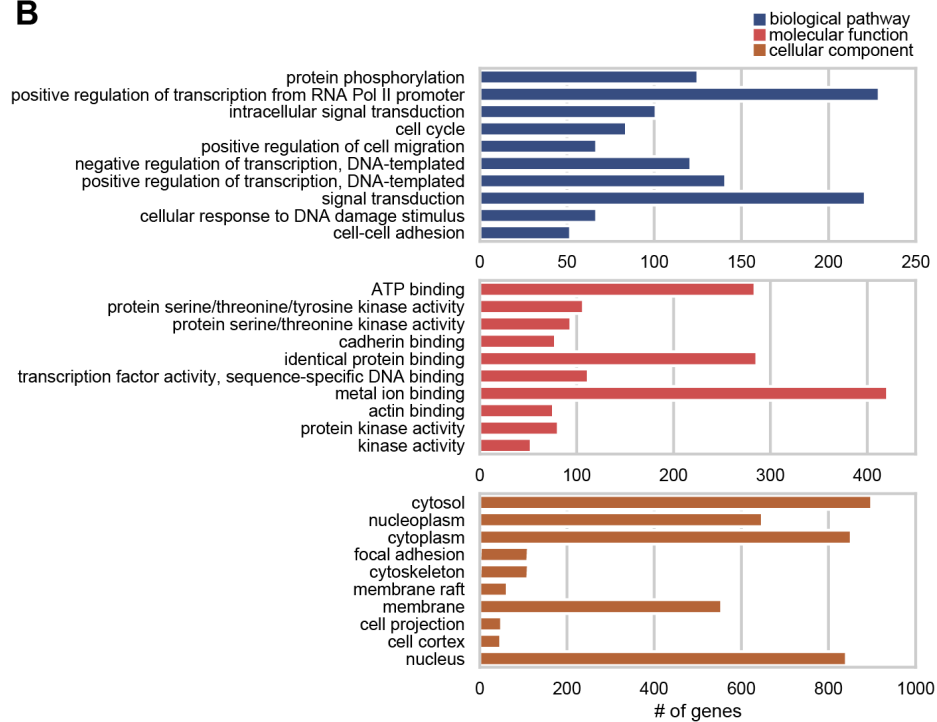**Figure 3.2 Genes containing both HIF-1α and ZBTB2-myc peaks encode for proteins involved in various processes.** DAVID was used to perform KEGG Pathway (A) and Gene Ontology (GO) (B) analysis of genes with both HIF-1α and ZBTB2-myc peaks. (A) The 20 pathways with the highest fold enrichment are displayed. (B) The top 10 terms (ranked by false discovery rate (FDR)) for each GO category are displayed.

Next, I investigated HIF-1 and ZBTB2 binding at several genes further. First, I examined EGFR Antisense RNA 1 (EGFR-AS1) and ATPase Na+/K+ Transporting Subunit Alpha 2 (ATP1A2), two genes that contained both HIF-1 and ZBTB2-myc peaks. Visualization of the ZBTB2-myc ChIP-Seq data and HIF-1α/β genomic intervals from ChIP-Atlas showed that these genes contained ZBTB2-myc peaks that overlapped with reported HIF-1 binding regions (Figure 3.3A). On the other hand, previously reported representative HIF-1 targets carbonic anhydrase 9 (CA9) and BCL2/adenovirus E1B 19 kDa protein-interacting protein 3 (BNIP3) did not have increased ZBTB2-myc signal compared to the negative control (Figure 3.3B) (43–45). These results suggest that ZBTB2 is recruited to a subset of, but not necessarily all, HIF-1 target gene loci.
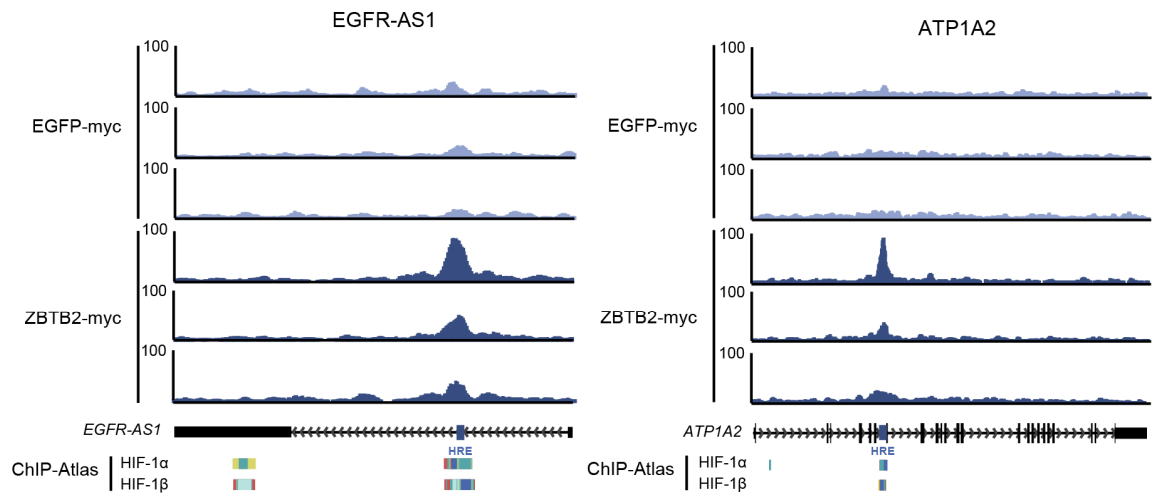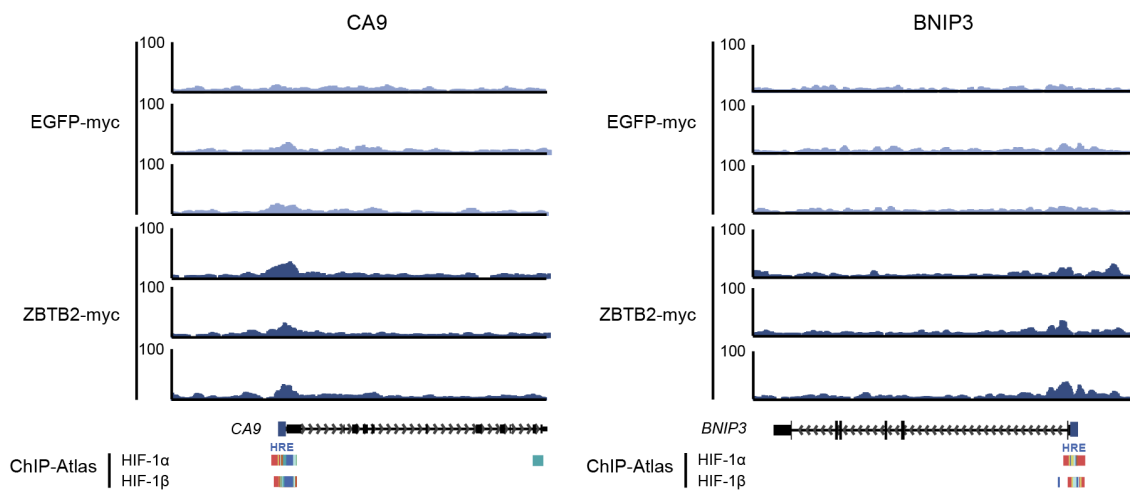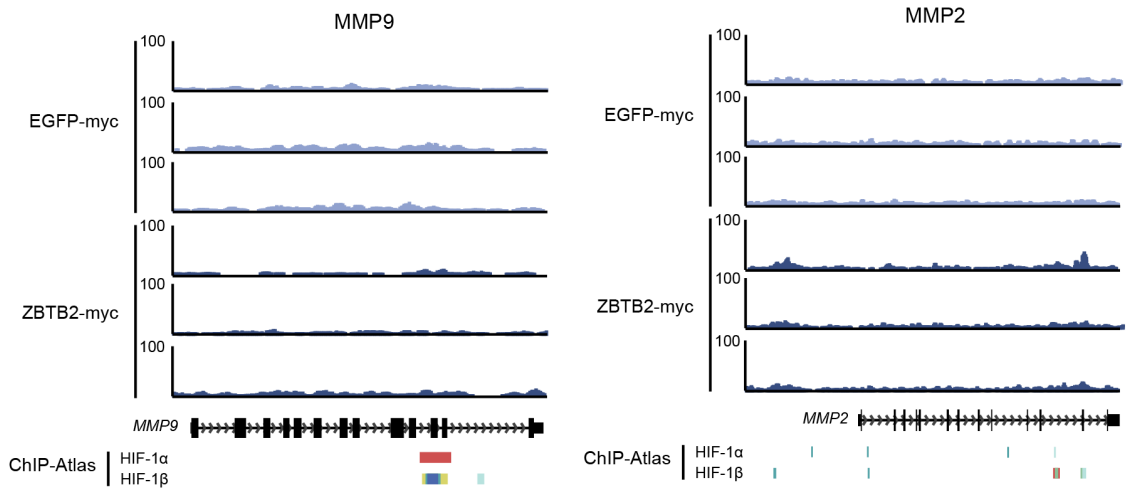
Figure 3.3 ZBTB2 peaks overlap with reported HIF-1 peaks at a subset of genes. UCSC Genome Browser view of EGFP-myc and ZBTB2-myc ChIP-Seq tracks. The location of putative and reported hypoxia response elements (HREs) are indicated (43, 45). (A) Representative genes with ZBTB2-myc peaks overlapping with reported HIF-1α and HIF-1β peaks. (B) Reported HIF-1 target genes that do not have overlapping ZBTB2 and HIF-1α or HIF-1β peaks. (C) Genes that were found in a previous study to be regulated in a ZBTB2/HIF-1-dependent manner.

3.2   Hypoxia-dependent upregulation of EGFR-AS1 is dependent on ZBTB2

To investigate the functional importance of the simultaneous recruitment of HIF-1 and ZBTB2 to a specific subset of genes, I selected one of the candidate HIF-1-ZBTB2 target genes, the long non-coding RNA EGFR-AS1, and investigated its regulation in more detail. EGFR-AS1 consists two exons separated by an intron with a putative HRE (Figure 3.3A). A ZBTB2-myc peak that overlaps with reported HIF-1α/β binding regions is located in the vicinity of the HRE. First, to confirm ZBTB2 binds to the vicinity of the EGFR-AS1 intron HRE, ChIP-qPCR was performed in HeLa cells transfected with a ZBTB2-V5 overexpression vector and treated under normoxia or hypoxia for 24 hours. Immunoprecipitation was performed using an anti-V5 antibody, and qRT-PCR was performed using primers amplifying a ~100 bp region around the HRE. It was found that hypoxic treatment leads to an increase in ZBTB2-V5 recruitment to the region of the intron HRE, but recruitment was not enriched under normoxia (Figure 3.4). This suggests that hypoxic conditions and HIF-1 are required for ZBTB2 to be recruited to the region.

Next, I examined whether hypoxic treatment affects EGFR-AS1 expression. HeLa cells were incubated under normoxia or hypoxia (< 0.1% O_2) for 24 hours, and qRT-PCR was used to quantify EGFR-AS1 transcript levels. While EGFR-AS1 was not present in detectable levels under normoxia, expression significantly increased after hypoxic treatment (Figure 3.5A). To see if ZBTB2 affects EGFR-AS1 expression, cells were treated either with two different ZBTB2 siRNA (siZBTB2#1, siZBTB2#2), or transfected with a ZBTB2-myc overexpression vector. Successful ZBTB2 knockdown or overexpression were confirmed by qRT-PCR and Western blotting. It was found that siRNA-mediated knockdown of ZBTB2 resulted in a significant decrease in EGFR-AS1 expression under hypoxia (Figure 3.5B). In contrast, overexpression of ZBTB2-myc resulted in a further increase in EGFR-AS1 expression under hypoxia (Figure 3.5C). However, ZBTB2 overexpression did not result in increased expression of CA9 or BNIP3, two HIF-1 target genes that lack strong ZBTB2-myc peaks (Figure 3.5D).

Collectively, these results show that ZBTB2 can enhance hypoxia-induced expression of the subset of HIF-1 target genes it is recruited to.

Our previous research showed that, in order for ZBTB2 to increase HIF-1 transactivation activity, several important domains were required (24). One is the N-terminal homodimerization domain. We found that a ZBTB2 mutant containing alanine substitutions in four key residues in this region (ZBTB2 4A) was not able to induce HIF-1 transactivation activity. Likewise, deletion of the zinc finger domain 3 (ZBTB2 ΔZF3) abrogated ZBTB2's ability to increase HIF-1 transactivation activity. To assess the importance of these domains in the regulation of EGFR-AS1 expression, I overexpressed either myc-tagged wild type ZBTB2, ZBTB2 4A, or ZBTB2 ΔZF3 in HeLa cells and incubated them under normoxia or hypoxia (< 0.1% O_2) for 24 hours. Western blotting was performed and it was confirmed that overexpression was successful and that the ZBTB2 variants are expressed at comparable levels. I performed qRT-PCR to quantify the relative amount of EGFR-AS1, and found that ZBTB2 4A and ZBTB2 ΔZF3 were unable to enhance EGFR-AS1 expression under hypoxia to the extent that wild-type ZBTB2 was able to (Figure 3.5E), indicating that the two domains are important for this mode of regulation.
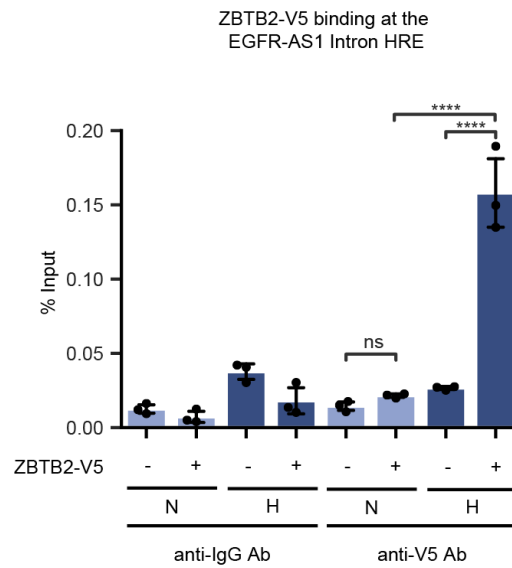
Figure 3.4 ZBTB2 is recruited to the EGFR-AS1 intron HRE under hypoxia. ChIP-qPCR was performed on HeLa cells transfected with ZBTB2-V5 and incubated under normoxia or hypoxia for 24 hours. Immunoprecipitation was performed using an anti-V5 antibody, and qRT-PCR was performed using primers amplifying the HRE in the EGFR-AS1 Intron.
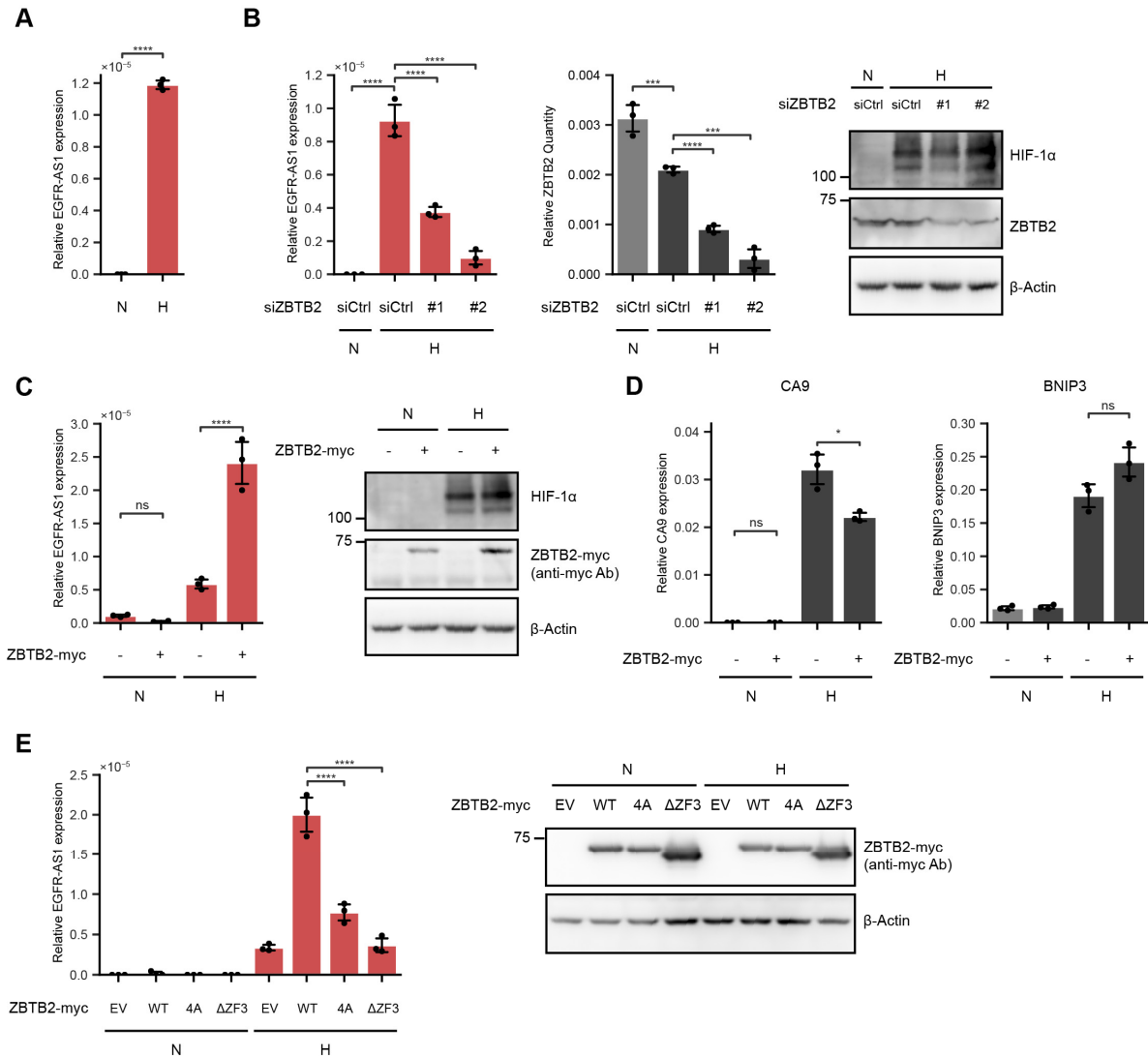
Figure 3.5 ZBTB2 enhances hypoxia-induced expression of EGFR-AS1. (A) qRT-PCR was performed on HeLa cells were incubated under normoxia or hypoxia (<0.1% O2) for 24 hours to determine EGFR-AS1 expression levels. (B-C) HeLa cells were treated with siRNA targeting ZBTB2 (B) or transfected with a vector for overexpression of ZBTB2-myc (C) and incubated under normoxia or hypoxia for 24 hours. EGFR-AS1 expression was quantified by qRT-PCR. qRT-PCR and Western blotting were performed to confirm successful knockdown or overexpression (D) The expression of HIF-1 target genes CA9 and BNIP3 in HeLa cells overexpressing ZBTB2 and incubated under normoxia or hypoxia for 24 hours was quantified by qRT-PCR. (E) HeLa cells were transfected with either an empty vector, or overexpression vectors for wild type (WT), ZBTB2 4A (4A), or ZBTB2 ΔZF3 (ΔZF3) and incubated under normoxia or hypoxia for 24 hours. EGFR-AS1 expression was quantified by qRT-PCR. Western blotting was performed to inspect the expression levels of the ZBTB2 variants.

3.3   Hypoxia-dependent upregulation of EGFR-AS1 is dependent on HIFs

I next investigated the impact of HIFs on EGFR-AS1 expression. HeLa cells were treated with siRNA targeting either HIF-1α (siHIF1A #1, siHIF1A #2), HIF-2α (siHIF2A #1, siHIF2A #2), or HIF-1β (siHIF1B #1, siHIF1B#2) and incubated under normoxia or hypoxia (< 0.1% O_2) for 24 hours. Relative EGFR-AS1 expression was quantified by qRT-PCR. The knockdown efficiency of the siRNAs was confirmed by qRT-PCR and Western blotting. Knockdown of these HIFs resulted in a significant decrease in EGFR-AS1 expression under hypoxia (Figure 3.6A-C). Additionally, when HIF-1β knockout HeLa cells were incubated under hypoxia, no increase in EGFR-AS1 expression was observed (Figure 3.7A). The effect of hypoxia on EGFR-AS1 expression was rescued through transfecting the knockout cells with a HIF-1β overexpression vector.

Next, in order to see if ZBTB2 can increase EGFR-AS1 expression in the absence of HIFs, I transfected HIF-1β knockout cells with a ZBTB2 overexpression vector and incubated the cells under normoxia or hypoxia for 24 hours, and found ZBTB2 overexpression failed to increase EGFR-AS1 expression (Figure 3.7B). Finally, in order to see if ZBTB2 is recruited to the gene locus in the absence of HIFs, I performed ChIP-qPCR in HIF-1β knockout cells transfected with ZBTB2-V5 and incubated under normoxia or hypoxia for 24 hours. Immunoprecipitation was performed with an anti-V5 antibody, and qRT-PCR was performed with primers amplifying the ~100 bp region around the EGFR-AS1 intron HRE. It was found that ZBTB2 was not recruited to the EGFR-AS1 intron if HIF-1β was not present, regardless of if the cells were incubated under normoxia or hypoxia (Figure 3.7C). Together, this data clearly shows that HIFs are required for the recruitment of ZBTB2 to certain HIF-1 target loci under hypoxia and the subsequent increase in gene expression.
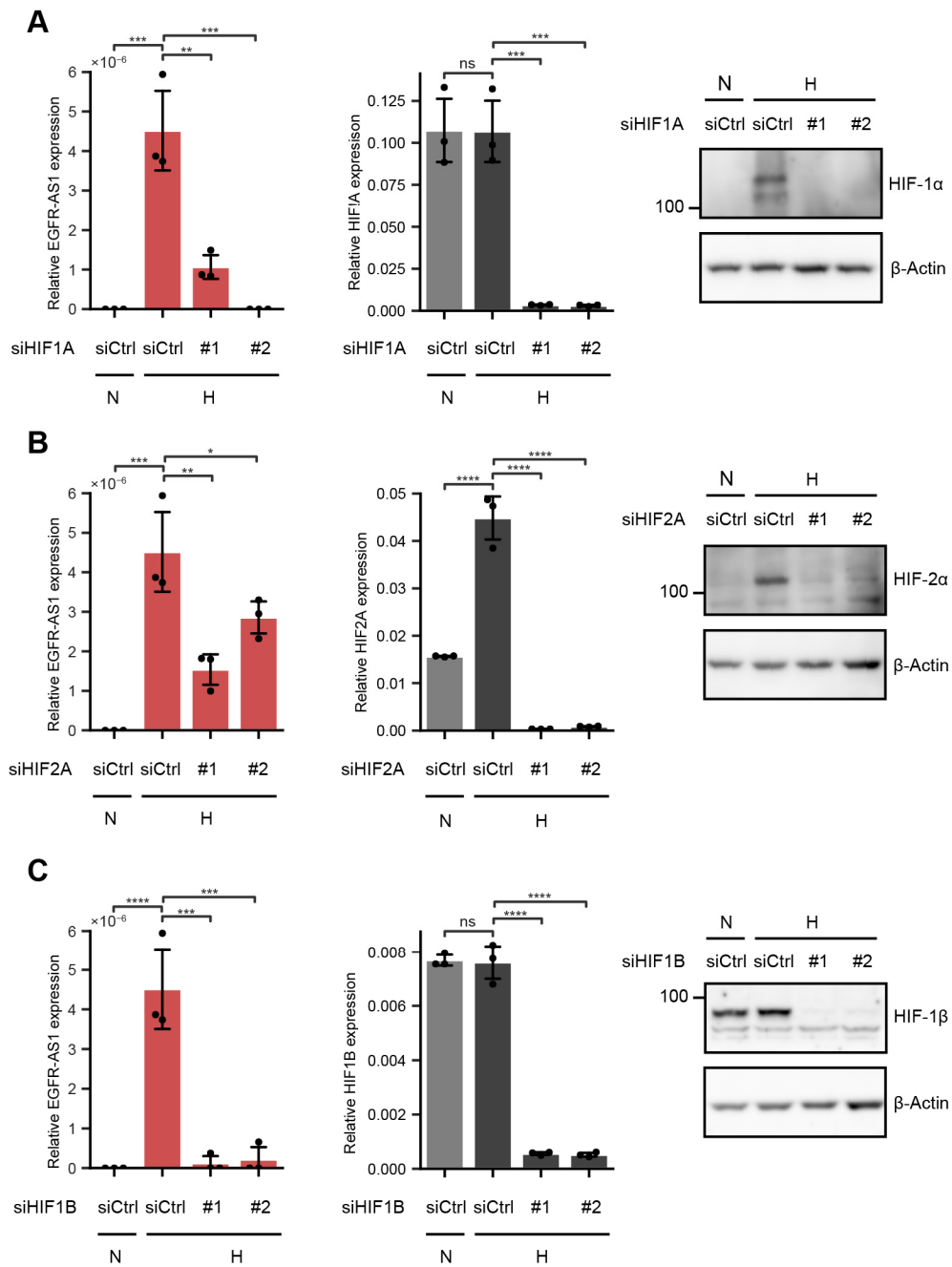
Figure 3.6 EGFR-AS1 is upregulated under hypoxia in a HIF-dependent manner. (A-C) HeLa cells were treated with siRNA targeting HIF1A (A), HIF2A (B), or HIF1B (C), and qRT-PCR was performed to quantify EGFR-AS1 expression. qRT-PCR and Western blotting were performed to confirm successful knockdown of the targets.
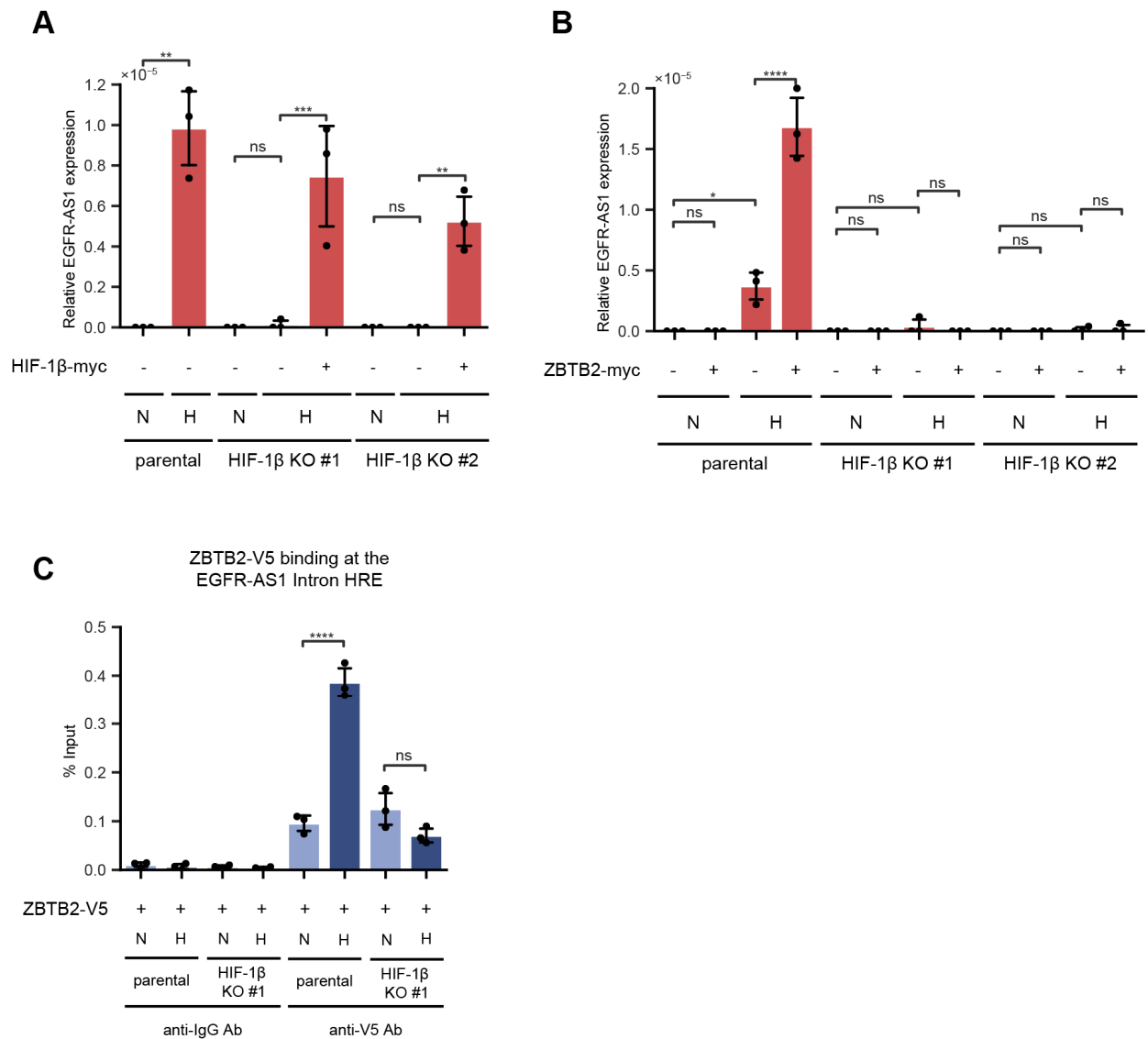
Figure 3.7 HIF-1 is required for ZBTB2-dependent upregulation of EGFR-AS1 and ZBTB2 recruitment to the EGFR-AS1 intron HRE. (A-B) Parental or HIF-1β KO HeLa cells were transfected with an empty vector or an overexpression vector for HIF-1β (A) or ZBTB2-myc (B) and incubated under normoxia or hypoxia for 24 hours. EGFR-AS1 expression was quantified by qRT-PCR. (C) ChIP-qPCR was performed on parental or HIF-1β KO HeLa cells overexpressing ZBTB2-V5 and incubated under normoxia or hypoxia for 24 hours. An anti-V5 antibody was used for immunoprecipitation, and primers annealing around the EGFR-AS1 intron HRE were used for qRT-PCR.

3.4 HIF-1 recruitment to the HRE is required for hypoxia- and ZBTB2-dependent induction of EGFR-AS1 expression

Next, I confirmed whether or not HIF-1 binds to the HRE in the intron of EGFR-AS1. First, ChIP-qPCR was performed on HeLa cells incubated under normoxia or hypoxia for 24 hours. An anti-HIF-1α antibody was used for immunoprecipitation and primers amplifying around the EGFR-AS1 intron HRE were used for qRT-PCR. As a positive control, I also performed qRT-PCR using primers amplifying around the HRE in the promoter of the known HIF-1 target gene CA9. It was found that, under hypoxic conditions, HIF-1α binding at the EGFR-AS1 intron HRE increased significantly to a similar degree as the positive control (Figure 3.8A). To see if HIF-1 binds to the HRE as a heterodimer, I next performed ChIP-qPCR on HeLa cells treated with siRNA targeting HIF-1β. Knockdown of HIF-1β greatly decreased HIF-1α occupancy at both the EGFR-AS1 intron HRE and CA9 promoter HRE (Figure 3.8B). Additionally, when a similar experiment was performed in HIF-1β knockout HeLa cells, it was found that the increase in HIF-1α binding at the EGFR-AS1 intron and CA9 promoter HREs was completely abrogated compared to in wild type cells (Figure 3.8C). These results show that HIF-1α and HIF-1β bind to the HRE at the EGFR-AS1 intron under hypoxia as a heterodimer.

To assess the importance of the intron HRE on the regulation of EGFR-AS1 expression, I employed a lentiviral CRISPR/Cas9 system to introduce mutations into the region. A guide RNA targeting the EGFR-AS1 intron was designed using CRISPRdirect, and was cloned into the lentiCRISPRv2 vector. The vector was introduced to HeLa cells *via* viral transduction, and positive clones were isolated through puromycin selection. I was able to successfully obtain two clones containing mutations in the EGFR-AS1 intron that resulted in the disruption of the HRE sequence on both alleles (Figure 3.9A). For use as negative controls, HeLa cells were transduced with the empty lentiCRISPRv2 vector and two clones with wild type HREs were isolated. Next, to ensure that binding at the EGFR-AS1 intron HRE has been lost in the HRE

mutants, HIF-1α ChIP-qPCR was performed on cells incubated under normoxia or hypoxia for 24 hours. The increase in HIF-1α binding under hypoxia observed in cells with wild type HREs was confirmed to be abolished in the cells with mutations in the HREs (Figure 3.9B). In contrast, the hypoxia-dependent increase at CA9 was unaffected. Next, I examined the effects of mutating the HRE on EGFR-AS1 expression by performing qRT-PCR on wild type or mutant HRE clones incubated under normoxia or hypoxia for 24 hours. It was found that the induction of EGFR-AS1 expression was completely abrogated in cells with mutant HREs (Figure 3.9C). To see if ZBTB2 can enhance EGFR-AS1 expression in cells with mutant HREs, I overexpressed ZBTB2-myc in wild type or HRE mutant clones, and performed qRT-PCR. Consistent with the hypothesis that HIF-1 is required for ZBTB2 recruitment to target gene loci, ZBTB2 overexpression failed to further induce EGFR-AS1 expression in cells with mutant HREs (Figure 3.9D). Together, these results show that HIF-1 binding to HREs is required for ZBTB2-dependent enhancement of HIF-1 target gene expression.
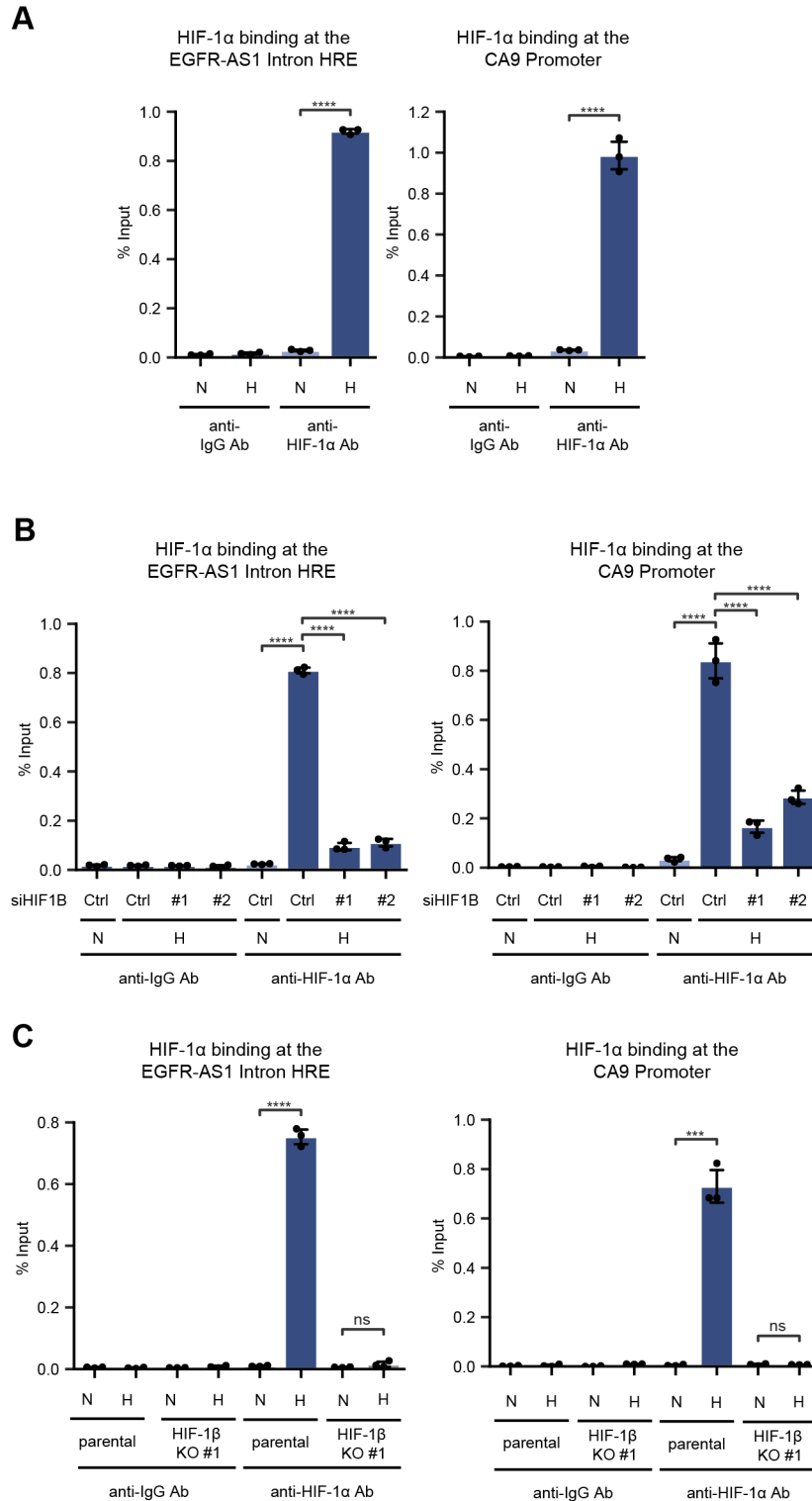
Figure 3.8 HIF-1 is recruited to the EGFR-AS1 intron HRE. (A-C) ChIP-qPCR was performed in parental HeLa cells (A), HeLa cell treated with siRNA targeting HIF1B (B), or HIF-1β knockout HeLa cells (C). Immunoprecipitation was performed using an anti-HIF-1α antibody. qRT-PCR was performed using primers annealing around the EGFR-AS1 intron HRE or CA9 promoter HRE.
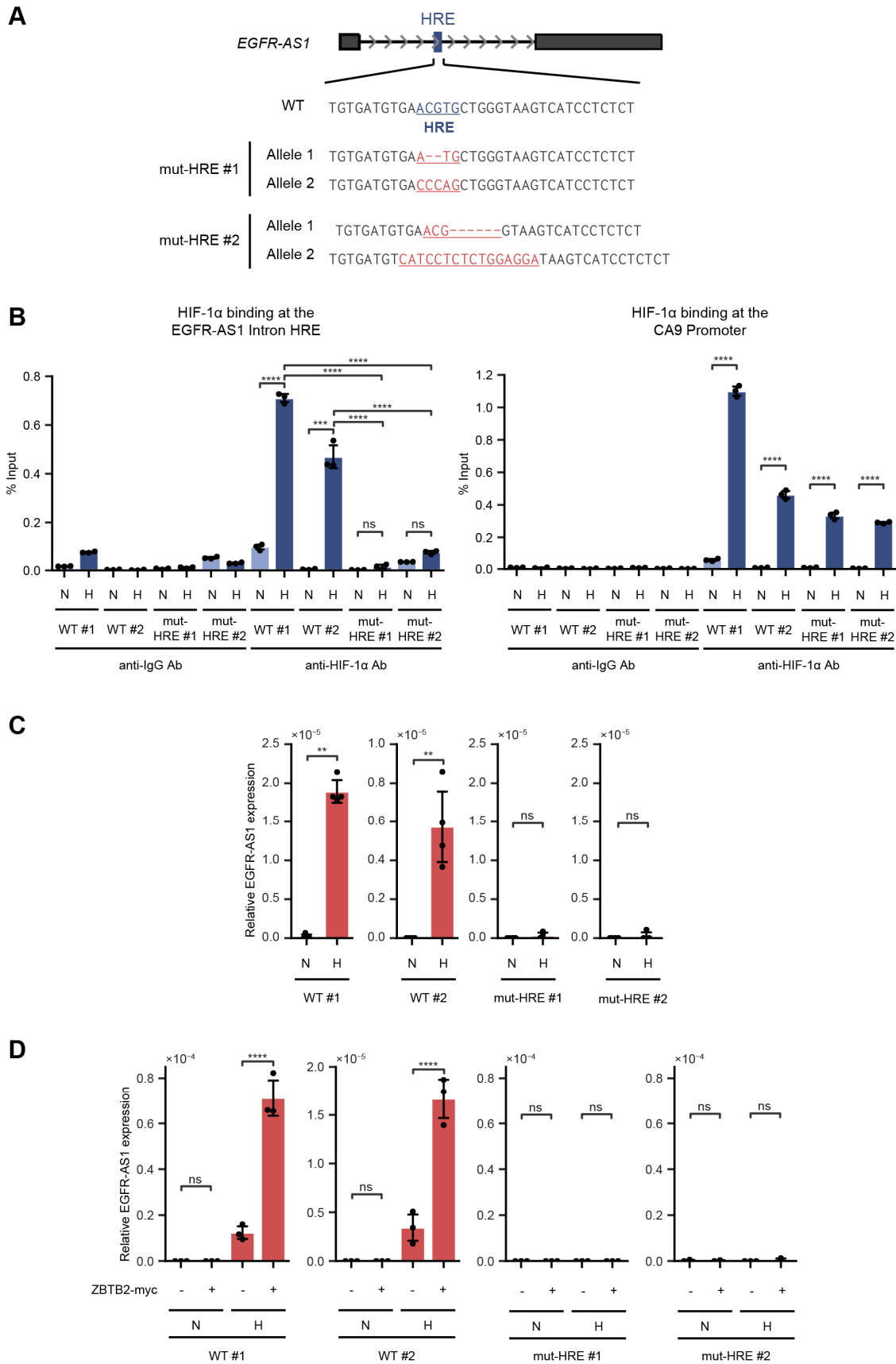
Figure 3.9 The EGFR-AS1 intron HRE is required for hypoxia- and ZBTB2-dependent upregulation of EGFR-AS1. (A) A schematic diagram showing the EGFR-AS1 locus in HRE mutant (mut-HRE) HeLa clones. Regions differing from wild-type HeLa cells are highlighted

in red. (B) ChIP-qPCR was performed on HeLa mut-HRE clones (mut-HRE #1 and #2) and control clones with intact HREs (WT #1 and WT #2). Immunoprecipitation was performed using and anti-HIF-1α antibody. qRT-PCR was performed using primers annealing around the EGFR-AS1 intron HRE or CA9 promoter HRE. (C) qRT-PCR was performed to quantify EGFR-AS1 expression in control or mut-HRE HeLa clones that were incubated under normoxia or hypoxia for 24 hours. (D) qRT-PCR was performed to quantify EGFR-AS1 expression in control or mut-HRE HeLa clones that were transfected with either an empty vector control or an overexpression vector for ZBTB2-myc and incubated under normoxia or hypoxia for 24 hours.

To further assess the importance of the HRE in HIF-1-ZBTB2 target gene regulation, I designed a split luciferase reporter construct containing the EGFR-AS1 intron. The intron of EGFR-AS1 was inserted after nucleotide residue 828 in the *Firefly* luciferase coding sequence to emulate the structure of endogenous EGFR-AS1 (Figure 3.10A). To examine the effects of hypoxia and HIF-1 on luciferase expression, HeLa cells were transfected with an expression vector containing the sequence for regular *Firefly* luciferase (pGL3/CMVmp No Intron) or a vector containing the split *Firefly* luciferase with the EGFR-AS1 Intron (pGL3/CMVmp EGFR-AS1 Intron). An expression vector for *Renilla* luciferase (pRL/CMV) was co-transfected as an internal control, and cells were also treated with siRNA targeting either HIF1A or HIF1B. It was found that after 24 hours of hypoxic treatment, luciferase activity in cells transfected with pGL3/CMVmp EGFR-AS1 Intron increased significantly compared to the activity observed under normoxia. Furthermore, luciferase activity significantly decreased after treatment with siHIF1A or siHIF1B (Figure 3.10B, C). A version of pGL3/CMVmp EGFR-AS1 Intron with a scrambled mutant HRE sequence (pGL3/CMVmp HRE mut) was also constructed. When HeLa cells were transfected with this variant and incubated under normoxia or hypoxia, the hypoxia-dependent increase in luciferase activity normally seen in cells expressing the wild type construct could no longer be observed, indicating that an intact HRE sequence is required for this process (Figure 3.10D). Together, these results show that the split luciferase reporter system recapitulates the effects of HIF-1 on endogenous EGFR-AS1 expression.

To see if the effects of ZBTB2 overexpression could be recapitulated as well, I transfected HeLa cells with expression vectors for ZBTB2-myc and pGL3/CMVmp EGFR-AS1 Intron, and was able to observe an increase in luciferase activity upon ZBTB2 overexpression under hypoxia (Figure 3.10E). Similarly, treatment of cells with siRNA targeting ZBTB2 resulted in a decrease in luciferase activity under hypoxia (Figure 3.10F). These data show that the effects

of hypoxia, HIF-1, and ZBTB2 on gene expression could be replicated on a reporter construct, and offers further evidence on the importance of these factors on the expression of EGFR-AS1.
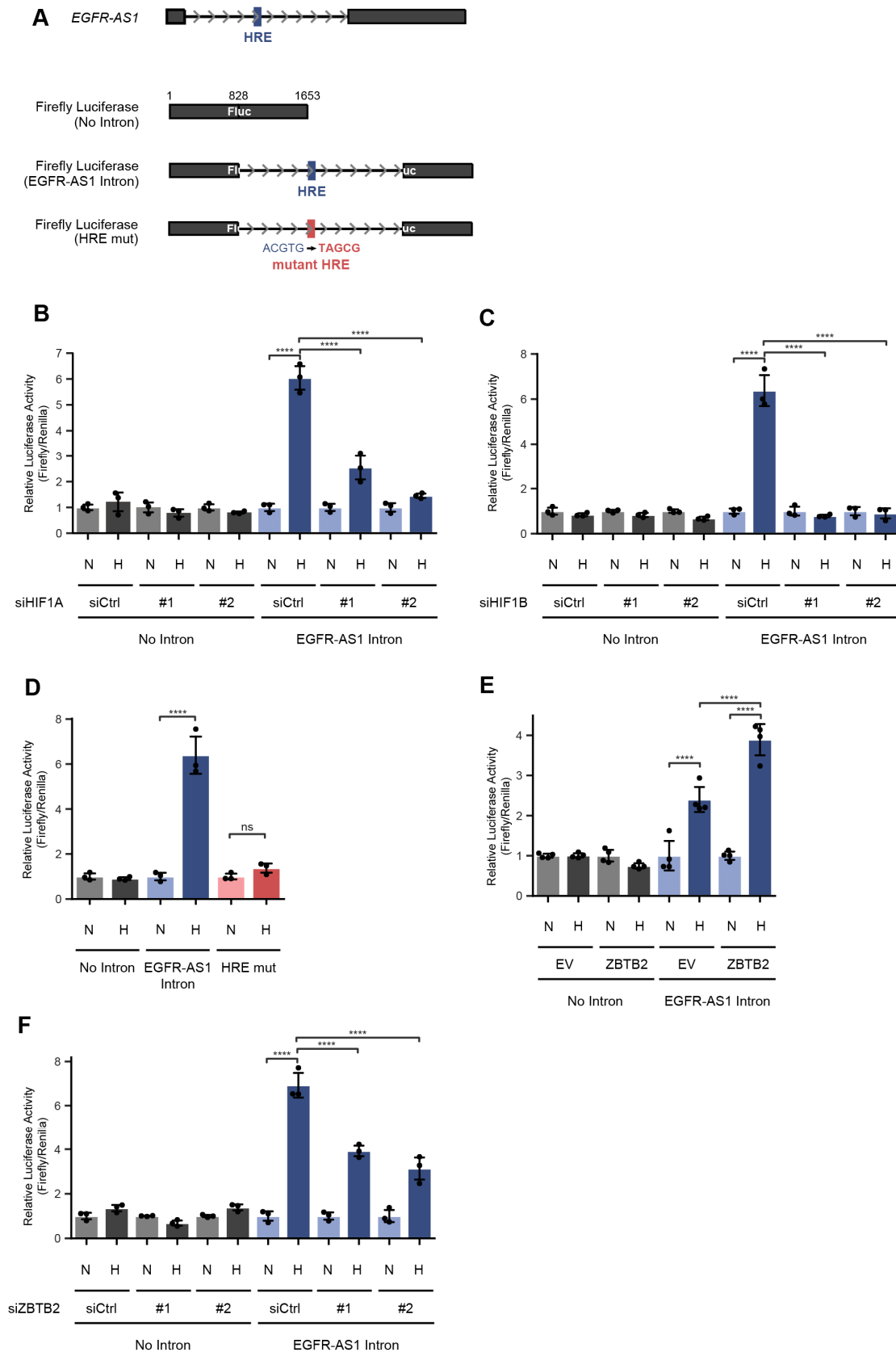
Figure 3.10 The effects of HIF-1 and ZBTB2 on HIF-1 target gene expression are recapitulated in luciferase reporter assays. (A) A schematic diagram showing wild type *Firefly* luciferase (No Intron), split *Firefly* luciferase containing the EGFR-AS1 intron (EGFR-AS1 Intron), and split *Firefly* luciferase containing the EGFR-AS1 intron with a scrambled

HRE sequence (HRE mut). (B-C) Luciferase assays were performed using HeLa cells expressing No Intron or EGFR-AS1 Intron luciferase that were treated with siRNA targeting HIF1A (B) or HIF1B (C) and incubated under normoxia or hypoxia for 24 hours. (D) Luciferase assays were performed on HeLa cells expressing either No Intron, EGFR-AS1 Intron, or HRE mutant luciferase that were incubated under normoxia or hypoxia for 24 hours. (E, F) Luciferase assays were performed on HeLa cells expressing either No Intron or EGFR-AS1 Intron luciferase that were transfected with either a vector for overexpression of ZBTB2-myc (E) or siRNA targeting ZBTB2 (F). In all experiments, cells were transfected with *Renilla* luciferase as a control. Results are normalized to the luciferase activity observed under normoxia.

3.5 Hypoxic treatment and ZBTB2 overexpression increase p300-dependent H3K27ac

Upregulation of gene expression by HIF-1 is known to involve p300, a transcriptional coactivator containing a histone acetyltransferase domain. I next investigated whether or not p300 is involved in the upregulation of EGFR-AS1 expression. To do so, I treated HeLa cells with siRNA targeting EP300, the gene that encodes p300, and incubated the cells under normoxia or hypoxia for 24 hours. Relative EGFR-AS1 expression and EP300 knockdown efficiency were assessed by qRT-PCR. Knockdown of EP300 abrogated the increase in EGFR-AS1 expression induced by hypoxic treatment (Figure 3.11A). To further confirm the results, HeLa cells were treated with the p300 bromodomain inhibitor SGC-CBP30. This also resulted in a significant decrease in EGFR-AS1 expression (Figure 3.11B). These results show that p300 activity is required for the induction of EGFR-AS1 gene expression under hypoxia.

p300's histone acetyltransferase domain allows it to modulate gene expression by modifying chromatin structure. Therefore, I next examined how hypoxia impacts H3K27ac, a marker associated with transcriptional activation, at the EGFR-AS1 intron. I performed ChIP-qPCR on HeLa cells incubated under normoxia or hypoxia for 24 hours using an anti-H3K27ac antibody that recognizes acetylated K27 on histone H3 and primers amplifying around the EGFR-AS1 intron. As a positive control, I also looked at H3K27ac at the CA9 promoter. It was found that hypoxic treatment increased H3K27ac acetylation at both the EGFR-AS1 intron and CA9 promoter (Figure 3.12A). To see if this increase is dependent on p300, cells were incubated under normoxia or hypoxia and treated with either siRNA targeting EP300 or with SGC-CBP30. Both treatments significantly reduced the hypoxia-dependent increase in H3K27ac at the loci (Figure 3.12B, C).

Next, to investigate if the increase in H3K27ac at the loci under hypoxia is dependent on HIF-1, I performed ChIP-qPCR using HIF-1β knockout HeLa cells incubated under normoxia or hypoxia for 24 hours. It was found that the increase in H3K27ac under hypoxia at both the EGFR-AS1 intron as well as the CA9 promoter were greatly reduced in HIF-1β knockout cells compared to in wild type cells (Figure 3.13A). I also performed a similar experiment in HeLa clones with mutations in the EGFR-AS1 intron HRE, and found that in the HRE mutants, H3K27ac at the EGFR-AS1 intron was significantly reduced while H3K27ac at the CA9 promoter remained largely unaffected (Figure 3.13B). These results show that H3K27 acetylation at the EGFR-AS1 intron is dependent on the recruitment on HIF-1 to the locus.

To see if ZBTB2 has an impact on H3K27ac, I performed anti-H3K27ac ChIP-qPCR on HeLa cells overexpressing ZBTB2. It was found that ZBTB2 overexpression further increased H3K27ac at the EGFR-AS1 intron HRE, but not at the CA9 promoter (Figure 3.14A). This suggests that ZBTB2 enhances the expression of the subset of HIF-1 targets it is recruited to by increasing H3K27ac. Additionally, anti-H3K27ac ChIP-qPCR was also performed in wild type or an EGFR-AS1 intron HRE mutant HeLa clone overexpressing ZBTB2. ZBTB2 overexpression could increase H3K27ac around the EGFR-AS1 intron HRE in the cells with wild type HREs, but did not have a significant effect in the clone with mutations in the HRE (Figure 3.14B). This indicates that an intact HRE sequence is required for ZBTB2 to increase H3K27ac.

Finally, to see if p300-induced H3K27ac alone is sufficient to increase EGFR-AS1 expression, I artificially induced the recruitment of p300 to the EGFR-AS1 intron HRE using by transfecting cells under normoxia with an expression vectors for a catalytically inactive Cas9 mutant (dCas9) fused with the p300 core histone acetyltransferase domain (dCas9-p300[Core]) and an expression vector for a sgRNA targeting the EGFR-AS1 intron HRE (46). To assess changes in acetylation, I first performed ChIP-qPCR, and found that co-expression of dCas9-

p300^{Core} and the EGFR-AS1 intron gRNA successfully caused an increase in H3K27ac at the intron (Figure 3.15A). Furthermore, when I checked the relative EGFR-AS1 transcript levels by qRT-PCR, I found that inducing H3K27ac at the locus increased EGFR-AS1 expression (Figure 3.15B). Collectively, these results suggest that HIF-1 binds to HREs of HIF-1 target genes, including EGFR-AS1, and recruits ZBTB2 and p300 to a subset of loci, thereby allowing ZBTB2 to further induce HIF-1 target gene expression by increasing H3K27ac.
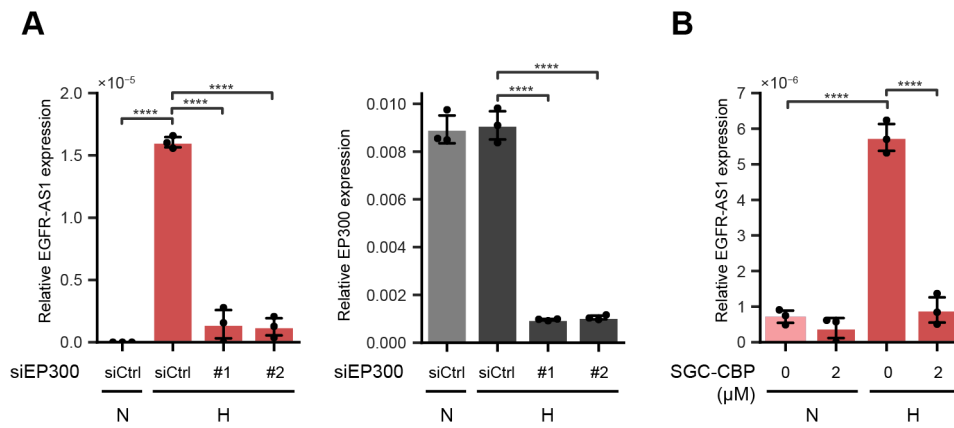
Figure 3.11 The activity of p300 is required for hypoxia-dependent induction of EGFR-AS1. (A-B) HeLa cells were treated with siRNA targeting EP300 (A) or the p300 bromodomain inhibitor SGC-CBP30 (SGC-CBP) (B) and incubated under normoxia or hypoxia for 24 hours. EGFR-AS1 expression and EP300 knockdown efficiency were quantified by qRT-PCR.
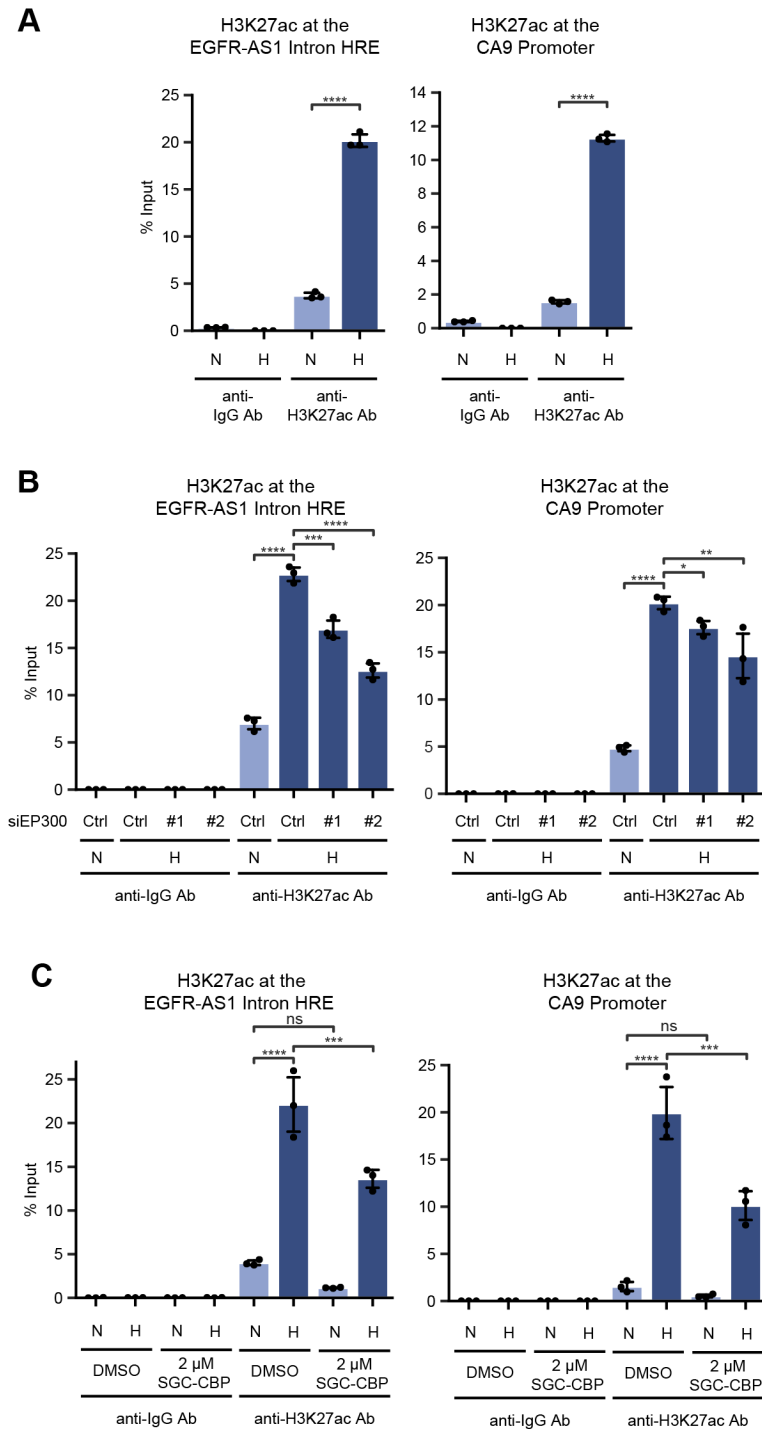
Figure 3.12 H3K27ac around the EGFR-AS1 intron HRE increases under hypoxia in a p300-dependent manner. (A-C) ChIP-qPCR was performed on untreated HeLa cells (A), cells treated with siRNA targeting EP300 (B), or cells treated with SGC-CBP30 (C). Cells were incubated under normoxia or hypoxia for 24 hours. Immunoprecipitation was performed using an anti-H3K27ac antibody. qRT-PCR was performed using primers annealing around the EGFR-AS1 intron HRE or the CA9 promoter HRE.
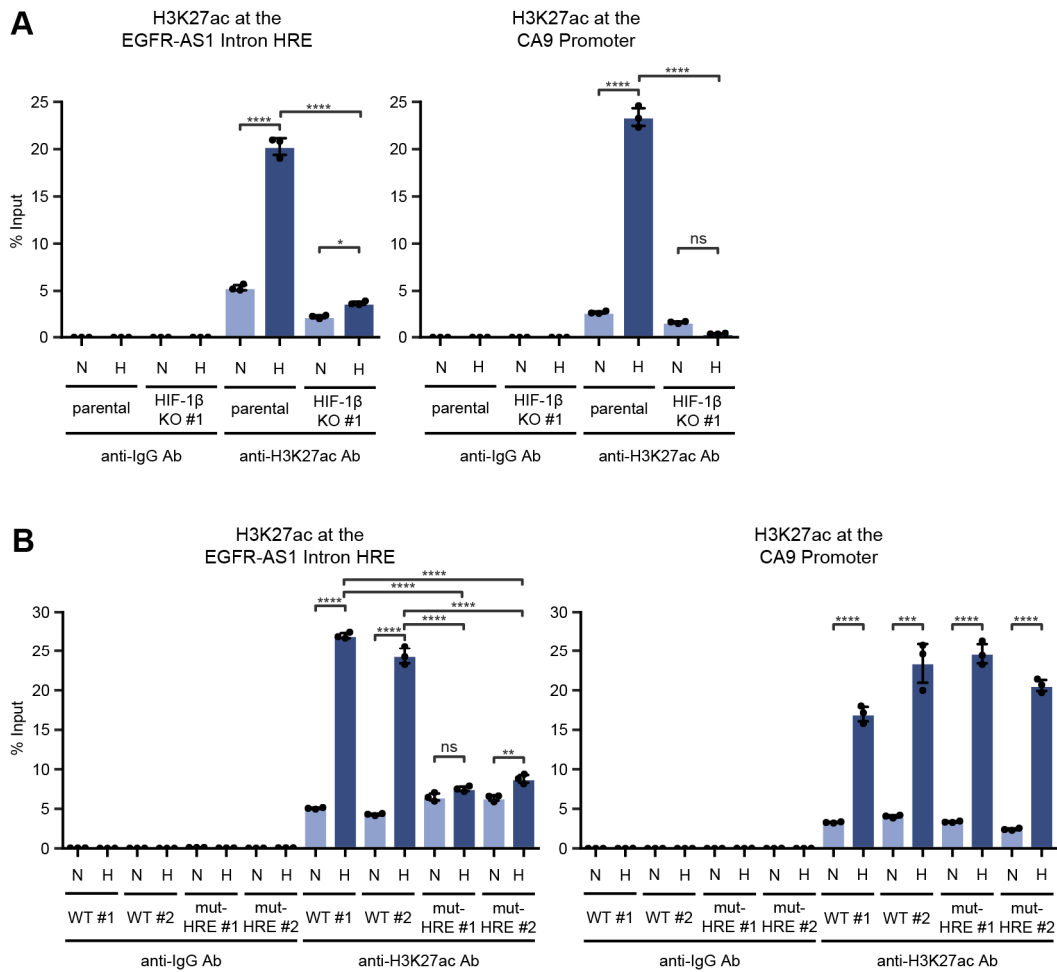
Figure 3.13 The hypoxia-dependent increase in H3K27ac at the EGFR-AS1 intron HRE is dependent on HIF-1 recruitment. (A-B) ChIP-qPCR was performed in parental and HIF-1β knockout HeLa cells (A), or mut-HRE HeLa clones (mut-HRE #1 and #2) and control clones with intact HREs (WT #1 and WT #2) (B). Immunoprecipitation was performed using anti-H3K27ac antibody. qRT-PCR was performed using primers annealing around the EGFR-AS1 intron HRE or CA9 promoter HRE.
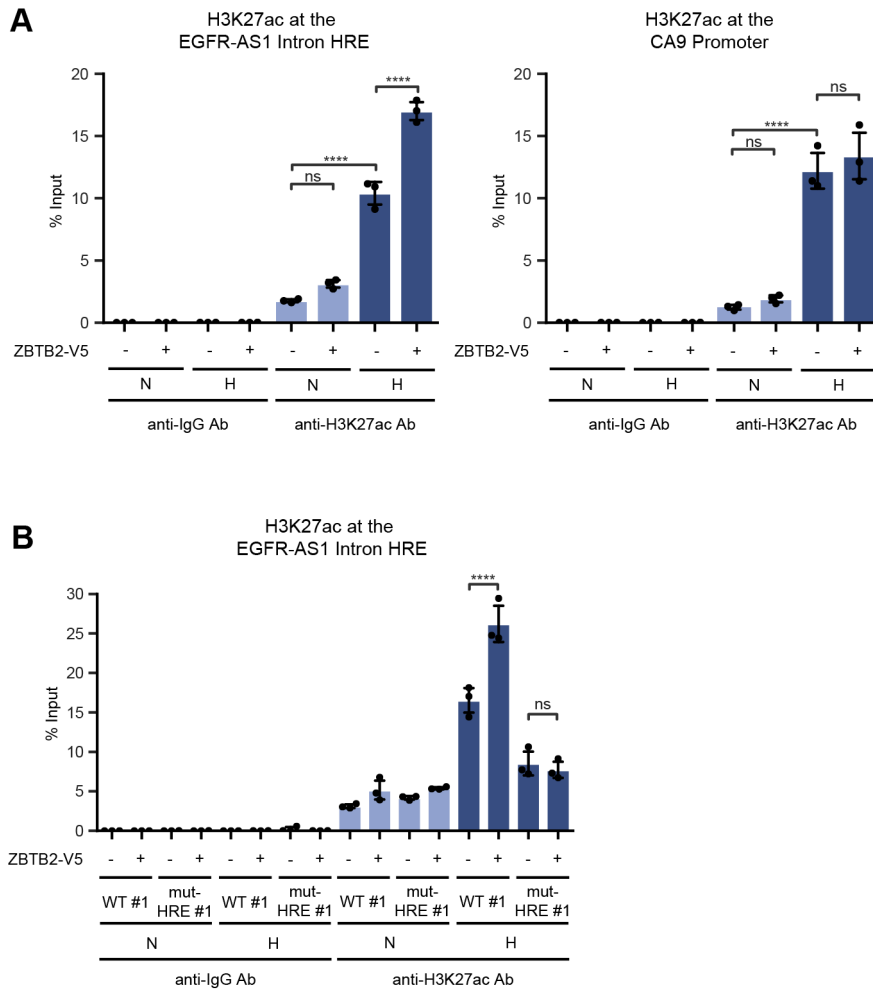
Figure 3.14 ZBTB2 increases H3K27ac at the EGFR-AS1 intron HRE. (A, B) ChIP-qPCR was performed in parental HeLa cells (A) or a mut-HRE HeLa clone (mut-HRE #1) and control clone with an intact HRE (WT #1) (B), transfected with an overexpression vector for ZBTB2-V5 and incubated under normoxia or hypoxia for 24 hours. Immunoprecipitation was performed with an anti-H3K27ac antibody, qRT-PCR was performed using primers annealing around the EGFR-AS1 intron HRE or CA9 promoter HRE.

Figure 3.15 EGFR-AS1 expression can be increased by artificially inducing H3K27ac at the gene locus. (A) ChIP-qPCR was performed on HEK293TN cells co-transfected with pCDNA/dCas9-p300 Core and either pX330-Cas9(-)/EGFR-AS1-sgRNA (+) or a corresponding empty vector (-). Immunoprecipitation was performed using an anti-H3K27ac antibody, and qRT-PCR was perfo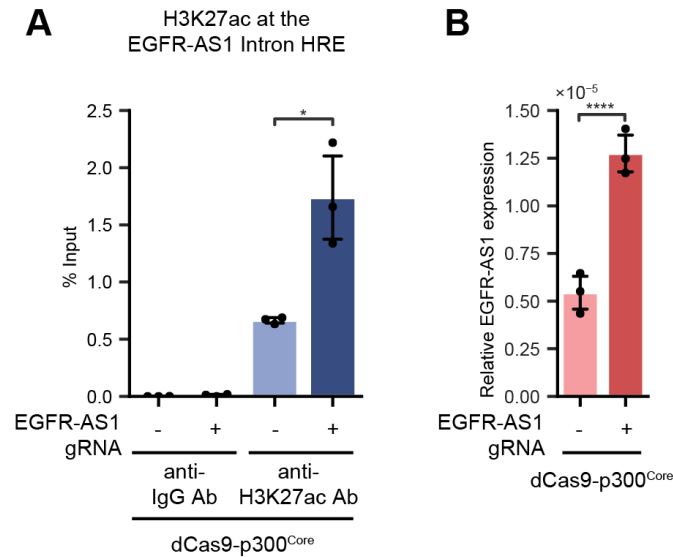rmed using primers annealing around the EGFR-AS1 intron HRE. (B) qRT-PCR was performed using the same conditions as (A) to quantify EGFR-AS1 expression.

3.6 Another candidate HIF-1/ZBTB2 target, ATP1A2, is regulated through similar mechanisms as EGFR-AS1

In order to see if the findings regarding EGFR-AS1 can be applied to other HIF-1 target genes that ZBTB2 is recruited to under hypoxia, I investigated the effects of HIF-1 and ZBTB2 on ATP1A2 gene expression. First, HeLa cells were treated with siRNA targeting either HIF1A or ZBTB2, and the cells were incubated the cells under normoxia or hypoxia for 24 hours. Subsequently, qRT-PCR was performed to quantify relative ATP1A2 transcript levels. Similar to what was seen with EGFR-AS1, hypoxic treatment increased expression of ATP1A2, and knockdown of either HIF-1α or ZBTB2 resulted in a significant decrease in gene expression (Figure 3.16A). I also overexpressed ZBTB2 in HeLa cells, and found that ZBTB2 overexpression further enhanced the hypoxia-dependent increase in ATP1A2 gene expression (Figure 3.16B). Additionally, this enhancement was not observed when the ZBTB2 4A and ΔZF3 mutants were overexpressed (Figure 3.16C). Finally, to see if hypoxia and ZBTB2 induce similar changes in histone acetylation at the ATP1A2 gene locus as it does at the EGFR-AS1 one, I performed ChIP-qPCR using an anti-H3K27ac antibody and primers amplifying around the respective HREs. Like with EGFR-AS1, hypoxic treatment increased the amount of H3K27ac around the ATP1A2 HRE, and overexpression of ZBTB2 increased it further (Figure 3.16D). These results demonstrate that the effects of HIF-1 and ZBTB2 can be observed on the other candidate gene identified by ChIP-Seq.
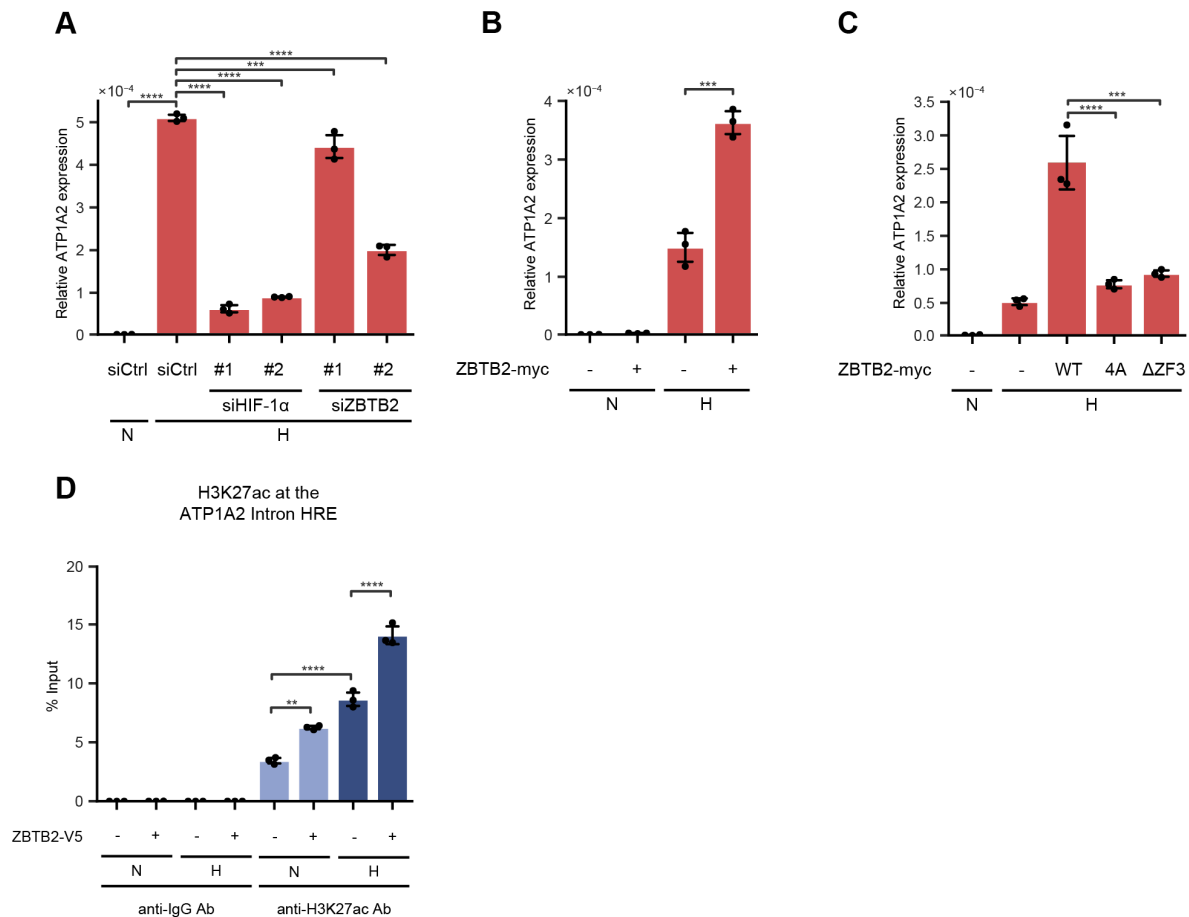
Figure 3.16 ZBTB2 regulates the expression of a subset of HIF-1 target genes. (A, B) HeLa cells were transfected with either siRNA targeting HIF1A or ZBTB2 (A) or transfected with a ZBTB2-myc overexpression vector (B) and incubated under normoxia or hypoxia for 24 hours. qRT-PCR was used to quantify ATP1A2 expression. (C) HeLa cells were transfected with wild type (WT), 4A mutant (4A), or Zinc Finger 3 deletion mutant (ΔZF3) ZBTB2-myc overexpression vectors and incubated under normoxia or hypoxia for 24 hours. qRT-PCR was used to quantify ATP1A2 expression. (D) ChIP-qPCR was performed on HeLa cells transfected with a ZBTB2-V5 overexpression vector and incubated under normoxia or hypoxia for 24 hours. Immunoprecipitation was performed using an anti-H3K27ac antibody. qRT-PCR was performed using primers annealing around the ATP1A2 intron HRE.

Chapter 4

Investigation of ZBTB2's binding motif

In the previous chapter, I established that ZBTB2 is recruited to a subset of HIF-1 genes to enable their full expression under hypoxia. I also showed that one of the zinc finger domains (ZF3) is required for the process. As zinc finger domains are known to recognize and bind to specific DNA sequences, I reasoned that ZBTB2 should have a unique DNA binding motif. Characterization of such a motif could enable further identification of ZBTB2 target genes. Therefore, I next attempted to identify ZBTB2 binding motifs through several means.

4.1   Motifs from ZBTB2-myc ChIP-Seq

Previously, I performed ZBTB2-myc ChIP-Seq and discovered that it was recruited to certain gene loci. If ZBTB2 binds directly to the DNA sequences at the gene loci, it should be possible to identify ZBTB2 binding motifs through examining the genomic sequences around the vicinity of ZBTB2 peaks. I searched for potential ZBTB2 binding motifs by analyzing the ChIP-Seq data using two different methods. First, Homer *de novo* motif analysis was used to identify enriched sequences within 100 bases of the 1000 strongest peaks (33). The top 10 identified motifs are displayed in Table 4.1. Interestingly, many of the motifs were highly similar to those of known transcription factors: for instance, the motifs 5'-TGA(C/G)TCA'-3' and 5'-TGACGTCA-3' were among the top hits of the analysis, and these are reported motifs for ATF/CREB transcription factors containing basic region-leucine zipper (bZIP) domains and AP-1 transcription factors respectively. Additionally, the HIF-1 HRE was also one of the top enriched binding motifs. These findings may indicate that ZBTB2 is often recruited to binding sites of other transcription factors.

Next, the MEME suite analysis tool (https://meme-suite.org/meme/tools/meme) was employed to identify enriched motifs in a 60 base pair region around the top 1000 peaks (39). The significant motifs identified for each of the three replicates is displayed in Table 4.2. Similar

to the Homer analysis, MEME analysis also identified 5'-TCAGTCA-3' as an enriched motif in two of the three replicates. Inspection of the other enriched sequences did not reveal a clear binding motif, although all three replicates had T-rich and G-rich motifs significantly enriched.

A closer look at the sequence of EGFR-AS1 revealed that one of the motifs enriched near ZBTB2-myc ChIP-Seq peaks, 5'-TCA(C/G)TCA-3', was located in close proximity to the HRE in the intron. To see if this sequence is important in regulating EGFR-AS1 expression, I once again utilized the split luciferase reporter assay. I generated a version of the reporter construct containing the EGFR-AS1 intron with a scrambled ChIP-Seq motif (ChIP motif mut) and investigated the effects of hypoxia on induction of luciferase activity (Figure 4.1A). Interestingly, the hypoxia-dependent increase in luciferase activity normally observed in cells expressing luciferase with a wild type EGFR-AS1 intron was abrogated in cells expressing ChIP motif mut luciferase (Figure 4.1). This indicates that this sequence is also important for regulation of EGFR-AS1 expression under hypoxia.

4.2   Motifs from previously published literature

A previous study by Yin *et al* analyzing the binding of various transcription factors by High Throughput Systematic Evolution of Ligands by Exponential Enrichment (HT-SELEX) found the motif shown in Figure 4.2 to be an *in vitro* ZBTB2 binding motif (47). To see if this motif was enriched around ZBTB2-myc ChIP-Seq peaks, I used the Find Individual Motif Occurrences (FIMO) tool in the MEME suite (https://meme-suite.org/meme/tools/fimo) to search for 5'-GTTTCCGGTA-3' in the 60 base pair region around the top 1000 peaks in both the negative control EGFP-myc samples as well as the ZBTB2-myc samples (Table 4.1) (48). However, enrichment in the previously reported binding motif was not observed in the ZBTB2-

myc samples compared to the EGFP-myc samples, indicating that this is likely not a ZBTB2

binding motif *in vivo*.

Table 4.1 Enriched motifs from ChIP-Seq were identified by Homer motif search.
Sequences within 100 bp the top 1000 peaks from each replicate were used for analysis. The top 10 binding motifs identified from Homer *de novo* analysis of ZBTB2-myc (replicate 1) ChIP-Seq results and the transcription factor (TF) motif they are the most similar to are shown.

	TF	Motif	P-Value	% of Targets	% of Background
1	ATF3		1×10^{-255}	36.49%	2.73%
2	HES7		1×10^{-36}	7.04%	0.77%
3	ARNT1 (HIF-1β)		1×10^{-22}	16.63%	6.68%
4	ATF1		1×10^{-17}	12.47%	4.90%
5	ATF4		1×10^{-16}	3.12%	0.34%
6	TEAD3		1×10^{-14}	16.05%	7.86%
7	TBX29		1×10^{-14}	3.35%	0.49%
8	EBF1		1×10^{-13}	1.39%	0.05%
9	FOXO3		1×10^{-13}	8.55%	3.14%
10	ZBED1		1×10^{-12}	2.89%	0.40%

Table 4.2 Enriched motifs from ChIP-Seq were identified by MEME Suite motif search.
60 bp sequences of the top 1000 peaks from each replicate were used for analysis. Motif searches were conducted with a minimum motif width of 6 and maximum motif with of 50. Significantly enriched motifs from each replicate are shown. The E-value represents the statistical significance of the identified motif. Motifs with E-values < 0.05 are considered significant.

		Motif	E-Value	% of Sequences
ZBTB2-myc Replicate 1	1		6.6×10^{-147}	18.6%
	2		2.2×10^{-19}	25.1%
	3		1.4×10^{-9}	2.9%
	4		8.7×10^{-3}	0.7%
ZBTB2-myc Replicate 2	1		2.8×10^{-64}	10.7%
	2		6.5×10^{-22}	10.3%
	3		6.5×10^{-15}	13.1%
	4		8.8×10^{-4}	1.6%
ZBTB3-myc Replicate 3	1		2.0×10^{-35}	4.1%
	2		5.9×10^{-8}	10.0%
	3		3.6×10^{-3}	6.6%

Figure 4.1 Mutation of a putative binding motif identified through ZBTB2-myc ChIP Seq in the luciferase reporter gene results in loss of hypoxia-dependent induction. (A) A schematic diagram showing wild type *Firefly* luciferase (No Intron), split *Firefly* luciferase containing the EGFR-AS1 intron (EGFR-AS1 Intron), and split *Firefly* luciferase containing the EGFR-AS1 intron with a scrambled ChIP-Seq motif sequence (ChIP motif mut). (B) Luciferase assays were performed on HeLa cells expressing either No Intron, EGFR-AS1 Intron, or ChIP motif mutant luciferase that were incubated under normoxia or hypoxia for 24 hours.
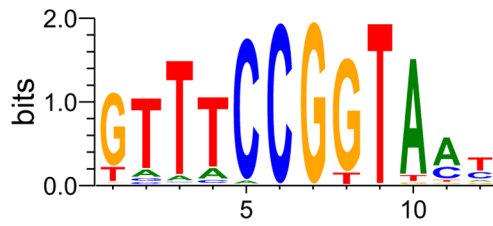
Figure 4.2 An *in vitro* ZBTB2 binding motif reported by Yin et al, 2017 (47). The position weight matrix (PWM) for the motif was obtained from the supplementary data of the cited paper and converted into a sequence logo with WebLogo 3 (https://weblogo.threeplusone.com/) (49, 50).

Table 4.3 FIMO was used to search for a previously reported ZBTB2 *in vitro* binding motif in ChIP-Seq samples. 60 bp sequences of the top 1000 peaks from each replicate were used for analysis. Only motif occurrences with a p value of $< 1 \times 10^{-4}$ were counted.

	# of motif occurrences
EGFP-myc Replicate 1	21
EGFP-myc Replicate 2	21
EGFP-myc Replicate 3	18
ZBTB2-myc Replicate 1	6
ZBTB2-myc Replicate 2	21
ZBTB2-myc Replicate 3	16

4.3   Motifs from SELEX

As an alternate approach to identifying ZBTB2 binding motifs, I performed Systematic Evolution of Ligands by Exponential Enrichment (SELEX) myself to identify *in vitro* binding motifs (Figure 4.3). HeLa cells overexpressing either EGFP-myc (negative control) or ZBTB2-myc and incubated under hypoxia (< 0.1% O_2) for 24 hours was used for the experiment. Nuclear lysates were harvested from the cells, and binding reaction mixtures were set up using the lysates and a random nucleotide library. The resulting reaction mixtures were incubated at 37ºC for 30 minutes. ZBTB2 and ZBTB2-bound DNA were then immunoprecipitated from the mixture using an anti-myc tag antibody. The DNA was isolated and amplified by PCR. Another binding reaction was then assembled using the PCR product in place of the random nucleotide library. This process was repeated for 9 cycles, and the resulting DNA fragments were subcloned into the pBlueScript plasmid for sequencing. A total of 24 sequences were obtained, and candidate binding motifs were then identified using the motif search module of the MEME suite (https://meme-suite.org/meme/tools/meme) (Table 4.4). The motif 5'-GTCTTKKT-3'was found to be significantly enriched among the obtained sequences.
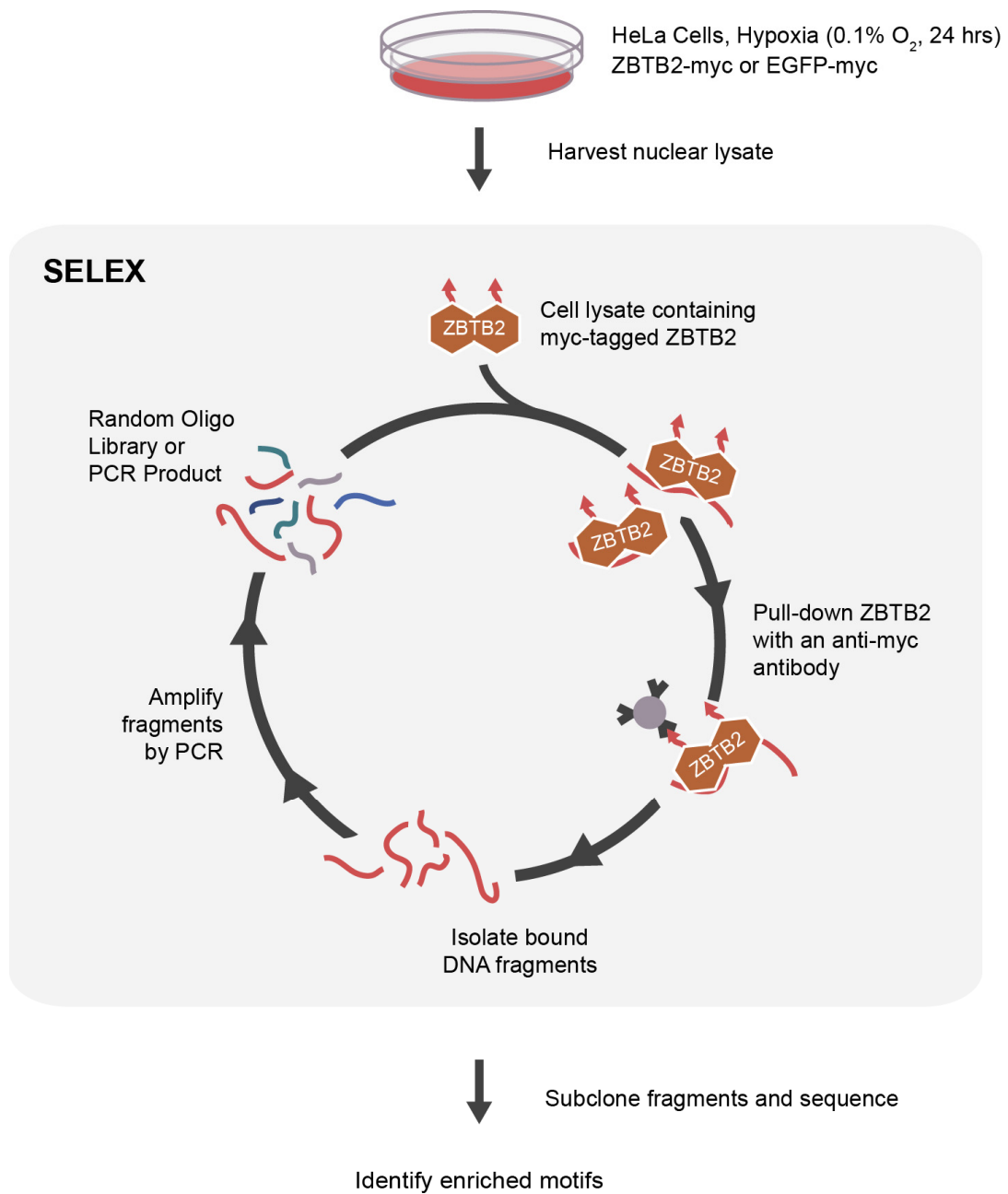
Figure 4.3 Systematic Evolution of Ligands by Exponential Enrichment (SELEX) was used to identify potential ZBTB2 binding motifs *in vitro*.

Table 4.4 Enriched motifs in sequences obtained from SELEX were identified by MEME Suite motif search. Motif searches were conducted with a minimum motif width of 4 and maximum motif with of 8. The top three motifs found are shown. The E-value represents the statistical significance of the identified motif. Motifs with E-values < 0.05 are considered significant.

	Motif	E-Value	Present in % of Sequences
1		4×10^{-3}	100%
2		1.8×10^{5}	16.67%
3		2.8×10^{5}	8.33%

Table 4.5 The Interactive PWN Predictor was used to predict ZBTB2's binding motif (30). Binding motifs for all 4 zinc fingers and only zinc fingers 2 and 3 in ZBTB2 were predicted. The SVM expanded linear model was used for prediction.

	ZF1-ZF4	ZF2/3 Only
Motif		
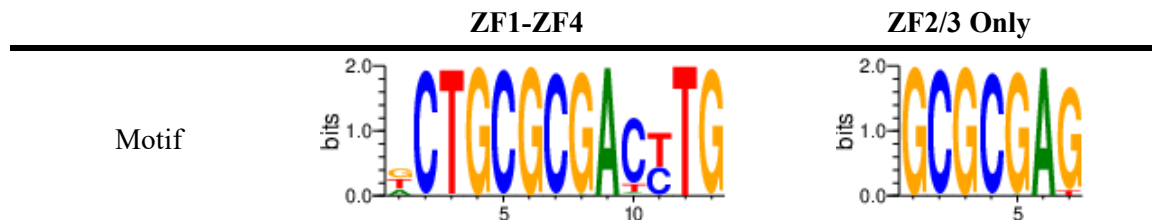
4.4 Motifs from *de novo* prediction of zinc finger binding sites

Finally, I employed an online tool that predicts position weight matrices (PWMs) representing Cys2His2 (C2H2)-type zinc finger DNA-binding specificities (http://zf.princeton.edu/) (30). In this model, it is assumed that every C2H2 zinc finger binds independently 4 bp of DNA. The binding energy for a zinc finger and every possible 4 bp combination is calculated and scored, and the probability the zinc finger binds a specific is calculated. From that, PWMs showing the probability of each nucleotide occupying each position in the 4 bp sequence can be determined. In proteins with multiple zinc fingers, there are often overlapping nucleotides in the 4 bp binding sequence, so in this case the PWMs are merged accordingly. Predictions were performed on either all 4 zinc fingers of ZBTB2 or just zinc fingers 2 and 3, the two zinc fingers previously shown to be involved in increasing HIF-1 transactivation activity (24). The predicted motifs are listed in Table 4.5. The motifs did not resemble any of the putative motifs identified through the other methods.

4.5 Comparison between motifs identified through different methods and their occurrence in HIF-1/ZBTB2 target genes

I next investigated the sequences of the ZBTB2 target genes that were identified in Chapter 3 (EGFR-AS1 and ATP1A2) to see whether or not the putative motifs identified through various methods are present near the vicinity of the ZBTB2-myc peak regions. The results are summarized in Figure 4.4. The motif reported in literature and the motifs predicted by the online tool were not found in any of the ZBTB2 target gene sequences. The motif identified through ChIP-Seq and the one identified by SELEX were present in both genes, but were only situated near the ZBTB2-myc peak in EGFR-AS1. From these results, it does not appear that any of the methods were able to identify a clear ZBTB2 binding motif.
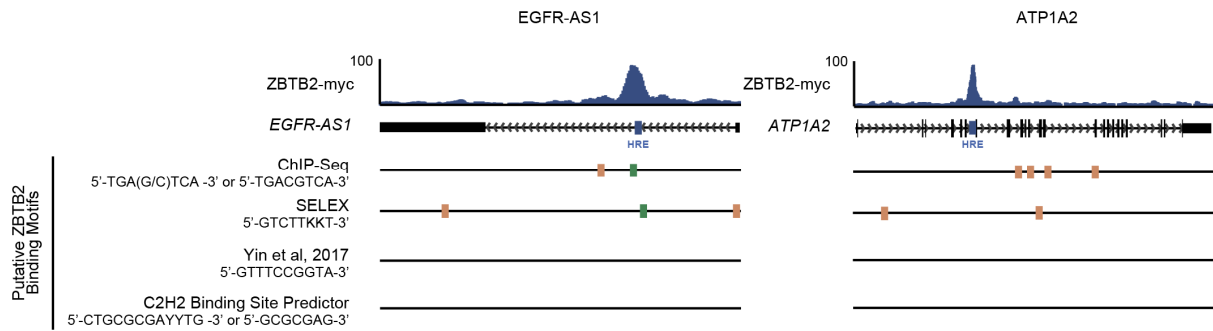
Figure 4.4 The sequences of ZBTB2 target genes were investigated for the presence of putative binding motifs. UCSC Genome Browser view of the ZBTB2-myc ChIP-Seq tracks of EGFR-AS1 and ATP1A2 are shown, along with the locations of the HREs. The locations of putative ZBTB2 binding motifs identified by each method are also shown. Green-coloured marks indicate that the putative motif was identified within 1000 bp of the ZBTB2-myc peak summit, while orange-coloured marks represent motifs that are not near the ZBTB2-myc peak.

Chapter 5

Discussion

The ultimate aim for this project was to further elucidate the mechanisms behind the cellular response to hypoxia, with a focus on how coactivating factors impact the expression of HIF-1 target genes. I investigated in detail how ZBTB2, a protein we previously found could act as a coactivator for HIF-1, can influence HIF-1-dependent gene regulation. I established that ZBTB2 is recruited to a portion of HIF-1 target genes to enable their full expression under hypoxia (Figure 5.1). Close examination of the regulation behind one of these genes, EGFR-AS1, revealed that it is upregulated under hypoxia in a HIF-1/ZBTB2/p300-dependent manner. ZBTB2 overexpression was found to further increase gene expression, but these effects were only observed if HIF-1 was present and if the HRE in the intron of EGFR-AS1 was intact. I showed that ZBTB2 overexpression resulted in an increase in H3K27ac in the vicinity of the HRE, indicating a possible mechanism through which ZBTB2 can promote HIF-1 target gene expression. Finally, I investigated the regulation of another putative HIF-1/ZBTB2 target, ATP1A2, and demonstrated that it is regulated through similar mechanisms as EGFR-AS1. These findings show a novel mechanism where ZBTB2 is a coactivator that is recruited to a specific subset of HIF-1 target genes to promote their full expression.
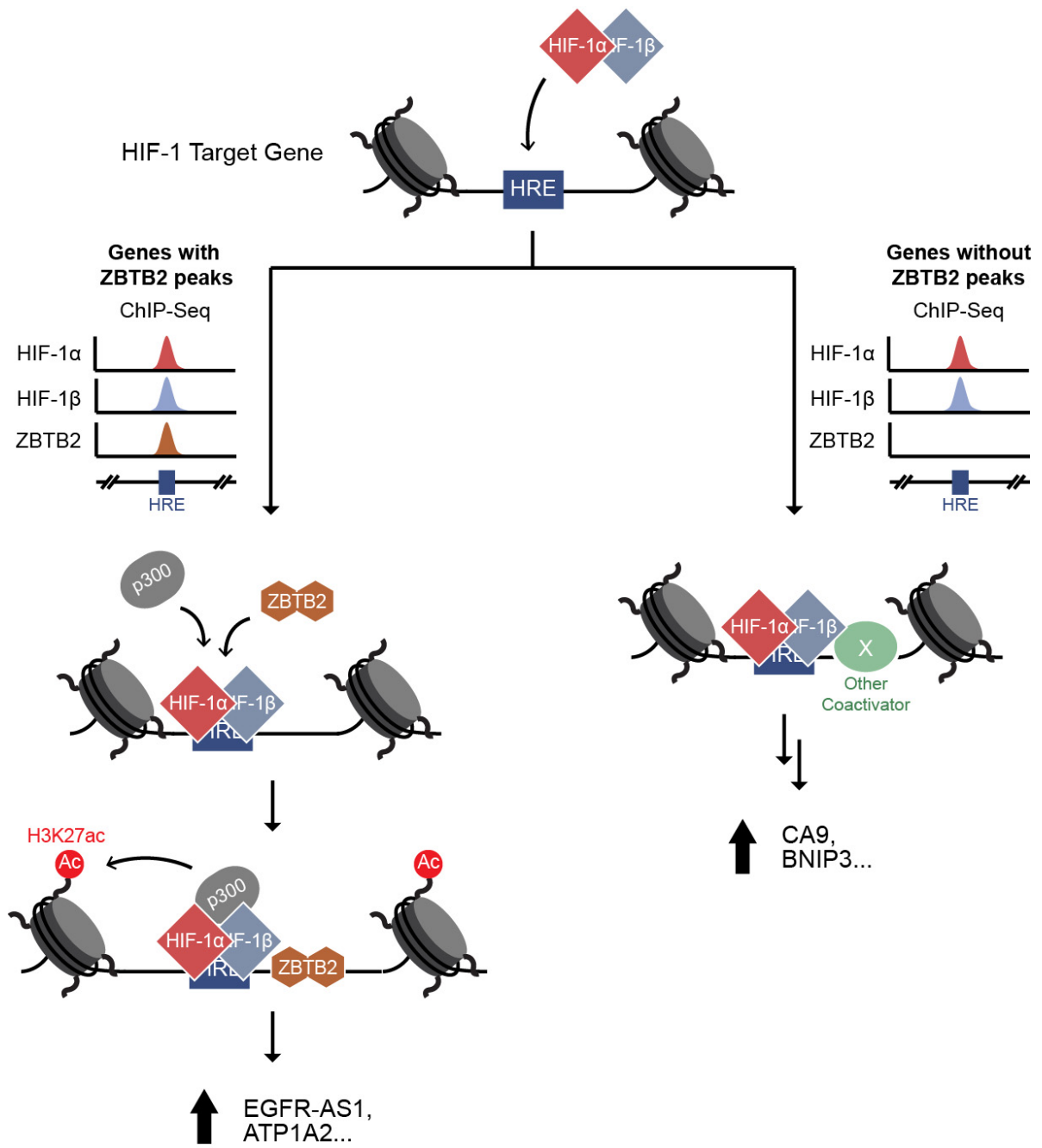
Figure 5.1 ZBTB2 is recruited to a subset of HIF-1 target genes under hypoxia and regulates their expression.

5.1 ZBTB2 regulates the expression of a subset of HIF-1 target genes involved in the hypoxia-associated phenotypes

I demonstrated that ZBTB2 is a coactivator that promotes the full expression of a subset of HIF-1 target genes under hypoxia. Comparison of ZBTB2 ChIP-Seq data with public HIF-1 ChIP data from ChIP-Atlas revealed that certain genes contained both ZBTB2 and HIF-1α peaks. Interestingly, when KEGG pathway enrichment analysis was performed, it was found that genes with both ZBTB2-myc peaks and reported HIF-1α peaks encoded for proteins involved in pathways associated with cancer and cardiomyopathy, which are two pathophysiological conditions where hypoxia plays an important role. I looked at the regulation of two genes, EGFR-AS1 and ATP1A2, both of which have overlapping HIF-1α and ZBTB2-myc peaks. I was able to confirm *via* qRT-PCR that hypoxia resulted in increased the expression of both genes, and that siRNA-mediated knockdown of ZBTB2 decreased expression while overexpression further increased expression (Figure 3.5). EGFR-AS1 has been reported to contribute to increased cell invasion and/or proliferation (51, 52). On the other hand, ATP1A2 has been implicated to play roles in cardiac function and heart disease (53). These results demonstrate that ZBTB2 and HIF-1 can co-regulate the expression of a subset of HIF-1 target genes, and may contribute to phenotypes observed in pathological conditions associated with hypoxia.

An important caveat to these observations is that just because a gene has both HIF-1α and ZBTB2 ChIP-Seq peaks, it does not necessarily mean that it is a HIF-1α/ZBTB2 target gene. While I was able to validate that the two candidate genes examined responded to hypoxic treatment in a HIF-1 and ZBTB2-dependent manner, it cannot be assumed that this holds true for all the other genes. A possible further experiment would be to perform RNA-Seq on cells treated under normoxia and hypoxia, with either ZBTB2 overexpression or with ZBTB2 depletion *via* knockdown or knockout. By comparing changes in the transcriptomes, genes that

have altered expression levels can be identified, and then these genes can be cross-referenced with the ChIP-Seq data to more reliably identify direct HIF-1/ZBTB2 target genes. The preliminary data described in this work suggests that HIF-1/ZBTB2 target genes may in part contribute to cancer and cardiomyopathy, indicating that further discovery and characterization of these genes may lead to new opportunities for therapeutic intervention.

5.2   ZBTB2 and HIF-2

HIF-2, another member of the HIF family of transcription factors that is associated with the response to chronic hypoxia, shares high structural similarity with HIF-1, is regulated through many of the same mechanisms, and binds to the same HRE consensus sequence. However, although HIF-2 shares some target genes with HIF-1, it is also known to regulate to distinct targets (9, 19, 40). While the mechanisms determining if a gene is regulated by either HIF or both have not completely been elucidated, it is known that certain HIF coactivators exclusively interact with one HIF isoform and only regulate expression of the target genes of one HIF (54). In light of this fact, I decided to examine if ZBTB2 may be one such coactivator. I compared HIF-1α/HIF-2α genomic occupancy data from ChIP-Atlas with my own ZBTB2-myc ChIP-Seq results, and discovered that most of the genes that had both HIF-1α and ZBTB2 peaks also had HIF-2α peaks, indicating that ZBTB2 is mostly recruited to genes that are both HIF-1 and HIF-2 targets (Figure 3.1). In addition, it was observed that siRNA-mediated knockdown of both HIF-1α and HIF-2α caused a decrease in the expression of HIF-1/ZBTB2 target gene EGFR-AS1 under hypoxia, indicating that EGFR-AS1 is likely target gene for both HIFs. This is further supported by the observation that knockdown of either HIF-1α or HIF-2α result in a smaller decrease in EGFR-AS1 expression than knockdown of HIF-1β, which suggests there may be some compensatory mechanism between the two HIF-αs. Therefore, based on these

observations, it is unlikely that ZBTB2 is a coactivator that exclusively interacts with one of the HIFs and confers target specificity. While the present study mainly focused on identifying HIF-1/ZBTB2 targets, it may be of interest to examine potential HIF-2/ZBTB2 targets in the future.

5.3   Not all HIF-1 targets are affected by ZBTB2

It is important to note that not all HIF-1 targets appear to be subjected to HIF-1/ZBTB2 co-regulation through the mechanisms described in this thesis. HIF-1 target genes such as CA9 and BNIP3 were unaffected by ZBTB2 overexpression (Figure 3.5D), and specific ZBTB2 peaks could not be observed at their promoter regions in the ChIP-Seq data (Figure 3.3B). The full expression of these genes does not depend on ZBTB2, and may instead require the participation of other coactivators. In addition, in our previous study, we identified matrix metalloproteinase 2 (MMP2) and MMP9 as ZBTB2 target genes upregulated under hypoxia (24). However, overlapping HIF-1 and ZBTB2 peaks at these genes could not be observed from the ChIP-Seq data (Figure 3.3C). Furthermore, the previous study showed that regulation of MMP2/9 proceeded through a p300-independent mechanism. This suggests that there may be multiple mechanisms through which ZBTB2 can positively influence the expression of HIF-1 target genes, or that there may be differences in HIF-1/ZBTB2 target genes depending on the cell type.

5.4   ZBTB2 increases H3K27ac at loci of certain HIF-1 target genes to promote transcription

I examined the mechanism behind HIF-1/ZBTB2-dependent gene regulation in greater detail through looking at the regulation of EGFR-AS1, and found that overexpression of ZBTB2

increases H3K27ac around the EGFR-AS1 intron HRE (Figure 3.14). In addition, I found that artificially inducing H3K27ac at the gene locus increases transcription of EGFR-AS1 (Figure 3.15). These results suggest that the mechanism through which ZBTB2 promotes HIF-1 target gene expression is through increasing histone acetylation. The coactivator and histone acetyltransferase usually associated with HIF-1-dependent regulation is p300/CBP, so it is possible that ZBTB2 may promote p300 activity. This is in contrast to the findings in our earlier study: we previously established that ZBTB2 increases HIF-1 transactivation activity through a mechanism that is not dependent on interaction between HIF-1 and p300 (24).

An area that requires further study is how ZBTB2 promotes histone acetylation. Published literature has shown that ZBTB2 and other BTB-domain containing proteins can interact with chromatin remodeling factors, although in most cases they function as transcriptional repressors *via* interaction with histone deacetylates (55–58). Interestingly, it has been reported that zinc finger protein Zac can interact with the C-terminus of p300 through its zinc finger domains and activate histone acetyltransferase activity (59). Further research can be performed to investigate the possibility that ZBTB2 may promote H3K27ac through similar mechanisms.

5.5   The challenge in identifying ZBTB2's consensus binding motif

Because ZBTB2's zinc finger domains have been shown to be required to modulate HIF-1 target gene expression both in a previous study and in the present one (Figure 3.5E), I reasoned that ZBTB2 may function by binding to DNA directly, and that characterization of a binding motif may assist in the discovery and investigation of other HIF-1/ZBTB2 target genes. I attempted to identify ZBTB2's consensus binding motif through various methods; however, none of the methods gave a clear motif that could be found near the ZBTB2 binding region in both the target genes that were investigated in this study. This is perhaps unsurprising: a

previous publication that performed ChIP-Seq to investigate ZBTB2's recruitment to CpG islands in mouse embryonic stem cells also failed to identify a clear motif through *de novo* searches (60). Furthermore, studies using HT-SELEX have reported that there is a low success rate in identifying motifs for transcription factors containing C2H2 zinc fingers, in part due to their long recognition motifs (47, 61). Additionally, ZBTB2 has 4 zinc finger domains and has the ability to form dimers both with itself and other zinc finger transcription factors (60), all which may recognize different DNA sequences, adding another layer of difficulty in identifying a clear binding motif.

Another possibility as to why I was unable to find ZBTB2's binding motif is that the ability of the zinc fingers in ZBTB2 to modulate HIF-1 activity may be independent from their ability to bind DNA directly. Zinc finger domains in proteins have been reported to be able to facilitate protein-protein interactions (59, 62). From my own data, ZBTB2 does not appear to be recruited to the EGFR-AS1 intron HRE under normoxic conditions despite being expressed, and is only recruited to under hypoxia in the presence of HIF-1 (Figure 3.4, Figure 3.5B). A possibility is that ZBTB2 does not bind to HIF-1 target genes directly and is observed at HREs because it is recruited to HREs indirectly through interaction with HIF-1 or other factors. Investigating whether or not this is the case, and whether or not the zinc finger domains play a role is the process, is a possible avenue for further studies.

5.6 ATF/CREB/AP-1 transcription factor binding sites are enriched near ZBTB2 peaks

When Homer and MEME analysis were performed on the ZBTB2 ChIP-Seq data, it was found that the motifs 5'-TCACGTCA-3' and 5'-TCA(C/G)TCA-3' were enriched near the top 1000 peaks (Table 4.1, Table 4.2). These motifs are actually known binding motifs for other

transcription factors: the former is known as the cyclic AMP response element (CRE) and is the canonical binding motif for activating transcription factor (ATF)/cAMP responsive element binding protein (CREB) transcription factors containing basic region-leucine zipper (bZIP) domains (63, 64), while the latter is known as the Activator protein 1 (AP-1) site, which is recognized by dimers formed with members of the ATF, Fos, and Jun transcription factor families (65, 66). These sequences are found on a wide variety of genes, and the transcription factors that bind to them regulate a diverse range of biological processes, including cell proliferation, lipid and glucose metabolism, and regulation of the immune response (65, 67, 68). Intriguingly, it has been reported that ATF-1 and CREB-1 can form a multiprotein complex with HIF-1 and p300/CBP, and that this complex is required for p300-dependent upregulation of HIF-1 target lactate dehydrogenase A (LDHA) (69). There are also experimental results that point to the possible importance of ATF/CREB/AP-1 transcription factors in regulation of HIF-1/ZBTB2 target genes: when I performed a split luciferase reporter assay with a construct containing the EGFR-AS1 intron and a mutated AP-1 site, I found that hypoxic induction of luciferase activity was completely abrogated (Figure 4.1). This suggests that a possible mechanism through which ZBTB2 increase acetylation at HIF-1 target genes is by promoting their expression through interaction with the reported multiprotein complex.

5.7   Summary and Future Perspectives

Hypoxia arises in many physiological and pathophysiological contexts, and therefore it is crucial to understand its underlying mechanisms in detail. While HIF-1 is known to regulate the transcription of many genes in response to hypoxia, it is also known that HIF-1 alone is often insufficient for full target gene expression and that additional cofactors are required. The aim of this study was to shed further light on the cellular response to hypoxia through

investigating how the coactivator ZBTB2 works with HIF-1 to influence gene expression under hypoxia. I showed that ZBTB2 is recruited to the vicinity of HREs in a subset of HIF-1 target genes, including those involved in cancer progression and heart disease, and demonstrated that ZBTB2 promotes H3K27ac at certain HIF-1 target gene loci. This leads to increased gene expression under hypoxic conditions. The effects of ZBTB2 are dependent on the presence of functional HIF-1 and on HIF-1 recruitment to the HRE. These results show a new mechanism through which ZBTB2 can act as a coactivator for HIF-1, and demonstrate that it is one cofactor that enables the full expression of certain HIF-1 target genes.

In hopes to better understand the targets of and mechanisms behind ZBTB2-dependent gene regulation under hypoxia, I also attempted to identify ZBTB2's consensus binding motif through various experimental and *in silico* methods. However, I was unable to obtain a clear result. Each method employed yielded different motifs, and none of the putative ZBTB2 binding motifs could be consistently identified in the HIF-1/ZBTB2 target genes investigated in this study. The challenge I faced when searching for ZBTB2 binding motifs may be due to the inherent difficulty in identifying C2H2 zinc finger binding motifs, or due to the possibility that ZBTB2 does not bind directly to *cis*-regulatory elements in HIF-1 target genes.

While I have met the original aims of the study and further elucidated how ZBTB2 can influence HIF-1's role in the cellular response to hypoxia, I have also identified several areas in this study that require additional research. I have identified several genes that undergo HIF-1/ZBTB2-dependent gene induction under hypoxia, but have not yet explored HIF-1/ZBTB2 targets on a transcriptome-wide scale. Additionally, I have not fully characterized the mechanisms through which ZBTB2 promotes an increase in H3K27ac at target gene loci. New findings in these areas will shed further light on HIF-1 and ZBTB2's role in regulating the response to hypoxic stimuli.

References

1. J. Pouyssegur, J. López-Barneo, Hypoxia in health and disease. *Mol Aspects Med* **47–48**, 1–2 (2016).

2. P. Vaupel, A. Mayer, M. Höckel, Tumor hypoxia and malignant progression. *Methods Enzymol* **381**, 335–354 (2004).

3. B. J. Moeller, R. A. Richardson, M. W. Dewhirst, Hypoxia and radiotherapy: opportunities for improved outcomes in cancer treatment. *Cancer Metastasis Rev* **26**, 241–248 (2007).

4. E. B. Rankin, A. J. Giaccia, The role of hypoxia-inducible factors in tumorigenesis. *Cell Death Differ* **15**, 678–685 (2008).

5. B. H. Jiang, E. Rue, G. L. Wang, R. Roe, G. L. Semenza, Dimerization, DNA binding, and transactivation properties of hypoxia-inducible factor 1. *J Biol Chem* **271**, 17771–17778 (1996).

6. S. Koyasu, M. Kobayashi, Y. Goto, M. Hiraoka, H. Harada, Regulatory mechanisms of hypoxia-inducible factor 1 activity: Two decades of knowledge. *Cancer Sci* **109**, 560–571 (2018).

7. H. Tian, S. L. McKnight, D. W. Russell, Endothelial PAS domain protein 1 (EPAS1), a transcription factor selectively expressed in endothelial cells. *Genes Dev* **11**, 72–82 (1997).

8. A. Pasanen, *et al.*, Hypoxia-inducible factor (HIF)-3alpha is subject to extensive alternative splicing in human tissues and cancer cells and is regulated by HIF-1 but not HIF-2. *Int J Biochem Cell Biol* **42**, 1189–1200 (2010).

9. M. Y. Koh, G. Powis, Passing the baton: the HIF switch. *Trends Biochem Sci* **37**, 364–372 (2012).

10. M. A. Maynard, *et al.*, Human HIF-3alpha4 is a dominant-negative regulator of HIF-1 and is down-regulated in renal cell carcinoma. *FASEB J* **19**, 1396–1406 (2005).

11. T. Tanaka, M. Wiesener, W. Bernhardt, K.-U. Eckardt, C. Warnecke, The human HIF (hypoxia-inducible factor)-3alpha gene is a HIF-1 target gene and may modulate hypoxic gene induction. *Biochem J* **424**, 143–151 (2009).

12. K. Hirota, G. L. Semenza, Regulation of hypoxia-inducible factor 1 by prolyl and asparaginyl hydroxylases. *Biochem Biophys Res Commun* **338**, 610–616 (2005).

13. M. Ivan, *et al.*, HIFalpha targeted for VHL-mediated destruction by proline hydroxylation: implications for O2 sensing. *Science* **292**, 464–468 (2001).

14. F. Yu, S. B. White, Q. Zhao, F. S. Lee, HIF-1alpha binding to VHL is regulated by stimulus-sensitive proline hydroxylation. *Proc Natl Acad Sci U S A* **98**, 9630–9635 (2001).

15. P. Jaakkola, *et al.*, Targeting of HIF-alpha to the von Hippel-Lindau ubiquitylation complex by O2-regulated prolyl hydroxylation. *Science* **292**, 468–472 (2001).

16. D. Lando, D. J. Peet, D. A. Whelan, J. J. Gorman, M. L. Whitelaw, Asparagine hydroxylation of the HIF transactivation domain a hypoxic switch. *Science* **295**, 858–861 (2002).

17. V. L. Dengler, M. Galbraith, J. M. Espinosa, Transcriptional regulation by hypoxia inducible factors. *Crit Rev Biochem Mol Biol* **49**, 1–15 (2014).

18. R. H. Wenger, D. P. Stiehl, G. Camenisch, Integration of oxygen signaling at the consensus HRE. *Sci STKE* **2005**, re12 (2005).

19. D. R. Mole, *et al.*, Genome-wide association of hypoxia-inducible factor (HIF)-1alpha and HIF-2alpha DNA binding with expression profiling of hypoxia-inducible transcripts. *J Biol Chem* **284**, 16767–16775 (2009).

20. N. C. Denko, *et al.*, Investigating hypoxic tumor physiology through gene expression patterns. *Oncogene* **22**, 5907–5914 (2003).

21. Y. Benita, *et al.*, An integrative genomics approach identifies Hypoxia Inducible Factor-1 (HIF-1)-target genes that form the core response to hypoxia. *Nucleic Acids Res* **37**, 4587–4602 (2009).

22. T. Tsuchiya, Y. Kominato, M. Ueda, Human hypoxic signal transduction through a signature motif in hepatocyte nuclear factor 4. *J Biochem* **132**, 37–44 (2002).

23. M. R. Pawlus, L. Wang, C.-J. Hu, STAT3 and HIF1α cooperatively activate HIF1 target genes in MDA-MB-231 and RCC4 cells. *Oncogene* **33**, 1670–1679 (2014).

24. S. Koyasu, *et al.*, ZBTB2 links p53 deficiency to HIF-1-mediated hypoxia signaling to promote cancer aggressiveness. *EMBO Rep* **24**, e54042 (2023).

25. M.-Y. Kim, *et al.*, ZBTB2 increases PDK4 expression by transcriptional repression of RelA/p65. *Nucleic Acids Res* **43**, 1609–1625 (2015).

26. R. Russo, *et al.*, ZBTB2 protein is a new partner of the Nucleosome Remodeling and Deacetylase (NuRD) complex. *Int J Biol Macromol* **168**, 67–76 (2021).

27. J. W. Bruce, M. Bracken, E. Evans, N. Sherer, P. Ahlquist, ZBTB2 represses HIV-1 transcription and is regulated by HIV-1 Vpr and cellular DNA damage responses. *PLoS Pathog* **17**, e1009364 (2021).

28. P. J. Stogios, G. S. Downs, J. J. S. Jauhal, S. K. Nandra, G. G. Privé, Sequence and structural analysis of BTB domain proteins. *Genome Biol* **6**, R82 (2005).

29. A. V. Persikov, M. Singh, An expanded binding model for Cys2His2 zinc finger protein-DNA interfaces. *Phys Biol* **8**, 035010 (2011).

30. A. V. Persikov, M. Singh, De novo prediction of DNA-binding specificities for Cys2His2 zinc finger proteins. *Nucleic Acids Res* **42**, 97–108 (2014).

31. Y. Naito, K. Hino, H. Bono, K. Ui-Tei, CRISPRdirect: software for designing CRISPR/Cas guide RNA with reduced off-target sites. *Bioinformatics* **31**, 1120–1123 (2015).

32. W. J. Kent, *et al.*, The human genome browser at UCSC. *Genome Res* **12**, 996–1006 (2002).

33. S. Heinz, *et al.*, Simple combinations of lineage-determining transcription factors prime cis-regulatory elements required for macrophage and B cell identities. *Mol Cell* **38**, 576–589 (2010).

34. S. Oki, *et al.*, ChIP-Atlas: a data-mining suite powered by full integration of public ChIP-seq data. *EMBO Rep* **19**, e46255 (2018).

35. R. Edgar, M. Domrachev, A. E. Lash, Gene Expression Omnibus: NCBI gene expression and hybridization array data repository. *Nucleic Acids Res* **30**, 207–210 (2002).

36. D. Karolchik, *et al.*, The UCSC Table Browser data retrieval tool. *Nucleic Acids Res* **32**, D493-496 (2004).

37. Z. Zou, T. Ohta, F. Miura, S. Oki, ChIP-Atlas 2021 update: a data-mining suite for exploring epigenomic landscapes by fully integrating ChIP-seq, ATAC-seq and Bisulfite-seq data. *Nucleic Acids Res* **50**, W175–W182 (2022).

38. E. Afgan, *et al.*, The Galaxy platform for accessible, reproducible and collaborative biomedical analyses: 2016 update. *Nucleic Acids Res* **44**, W3–W10 (2016).

39. T. L. Bailey, C. Elkan, Fitting a mixture model by expectation maximization to discover motifs in biopolymers. *Proc Int Conf Intell Syst Mol Biol* **2**, 28–36 (1994).

40. C.-J. Hu, L.-Y. Wang, L. A. Chodosh, B. Keith, M. C. Simon, Differential roles of hypoxia-inducible factor 1alpha (HIF-1alpha) and HIF-2alpha in hypoxic gene regulation. *Mol Cell Biol* **23**, 9361–9374 (2003).

41. B. T. Sherman, *et al.*, DAVID: a web server for functional enrichment analysis and functional annotation of gene lists (2021 update). *Nucleic Acids Res* **50**, W216–W221 (2022).

42. D. W. Huang, B. T. Sherman, R. A. Lempicki, Systematic and integrative analysis of large gene lists using DAVID bioinformatics resources. *Nat Protoc* **4**, 44–57 (2009).

43. S. Kaluz, M. Kaluzová, S.-Y. Liao, M. Lerman, E. J. Stanbridge, Transcriptional control of the tumor- and hypoxia-marker carbonic anhydrase 9: A one transcription factor (HIF-1) show? *Biochim Biophys Acta* **1795**, 162–172 (2009).

44. K. Guo, *et al.*, Hypoxia induces the expression of the pro-apoptotic gene BNIP3. *Cell Death Differ* **8**, 367–376 (2001).

45. K. Tracy, *et al.*, BNIP3 is an RB/E2F target gene required for hypoxia-induced autophagy. *Mol Cell Biol* **27**, 6229–6242 (2007).

46. I. B. Hilton, *et al.*, Epigenome editing by a CRISPR-Cas9-based acetyltransferase activates genes from promoters and enhancers. *Nat Biotechnol* **33**, 510–517 (2015).

47. Y. Yin, *et al.*, Impact of cytosine methylation on DNA binding specificities of human transcription factors. *Science* **356**, eaaj2239 (2017).

48. C. E. Grant, T. L. Bailey, W. S. Noble, FIMO: scanning for occurrences of a given motif. *Bioinformatics* **27**, 1017–1018 (2011).

49. G. E. Crooks, G. Hon, J.-M. Chandonia, S. E. Brenner, WebLogo: a sequence logo generator. *Genome Res* **14**, 1188–1190 (2004).

50. T. D. Schneider, R. M. Stephens, Sequence logos: a new way to display consensus sequences. *Nucleic Acids Res* **18**, 6097–6100 (1990).

51. J. Hu, *et al.*, Long Noncoding RNA EGFR-AS1 Promotes Cell Proliferation by Increasing EGFR mRNA Stability in Gastric Cancer. *Cell Physiol Biochem* **49**, 322–334 (2018).

52. A. Wang, *et al.*, Long noncoding RNA EGFR-AS1 promotes cell growth and metastasis via affecting HuR mediated mRNA stability of EGFR in renal cancer. *Cell Death Dis* **10**, 154 (2019).

53. C. Staehr, *et al.*, Migraine-Associated Mutation in the Na,K-ATPase Leads to Disturbances in Cardiac Metabolism and Reduced Cardiac Function. *J Am Heart Assoc* **11**, e021814 (2022).

54. C.-J. Hu, A. Sataur, L. Wang, H. Chen, M. C. Simon, The N-terminal transactivation domain confers target gene specificity of hypoxia-inducible factors HIF-1alpha and HIF-2alpha. *Mol Biol Cell* **18**, 4528–4542 (2007).

55. D. Olivieri, *et al.*, The BTB-domain transcription factor ZBTB2 recruits chromatin remodelers and a histone chaperone during the exit from pluripotency. *J Biol Chem* **297**, 100947 (2021).

56. P. Dhordain, *et al.*, Corepressor SMRT binds the BTB/POZ repressing domain of the LAZ3/BCL6 oncoprotein. *Proc Natl Acad Sci U S A* **94**, 10762–10767 (1997).

57. F. Guidez, *et al.*, Histone acetyltransferase activity of p300 is required for transcriptional repression by the promyelocytic leukemia zinc finger protein. *Mol Cell Biol* **25**, 5552–5566 (2005).

58. T. Maeda, Regulation of hematopoietic development by ZBTB transcription factors. *Int J Hematol* **104**, 310–323 (2016).

59. A. Hoffmann, T. Barz, D. Spengler, Multitasking C2H2 zinc fingers link Zac DNA binding to coordinated regulation of p300-histone acetyltransferase activity. *Mol Cell Biol* **26**, 5544–5557 (2006).

60. I. D. Karemaker, M. Vermeulen, ZBTB2 reads unmethylated CpG island promoters and regulates embryonic stem cell differentiation. *EMBO Rep* **19**, e44993 (2018).

61. A. Jolma, *et al.*, DNA-binding specificities of human transcription factors. *Cell* **152**, 327–339 (2013).

62. K. J. Brayer, D. J. Segal, Keep your fingers off my DNA: protein-protein interactions mediated by C2H2 zinc finger domains. *Cell Biochem Biophys* **50**, 111–131 (2008).

63. J. A. Bokar, *et al.*, Characterization of the cAMP responsive elements from the genes for the alpha-subunit of glycoprotein hormones and phosphoenolpyruvate carboxykinase (GTP). Conserved features of nuclear protein binding between tissues and species. *J Biol Chem* **263**, 19740–19747 (1988).

64. T. W. Hai, F. Liu, W. J. Coukos, M. R. Green, Transcription factor ATF cDNA clones: an extensive family of leucine zipper proteins able to selectively form DNA-binding heterodimers. *Genes Dev* **3**, 2083–2090 (1989).

65. M. Karin, Z. g Liu, E. Zandi, AP-1 function and regulation. *Curr Opin Cell Biol* **9**, 240–246 (1997).

66. P. Angel, *et al.*, Phorbol ester-inducible genes contain a common cis element recognized by a TPA-modulated trans-acting factor. *Cell* **49**, 729–739 (1987).

67. A. Cui, D. Ding, Y. Li, Regulation of Hepatic Metabolism and Cell Growth by the ATF/CREB Family of Transcription Factors. *Diabetes* **70**, 653–664 (2021).

68. A. G. Papavassiliou, A. M. Musti, The Multifaceted Output of c-Jun Biological Activity: Focus at the Junction of CD8 T Cell Activation and Exhaustion. *Cells* **9**, 2470 (2020).

69. B. L. Ebert, H. F. Bunn, Regulation of transcription by hypoxia requires a multiprotein complex that includes hypoxia-inducible factor 1, an adjacent transcription factor, and p300/CREB binding protein. *Mol Cell Biol* **18**, 4089–4096 (1998).

Acknowledgements

I would like to express my sincere gratitude to my advisor, Dr. Hiroshi Harada of the Graduate School of Biostudies at Kyoto University for his enthusiasm and insightful advice throughout the course of my degree. Dr. Harada has challenged me to tackle difficult problems and allowed me to grow as both a person and a scientist. I am also deeply thankful for the financial support from the Japanese Ministry of Education, Culture, Sports, Science and Technology in the form of the Monbukagakusho (MEXT) Scholarship.

My appreciation also extends to the current and former members of the Laboratory of Cancer Cell Biology. I would like first to thank Dr. Minoru Kobayashi for the invaluable input and knowledge he shared with me. I am also very grateful to Dr. Sho Koyasu for his guidance in the early stages of the project and his continued support even after leaving the lab. I am also thankful to Ms. Kumi Johchi for her technical assistance in constructing the HIF-1β knockout HeLa cells. I would also like to thank Mr. Gouki Kambe for his suggestions and advice on experiments, and Ms. Yukari Shirai for always being open for discussion. I am very fortunate to have been able to work among such an amazing group of people.

Last but not least, I would like to thank my family in for their overwhelming love and support. Without their encouragement, I would not be where I am today.

<div align="right">
Christalle Cheuk Tung Chow
Email: christalle.chow@outlook.com
</div>